Master of Science Thesis

Structure and dynamics of complex networks

Network epidemics and a geometric robustness measure

Karel Devriendt

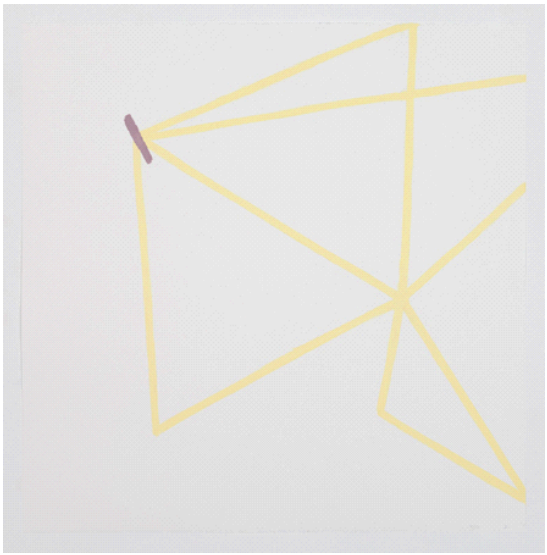
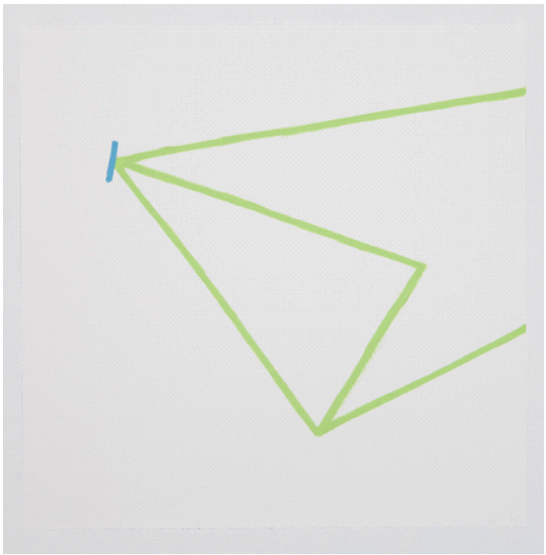
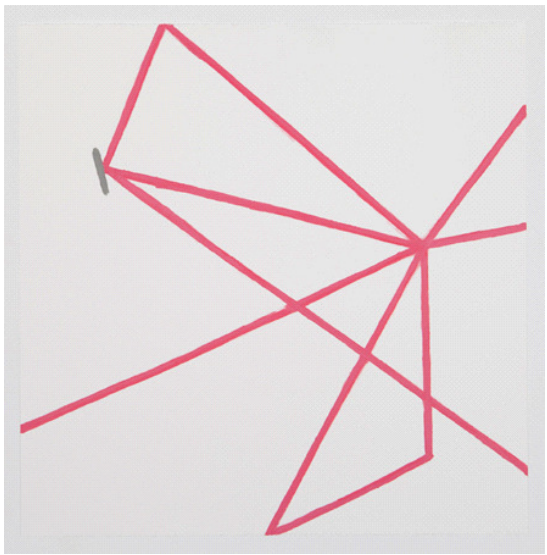
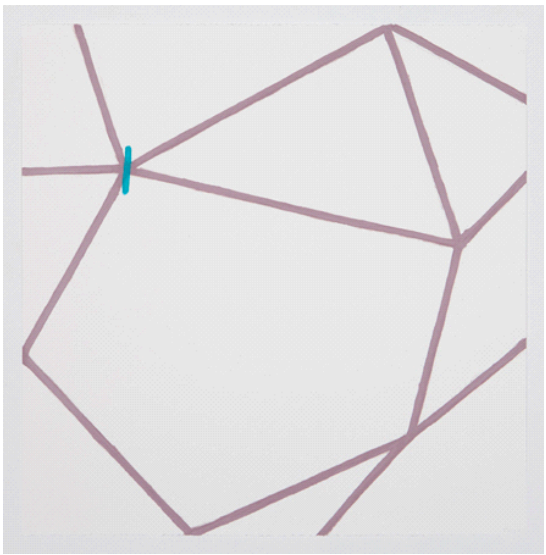

TU Delft Delft University of Technology

Network Architectures and Services

PVM 2017-091

Cover art:
Spencer Finch, "*Paths through the Studio*" (2012).
Series of 21 drawings based on walks taken through the studio on different days.
Copyright: Spencer Finch

Faculty of Electrical Engineering, Mathematics and Computer Science
Network Architectures and Services Group

Structure and dynamics of complex networks

Network epidemics and a geometric robustness measure

Karel Devriendt
4517024

Committee members:

Supervisor: Prof. Piet Van Mieghem
Member: Prof. Marco Loog
Member: Prof. Wioletta Ruszel

JULY 07, 2017
M.Sc. Thesis No: PVM 2017-091

Copyright © 2017 by Karel Devriendt
All rights reserved. No part of the material protected by this copyright may be reproduced or utilized in any form or by any means, electronic or mechanical, including photocopying, recording or by any information storage and retrieval system, without the permission from the author and Delft University of Technology.

Abstract

As new technologies continue to find their way into everyday life, the world becomes more and more connected. Airplanes and other means of transportation provide global connections in the physical world, while the omnipresence of the Internet means that information is shared around the globe, easier than ever before. But not only these man-made systems are distinctly connected, other complex systems like the human brain [1], or metabolic networks [2] are successfully being studied from the perspective of their constituting connections.
The combining concept in all these examples is the structure of the problem at hand: each system consists of interacting elementary components at the lowest level, from which a network structure emerges at the global level. The study of such networked systems, their observed features and the wide range of related analysis tools is commonly referred to as Network Science.

In this thesis, the specific problem of *how diseases spread over networks* is addressed. Better understanding this spreading behavior has significant practical importance, i.e. for the prediction and control of disease prevalence [3], and poses many interesting theoretical challenges. In the context of modeling epidemics on networks, we formulate the *Universal Mean-Field Framework*. This new and theoretically well-founded framework unifies and generalizes a number of existing approximate models, and brings forth new approaches to bound the approximations. Apart from the work on epidemics, some new insights are explored in the context of the connections between *electrical circuits, networks and simplices* (higher-dimensional triangles). These deep theoretical equivalences allow the tools and intuitions from electrical circuits and geometry to be used in the study of networks. A comprehensive introduction and discussion of the equivalent representations and their connections is given. Additionally, we derive a new formula for the volume of a hyperacute simplex and propose to use this volume as a network-robustness measure.

Preface

This thesis reports the work conducted during my graduation project at the Network Architectures and Services (NAS) group at Delft University of Technology. Under supervision of professor P. Van Mieghem, I had the opportunity to work on several interesting theoretical problems in the field of Network Science and graph theory. Starting from an initial interest in graph spectra, I was lead through a variety of topics, and ended up choosing two problem on which to focus my thesis work: Network epidemics and applications of the effective resistance in graphs.

A first word of thanks goes out to Piet Van Mieghem, for encouraging me to freely explore my interests and ideas, and for motivating me to put in my best effort. Thank you, Piet, for this great experience. Furthermore, I want to thank my colleagues at NAS, and all my friends in Delft, for the innumerous good moments we shared during these last two years.
And finally, the biggest thanks goes to my parents. Thank you for your advice and support, for my good 'nature and nurture', for keeping my feet on the ground and for everything else.
Thank you,
Bedankt.

Karel Devriendt
Delft, July 2017

Table of Contents

Chapter 1

Introduction

1-1 Network Science

Broadly speaking, the field of network science studies systems whose elementary structure can be described by some basic components and pairwise relationships between those components. These components and relationships, commonly called the *nodes* and *links*, are the building blocks of any network (Figure 1-1). Secondly, a dynamical process can be modeled

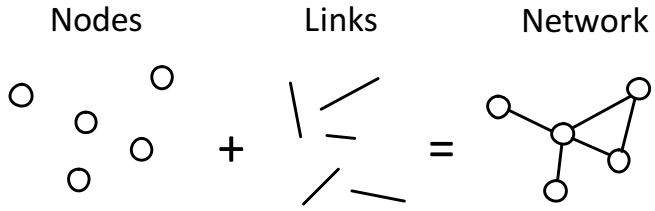

Figure 1-1: Nodes and links, the building blocks of any network

to take place on these networks. Such processes can often be stated in simple, local rules and can lead to complex, emergent behavior when taking place on networks. This combination of network topology and dynamical processes, enables Network Scientists to effectively study a large number of complex systems: cars driving on a road network [4], the spread of Internet worms [5] and even the communication between brain regions [1]. For every specific system and problem, the level of detail of the network and process needs to be chosen, such that only the necessary information is modeled.

A good example to illustrate the abstracting power of network models, is the first problem solved ever by graph theory. *Graph theory* is the mathematical field that studies graphs, which are the mathematical objects that correspond to networks. Graphs were invented by the famous mathematician Euler, who in the 18th century used them to solve the so-called Königsberg seven-bridges problem [6]. The Prussian city of Königsberg was divided in four parts by a river flowing through it. As Figure 1-2 illustrates, these parts were connected

by seven bridges. The open question at that time was: *Is there any route through the city that crosses all seven bridges without crossing any bridge twice?* Euler solved the problem

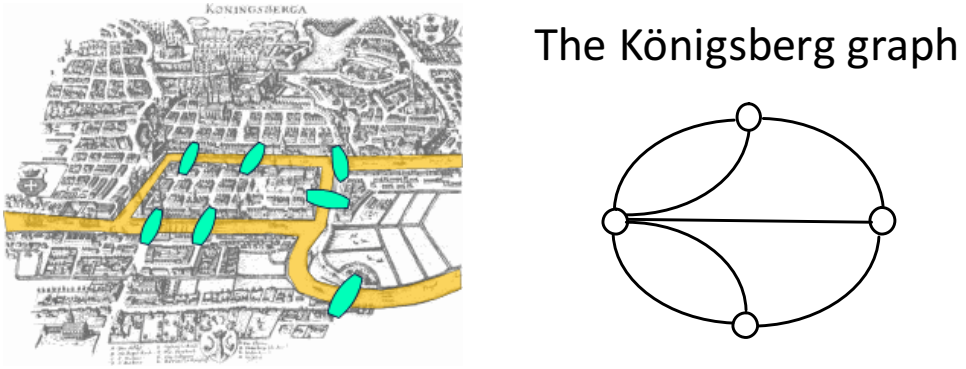

Figure 1-2: The Königsberg seven-bridges problem: is there any route through the city such that each of the seven bridges (green) is crossed exactly once? The city of Königsberg with the bridges highlighted in green is shown on the left[1]. On the right, the graph is shown which Euler used to solve this problem. Each separated part of the city corresponds to a node and each bridge corresponds to a link.

by considering the graph abstraction shown on the right in Figure 1-2. Based on this graph representation, Euler then ingeniously argued that for any connected graph a "non-returning route" only exists is there are exactly zero or two nodes with an odd number of nodes linked to them. Since the Königsberg bridge graph does not satisfy this condition Euler proved the non-existence of a route crossing all bridges only once.
This example shows how the correct level of abstraction leads to a better description of the problem. The shape of the city does not matter, the length of the bridges does not matter and neither does the relative position of the bridges. The only thing that matters is the number of bridges (links) between the different parts of the city (nodes), and the restrictions on the walk over the network. In the same spirit of Eulers approach, it is the attempt of network science to study complex systems by reducing a systems' description to a network. Once at the level of a network, the system can be studied using the rich mathematical tools of graph theory or the developments in the study of other networked systems. The power of this reductionist approach is seen clearly in the wide variety of fields that use it: social sciences, biology, mathematics, physics and many other.

The modern flavor of network science was largely developed at the transition between the 20th and 21st century. In a series of ground-breaking papers, it was shown that a wide range of real-world networks contained similar structures. In 1998, Watts and Strogatz [7] showed that networks constructed from actor collaborations, the US powergrid and the neural network of the C. Elegans worm, all had the so-called small-world property. Roughly speaking, a small-world network combines a good local efficiency with a good global efficiency. Soon after, in 1999, Barabasi and Albert [8] showed that networks constructed from websites in the world-wide-web, collaborations between actors and the US powergrid, all have a degree distribution that satisfy a power-law. The degree of a node is the number of nodes it is linked to, and the degree distribution of a network is then the distribution of all the node degrees in

a network. In a network with a power-law degree distribution, there is no "typical" degree and nodes with very high degree exist, which are also called hubs. The significance of these two results is that, probably unexpected at the time, a wide variety of real-world networks possess similar global structures, which seemed to imply some governing rules behind the growth and functioning of networks. Later, other ubiquitous structures were observed. Girvan and Newman [9], for instance, describe how community structure is another important feature in many network, illustrated by results in networks based on friendships, food webs and games between football teams.
The surprising generality of some network structures is an important motivation to further investigate complex systems from the network perspective. In the same spirit, the theoretical work in this thesis is motivated by the fact that any development in the network science tools or graph theory can potentially be used in a wide variety of contexts.

The main result in this thesis is related to dynamical processes on graphs, and an additional result connected to network structure is given. In Section 1-2, we give a brief discussion of dynamical processes and diseases spreading on graphs, as an introduction to the actual thesis contributions in Chapter 2. Then, in Section 1-3, we discuss the relationship between electrical circuits and weighted graphs as an introduction to Chapter 3.

1-2 Dynamical processes on graphs

1-2-1 Difference between classic and networked dynamical processes

The study of dynamical processes on networks is an important part of network science, but what makes it such an interesting problem to consider? If we only take the relevant properties of dynamical processes into account, then the spreading of a virus or a rumor is not much different from classic physical problems like wave propagation or diffusion. In both settings, the propagation of the energy, rumor or disease is governed by a local 'contact rule', i.e. the spreading takes place between neighbors. Then why is it not possible to simply translate the intuition and theoretical understanding of these classical physical problems (wave propagation or diffusion) to the setting of networked dynamical processes (diseases or rumors spreading)? By describing two experiments with a rough quantitative analysis, we will illustrate that, the network topology on which the processes take place makes a significant difference to the behavior of the process.

> Waves in a pool: We throw a rock in the middle of a circular pool of radius R and measure the time T_1 it takes for the first wave to reach the side of the pool. Then, we throw the same rock in a pool of radius $2R$ and measure again the time T_2.
> Since waves travel at a constant speed, say v, we can roughly calculate that $T_1 = R_1/v$ and $T_2 = R_2/v$, and thus $T_2 = 2T_1$. In other words, by quadrupling the size of the pool (i.e. doubling the radius), the waves take twice as long to travel through the pool.
>
> Gossip in a school: In a school with N students, Alice starts spreading a gossip to all of her friends. As is common, each of these friends will in turn share the gossip with all their friends during recess. We count the number of recesses L_1 it takes for the gossip to reach all the students. The following year, the number of students has quadrupled

to $4N$. Again, Alice starts spreading a gossip, and we measure the number of recesses L_2 it takes for the gossip to reach all students.
Since typical networks are small-world, all nodes are connected by short paths. Specifically, the shortest-path distance L between any two nodes in the network, grows about logarithmically with the network size N [7]. Hence if we call N the number of students in the first year, we can estimate the number of recesses as $L_1 = \log(N)$ and $L_2 = \log(4N)$, and thus $L_2 = L_1 + \log(4)$ or the second year. In other words, by quadrupling the number of students, the gossip takes only $\log(4)$ recesses longer.

These quick, first-order analyses illustrate the inherently different behavior of dynamical processes on networks, as compared to other, classic dynamical processes. The 'global spreading time' of waves is polynomially dependent on the system size, while for gossip spreading on small-world networks this dependence is logarithmic. This difference in behavior that stems from the process-topology dependence, motivates the further investigation dynamic processes on networks[2].

1-2-2 Epidemics on networks

A particular dynamical process that is widely studied, is the spreading of diseases on networks. While the mathematical study of epidemics dates back to the work of Bernoulli in the 18th century, the focus on the role of network topology only started at the transition between the 20th and 21st century with the work of Kephart and White [5], and Pastor-Satorras and Vespignani [10]. In their work, the importance of the interaction between network topology and spreading behavior was highlighted. A better understanding of this interaction could be crucial in managing epidemic outbreaks in the future, which motivates the continuous research in this field.
To investigate disease on a network, many disease models can be used. One of these models is the Susceptible-Infected-Susceptible model, further also called the SIS model. In SIS, each node in the network can be in one of two states: infected (I), which means that the node is infected by the disease, or susceptible (S), which means that the node is healthy but can be infected. The disease then spreads through the network because infected nodes can infect their susceptible neighbors according to a stochastic infection process. Similarly, infected nodes can become healthy by a stochastic curing process. The details of these infection and curing processes are further described in Chapter 2. At this point, it is enough to mention that by particular choices of stochastic processes, the SIS process becomes memoryless, and as a result, can be described analytically with tools from Markov theory. This tractability is a great advantage, since it means that the Markovian SIS model is simple enough to allow for a deep theoretical study while still exhibiting complex behavior linked to the network topology.

1-2-3 Context of the thesis contribution

While the Markovian SIS process can be described exactly, the complexity of the description grows exponentially with the network size [11]. As a result, a variety of approximation

[2]Roughly speaking, the classic physical problems can be considered to take place on a lattice topology, which is the 'neighborhood structure' of Euclidean space. Hence, the difference between dynamical processes on general complex networks and classic dynamical processes originates from the different properties of complex networks and lattices.

methods have been developed in the epidemics research community [12],[13]. One class of approximation methods are the mean-field approximations, which are inspired by approximation methods from statistical physics. Mean-field methods are widely used to study SIS epidemics, and have lead to important insights in the behavior of epidemics on networks, however, no real consensus exists about which mean-field method should be used for which problem. Related to this problem is the fact that no general framework exists that contains all mean-field methods.

In this thesis, such a framework is introduced: *the Universal Mean-Field Framework* (UMFF). This framework consists of a general and rigorous description of approximation steps that lead from the exact SIS equations to a general set of mean-field equations. In particular, we show that the UMFF equations contain a number of important mean-field methods: the N-Intertwined Mean-Field Approximation (NIMFA) [11], the Heterogeneous Mean-Field method (HMF) [10] and pairwise Quenched Mean-Field theory (pQMF) [14]. Apart from *unifying* the existing mean-field techniques, UMFF also *generalizes* them by providing a general description of the possible approximation steps. A second contribution in the description of UMFF is that we provide an interpretation of the mean-field approximations from the perspective of the *isoperimetric problem*. This perspective enables the formulation of new bounds on the mean-field approximations, and results in a theoretically interesting connection to other mathematical results, in particular Szemerédi's Regularity lemma (see Section 2-8). Roughly speaking, the isoperimetric problem for a certain geometry is related to the question: "Given a certain perimeter, or surface of size P, what are the bounds on the volume A that can be enclosed by this perimeter or surface?". The analogy with the epidemic process is explained in Section 2-7. To conclude, the thesis contributions related to network epidemics can be summarized as:

Thesis contribution (i)

The formulation of the Universal Mean-Field Framework contributes to the network epidemics research by unifying and generalizing the subclass of mean-field approximation methods of the SIS epidemic model. Additional intuition in the mean-field approximation methodology and accuracy bounds are provided by the analogy between the SIS process and the isoperimetric problem.

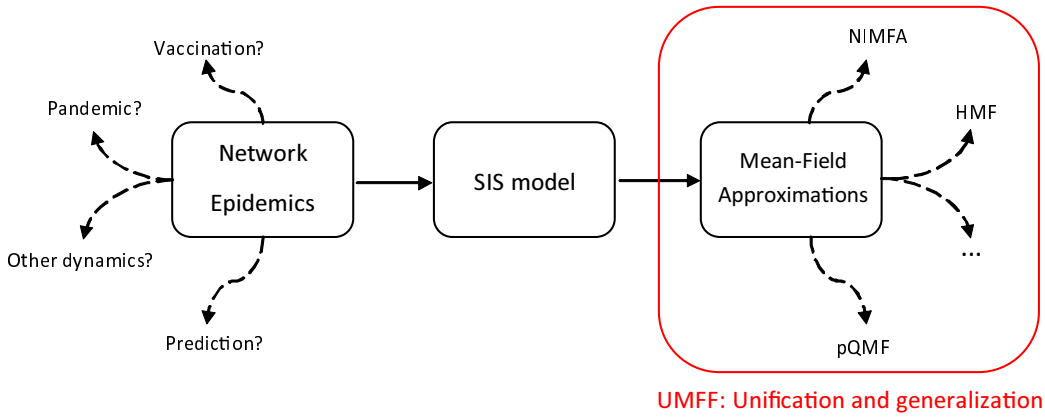

Figure 1-3: The role of the Universal Mean-Field Framework: unification and generalization of SIS mean-field approximations.

1-3 Electrical circuits and graphs

1-3-1 Equivalence between electrical circuits and weighted graphs

Electrical circuits consist of resistors connected by ideal wires, and are used to model the voltages in an interconnection of electrical components. Interestingly, such circuits can be translated directly to networks. There exists a one-to-one mapping between electrical circuits and weighted graphs, where nodes correspond to the connecting wires and links to the resistors. This equivalence has historically been proven to be a fruitful connection, since it allows the circuit laws to be handily rewritten using the characteristic matrices of the graph, and conversely enables the physical intuition of electrical circuits and equivalent systems to be used in network problems, as illustrated by Figure 1-4. A particular circuit concept that has

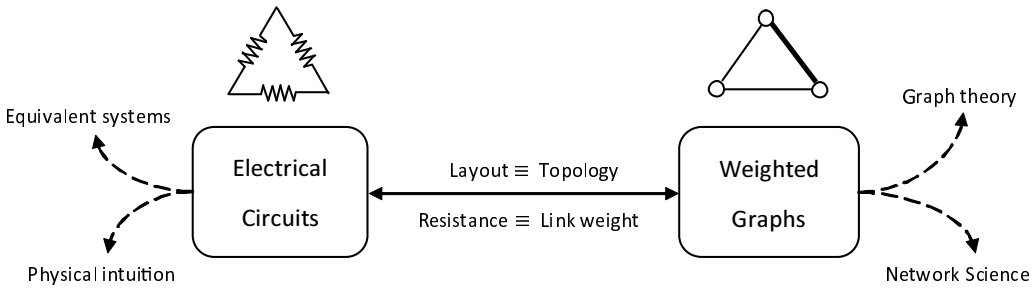

Figure 1-4: Each passive electrical is equivalent to a weighted graph, where ideal wires and resistors in the circuit correspond to nodes and links in the graph. This equivalence enables graph theory and tools from network science to be used in circuit-related problems. Conversely, the physical intuition of electrical circuits and equivalent systems have many useful applications in network-related problems.

had an important impact in graph theory is the effective resistance. In electrical circuits, the effective resistance has a clear physical meaning and is related to the circuit laws, but also in the context of graphs it has numerous applications and interpretations. The effective resistance has for instance been used to define graph invariants in molecular graphs [15], distance functions between nodes [16] or robustness measures [17].

1-3-2 Context of the thesis contribution

Since the effective resistance defines a distance function between nodes [16], which implies a certain geometric context, the circuit-graph equivalence can be extended by another representation: a simplex[3]. A simplex is a generalization to higher-dimensions of a triangle and a prism, i.e. a convex polyhedron with $N-1$ vertices in N dimensions (and other restrictions). We will refer to this three-way equivalence as the Circuit-Graph-Simplex (CGS) equivalence, and already in 1969, Sharpe [18] articulated the interesting potential that this equivalence provides[4] : "*As a consequence, problems on resistive networks are equivalent to geometric problems on acute-angled simplices (...) All the arsenal of knowledge acquired over many*

[3]The equivalence holds only for *hyperacute simplices*, as defined in Section 3-5
[4]In [18], only the circuits and simplices are discussed.

years which we possess on Euclidean spaces may therefore be utilised in the solution of the resistive n-port problem."
In the spirit of this quote by Sharpe, we introduce a new formula relating the geometric notion of the simplex volume to the graph-theoretical notion of Laplacian eigenvalues. Specifically, the thesis contribution can be summarized as:
Thesis contribution (ii)
In the context of the Circuit-Graph-Simplex equivalence, a new formula for the volume of a hyperacute simplex in terms of Laplacian eigenvalues is derived. Moreover, the relation of this new formula to the effective graph resistance [17] motivates the interpretation of the simplex volume as a network robustness measure.

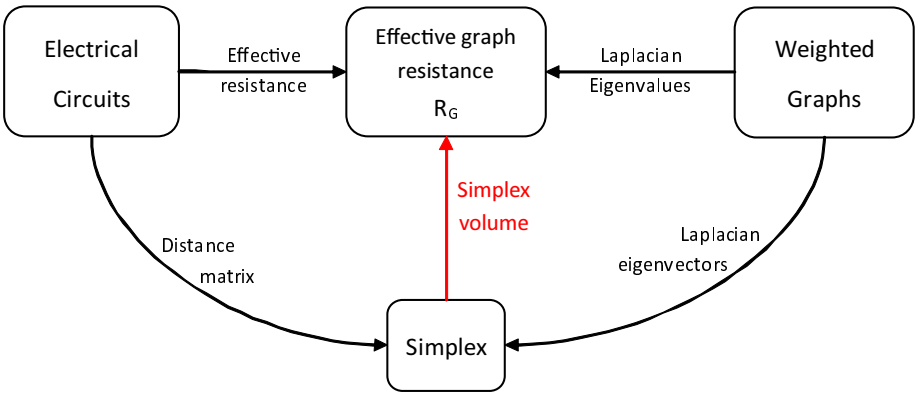

Figure 1-5: Chapter 3 describes how each equivalent circuit-graph pair also corresponds to an equivalent simplex. A novel expression is given for the volume of this simplex in terms of the graph description, which leads to a network robustness interpretation of the volume.

1-4 Notations

We introduce some mathematical notations that will be used throughout this article. The basic object of study is a graph $G(\mathcal{N}, \mathcal{L})$, where $\mathcal{N}$ represents the set of N nodes and $\mathcal{L}$ the set of L links between pairs of nodes. Unless stated otherwise, the graph is assumed to be connected (i.e. there is at least one path between each pair of nodes) and the links to be unweighted and undirected. A convenient way of representing the graph structure is the $N \times N$ adjacency matrix A, with elements:

$$a_{ij} = \begin{cases} 1 & \text{if } (i,j) \in \mathcal{L} \\ 0 & \text{otherwise} \end{cases}$$

The number of neighbors of a node in the graph, is called the degree of that node. For a node $i \in \mathcal{N}$ the degree is given by

$$d_i = \sum_{j=1}^{N} a_{ij}$$

Since we consider undirected and unweighted graphs, the adjacency matrix A is real and symmetric, possessing the following eigendecomposition:

$$A = X\Lambda X^T = \sum_{i=1}^{N} \lambda_i x_i x_i^T$$

where X is the orthogonal eigen-matrix with eigenvectors x_i as columns, and $\Lambda = \text{diag}(\lambda_1, \lambda_2, \ldots, \lambda_N)$ the diagonal matrix with eigenvalues on its diagonal. Because the adjacency matrix A is real and symmetric, all eigenvalues are real and can be ordered as $\lambda_1 \geq \lambda_2 \geq \cdots \geq \lambda_N$. Another matrix capturing the graph structure is the Laplacian matrix Q, defined as:

$$Q = \Delta - A$$

where $\Delta = \text{diag}(d_1, d_2, \ldots, d_N)$ is the diagonal matrix containing the node degrees. Since the Laplacian Q is also real and symmetric matrix, we can write the eigendecomposition:

$$Q = ZMZ^T = \sum_{i=1}^{N} \mu_i z_i z_i^T$$

where Z is the orthogonal eigen-matrix with eigenvectors z_i as columns, and $M = \text{diag}(\mu_1, \mu_2, \ldots, \mu_N)$. Since all rows of Q sum to zero, it holds that $Qu = 0$, where u is the all-one vector. The eigenvalue equation $Qu = \mu_N u$ with $\mu_N = 0$ illustrates that Q has at least one zero eigenvalue, according to the eigenvector $u/\sqrt{N}$. The Laplacian Q is positive semidefinite, which means that all eigenvalues are non-negative, i.e. $\mu_i \geq 0$ for all $i \leq N$. Additionally, the multiplicity of the zero eigenvalue μ_N is known to be one for connected graphs [19]. Hence, for any connected graph, we can write the ordered sequence of Laplacian eigenvalues $0 = \mu_N < \mu_{N-1} \leq \cdots \leq \mu_1$.
To use single-node information in formulas, we will often use the $N \times 1$ node indicator vector e_i, for which the k'th entry equals:

$$(e_i)_k = \begin{cases} 1 & \text{if } k = i \\ 0 & \text{otherwise} \end{cases}$$

With this vector, we can conveniently denote single entries from vectors and matrices, for instance $a_{ij} = e_i^T A e_j$.

Chapter 2

Universal mean-field framework for SIS epidemics

2-1 Overview

This chapter discusses the thesis contributions related to the modeling of epidemic diseases on networks. As introduced in Chapter 1, the study of epidemic diseases on networks is part of the more general study of dynamical processes on networks. With the example of "waves in a pool" and "gossip in a school", we illustrated the non-trivial coupling between network topology and the process running on a network. Hence, apart from the clear benefit in terms of prediction and control of diseases, also the a theoretical understanding of the topology-process interplay are motivations to further consider network epidemics.
Figure 1-3 sketched the specific context of this chapter and the contribution: the formulation of the Universal Mean-Field Framework (UMFF) as a unifying and generalizing framework for SIS approximations. Additionally, we further investigate the close connection between the infection process in network epidemics and the well-studied isoperimetric problem [20],[21]. This connection provides novel insights, e.g. about the scaling behavior of the SIS process on large graphs, and allows us to deduce new bounds on the UMFF approximations.

In Section 2-3, we start by defining the SIS epidemic model on networks and elaborate on the feasibility of the exact SIS description. Then, in Section 2-4, we define UMFF, which consists of two approximations and the resulting UMFF equations. In Section 2-5, we derive how the UMFF equations follow from the exact SIS equations by subsequently introducing the two approximations. In Section 2-6, we describe how the existing mean-field methods are contained by UMFF. Section 2-7 introduces the isoperimetric problem and describes its analogy with the infection process. This analogy leads to the topological UMFF approximation and bounds on this approximation. In Section 2-8, we discuss the relation between UMFF and Szemerédi's regularity lemma and explore the implications of this relation for the SIS process on large graphs. Section 2-9 overviews some related work. Finally, Section 2-10 concludes

the Chapter by summarizing the main properties of UMFF and by suggesting some future research directions.

2-2 Introduction: Epidemics on networks

The spread of epidemic diseases on complex networks is a widely studied topic in the field of network science [12]. While the mathematical study of epidemics dates back to the work of Bernoulli in the 18th century, the focus on the role of network topology only started at the end of the 20th century with the work of Kephart and White [5]. With the recent observations that network structures seem ubiquitous in both natural and man-made systems, a better understanding of the interplay between dynamic processes and network structure has become an important pursuit. For the case of diseases, a better knowledge of the interaction between network features and the resulting spreading behavior could be crucial in managing epidemic outbreaks in the future. More generally, the theoretical study of spreading diseases is related to a much wider class of dynamic processes on networks like the spreading of information, computer viruses or opinions.
In the study of epidemics on complex networks, the compartmental model of Kermack and McKendrick [22] from 1927 is regarded as a basic disease model. In compartmental models, each entity in the population is assumed to be in a certain state, for instance healthy, contagious, immune or others. The state of each entity, from now on called node, can change based on the current state of the node itself and, in the case of nodes in a network, its neighboring nodes. By these local interactions the disease can spread, die out or show other behaviors depending on the model. A more general overview of the basic models and current progress in the field of epidemics on complex networks is given in [12].
Like many network-epidemic studies, we will focus on one specific compartmental model: the SIS (Susceptible-Infected-Susceptible) model. The SIS model is often used because it is simple enough for a deep theoretical study while still being complex enough to exhibit global behavior that is non-trivially coupled to the small-scale process and the topology of the underlying network. In the SIS model, each node in the network can be in either of two states: susceptible (S) or infected (I). These states can change over time when an infected node is cured, or when a susceptible node is infected by a sick neighbor. These curing and infection events are stochastic processes that determine the dynamics of the disease. For a given initial distribution of infected nodes, the basic questions in studying the SIS model are then: what is the evolution of the state of the nodes in the network, how many nodes are infected in the metastable state, does the disease die out before reaching a significant fraction of the population, etc.
To address these questions, some further assumptions need to be made about the dynamics of the SIS process. In the Markovian SIS model, on which this article focuses, the infection and healing events are modeled as Poisson processes. More general distributions are possible [23], but with the Poisson assumption, the waiting times for infection or healing events are exponentially distributed which means that they satisfy the memoryless property, and the transitions between different configurations of the system become equivalent to state transitions in a Markov Chain. For specified rates of the Poisson processes, the evolution of the process can be exactly described based on Markov theory [11]. However, since the number of possible states of the system grows exponentially with the number of nodes, this exact description is not practical. Consequently, several methods have been developed that ap-

proximate the SIS model in order to make analysis possible and investigate the interesting interaction between the process and the underlying topology. Notably, the N-Intertwined Mean-Field Approximation (NIMFA) [11] and the Heterogeneous Mean-Field method (HMF) [10],[24] are two widely-used approximation methods, which we will show to be contained by the introduced framework. An overview of these two methods and other SIS approximation methods can be found in [12] and [13].

2-3 Background: the SIS epidemic model

In the study of epidemics on complex networks, the compartmental model of Kermack and McKendrick [22] from 1927 is regarded as a basic disease model. In compartmental models, each entity in the population is assumed to be in a certain state, for instance healthy, contagious, immune or others. The state of each entity, from now on called node, can change based on the current state of the node itself and, in the case of nodes in a network, its neighboring nodes. By these local interactions the disease can spread, die out or show other behaviors depending on the model. A more general overview of the basic models and current progress in the field of epidemics on complex networks is given in [12].
Like many network-epidemic studies, we will focus on one specific compartmental model: the SIS (Susceptible-Infected-Susceptible) model. The SIS model is often used because it is simple enough for a deep theoretical study while still being complex enough to exhibit global behavior that is non-trivially coupled to the small-scale process and the topology of the underlying network. In the SIS model, each node in the network can be in either of two states: susceptible or infected. For a specified graph $G(\mathcal{N}, \mathcal{L})$, the disease state at a given time t, is represented by the variable:

$$W_n(t) \in \{0, 1\}$$

The expression $W_n(t) = 0$ means that node n is healthy, but susceptible (S) to the disease, while $W_n(t) = 1$ means that the node is infected (I) and contagious. Figure 2-1 shows two examples of disease states and the corresponding state vector w. Since the SIS process is a

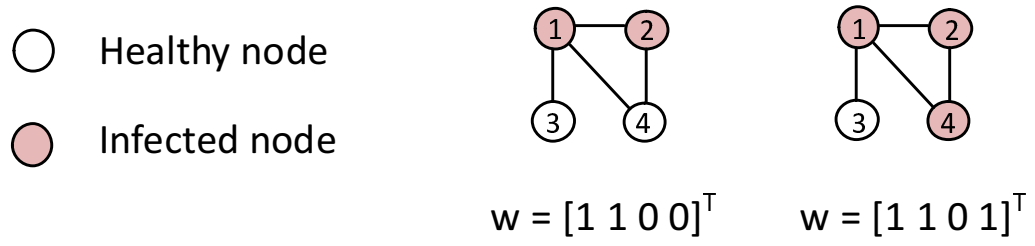

Figure 2-1: In the Susceptible-Infected-Susceptible compartmental disease model, each node n in the network can be in two states: susceptible ($w_n = 0$) or infected ($w_n = 1$). The disease state of an N-node network can then be represented by the $N \times 1$ disease state w. In this figure, two examples of disease states are given with their corresponding vector representations.

stochastic process, $W_n(t)$ is a Bernoulli random variable and the infection probability of node n equals $\Pr[W_n(t) = 1]$. The evolution of the state probabilities over time is governed by the

disease dynamics

$$S \to I \to S$$

which means that susceptible nodes can become infected nodes, which in turn can become susceptible. The $S \to I$ transition is called *infection* and can occur when a susceptible node n has an infected neighbor j in the network. The $I \to S$ transition is called *curing* and captures the process where each infected node has the possibility to be cured. Figure 2-2 illustrates how the infection and curing process lead to transitions of the disease state. To make the

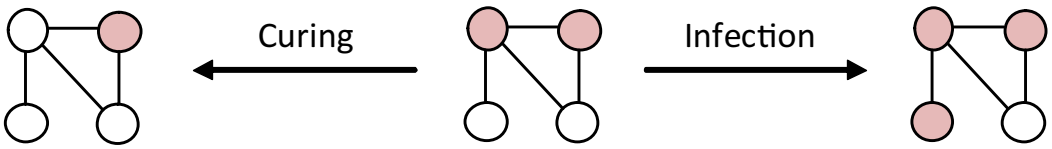

Figure 2-2: The SIS dynamics are governed by two processes: infection and curing. In the infection process, infected nodes infect their neighbors at a certain rate β. In the curing process, infected nodes are cured at a certain rate δ.

dynamics tractable, the infection and curing events are assumed to be independent Poisson processes. In particular, for the curing process,

$$\Pr[W_n(t+h) = 0 | W_n(t) = 1] = \delta e^{-\delta h} \tag{2-1}$$

means that, disregarding all other processes, the waiting time for the $I \to S$ transition is exponentially distributed with rate δ. In general, each node n can have a different, time-dependent rate $\delta_n(t)$, but further in this work we consider a fixed and time-independent rate δ. If we consider just one link between a susceptible node n and an infected node j, which we will call an infective link, then the infection process obeys

$$\Pr[W_n(t+h) = 1 | W_n(t) = 0] = \beta e^{-\beta h} \tag{2-2}$$

where the occurrence of other processes is ignored (which holds for $h \to 0$) and where we thus assume that the infected neighbor node j stays infected and does not cure, i.e. $W_j(t+s) = 1$ for $s \in [0, h]$. Again, each link $(n, j) \in \mathcal{L}$ can have a specific rate $\beta_{nj}(t)$, but for simplicity we assume a fixed and time-independent rate β. For notational purposes, we will often omit the time reference t in time-dependent variables by writing W_n instead of $W_n(t)$ and similarly for other time-dependent variables. It is also possible to model the infection and curing events as more general renewal processes [25], which results in different distributions for the waiting times (2-1) and (2-2). For non-Poissonian processes, the Markov property no longer holds but approaches still exist to describe the SIS process [23].

The expressions of the curing and infection processes show that the evolution of the SIS process at a given time, only depends on the disease state at that time. This means that the system is memoryless and can be described as a Markov process. In other words, the process evolution can be fully described based on the knowledge of (i) which state can transition to which other state and (ii) at which rate these transitions happen. Based on this transition structure, the Kolmogorov equations and the infinitesimal generator lead to an exact description of the SIS process, for any initial disease state distribution $\Pr[W(0) = w]$ for all w (see Appendix A-1-1). Figure 2-3 illustrates and summarizes the Markov chain structure of the

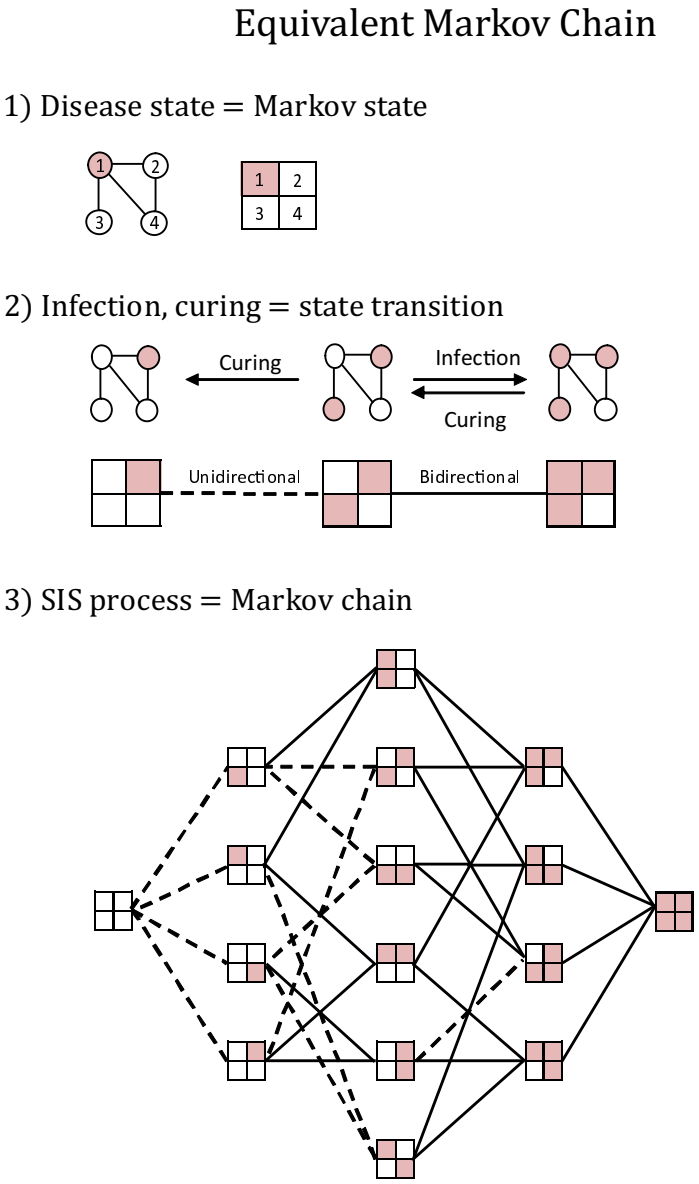

Figure 2-3: Based on the assumption that infection and curing are Poisson processes, the SIS process is equivalent to a continuous-time discrete-state Markov process, i.e. a Markov Chain. Each state in the Markov process corresponds to a disease state of the network, and the transition rates between the Markov states corresponds to the infection or curing rates, i.e. δ for healing nodes, and ($\beta \times$#Infected neighbors) for node infection. All transitions combined form a Markov Chain, which by means of the Kolmogorov equations or the infinitesimal generator leads to a exact description of the SIS process [11].

SIS process.
While the Markov property leads to an exact and tractable description of the full SIS process, the complexity of this description grows exponentially with the number of nodes. As Figure 2-3 already indicates, a network with N nodes has 2^N possible SIS disease states. This means that for roughly $N > 20$, finding a solution of the 2^N linear equations becomes infeasible. This complexity of representing all possible disease states on a network is the main problem in describing the SIS process and especially, as we will show later, because of the dependence of the number of infective links (and thus the transition rates) on the full state information. An exact description of the process requires to calculate the probability $\Pr[W(t) = w]$ that the state vector $W(t) = [W_1(t)\ W_2(t)\ \dots\ W_N(t)]^T$ equals a certain state vector w, for each possible state. Such a state w is a zero-one Bernoulli vector, or $w \in \{0,1\}^N$, which shows again that there are 2^N possible state vectors.
To resolve the complexity problem of the exact SIS equations, it is necessary to introduce approximations. The basic idea of approximating the SIS process lies in the description of the state by a different variable than the random variable $W(t)$, and to find the governing equations such that the exact dynamics are approximately described by that variable. UMFF relies on two different types of variables: the number of infected nodes $\widetilde{W}(t)$ (which is a random variable) and the (deterministic) expected number of infected nodes $\mathbf{E}[\widetilde{W}(t)]$. Apart from being a lower-dimensional description for the SIS process and thus addressing the exponential complexity problem, the number of infected nodes and the expected number of infected nodes are also more insightful variables.

2-4 Definition of the Universal Mean-Field Framework

To describe UMFF, we need a number of preliminary definitions and notations. Firstly, we define a graph partitioning as follows:

Definition 1 (Partitioning)**.** *A partitioning π of graph G defines a partitioning of the node-set $\mathcal{N}$ of G into K non-empty, disjoints partitions $\mathcal{N}_k \subseteq \mathcal{N}$ such that $\bigcup_{k=1}^{K} \mathcal{N}_k = \mathcal{N}$.*

By $N_k = |\mathcal{N}_k|$, we will denote the number of nodes in partition k, and by L_{km}, the number of links between nodes from partition k and m (and twice the number of links if $k = m$, see Table 2-1).
We will use the graph partitioning to group information of nodes belonging to the same partition, which results in a lower-dimensional description of the disease state and thus of the SIS process. A crucial concept of UMFF is to group nodes according to a partitioning π and to consider the $K \times 1$ *reduced-state vector* $\tilde{w}$ instead of the $N \times 1$ *full-state vector* w. The entry $\tilde{w}_k$ captures how many nodes are infected in partition k, which means that we have the relation:

$$\tilde{w}_k = \sum_{i \in \mathcal{N}_k} w_i \quad \text{for each } k = 1, 2, \dots, K \tag{2-3}$$

where $\tilde{w}_k$ is bounded as $0 \leq \tilde{w}_k \leq N_k$. Figure 2-4 shows some graph partitioning examples, and illustrates how these partitions influence the state reduction. The reduced-state vector $\tilde{w}$ contains less information about the disease state; it is a coarser description of the disease state than the full-state w. In other words, one reduced state $\tilde{w}$ can correspond to a number

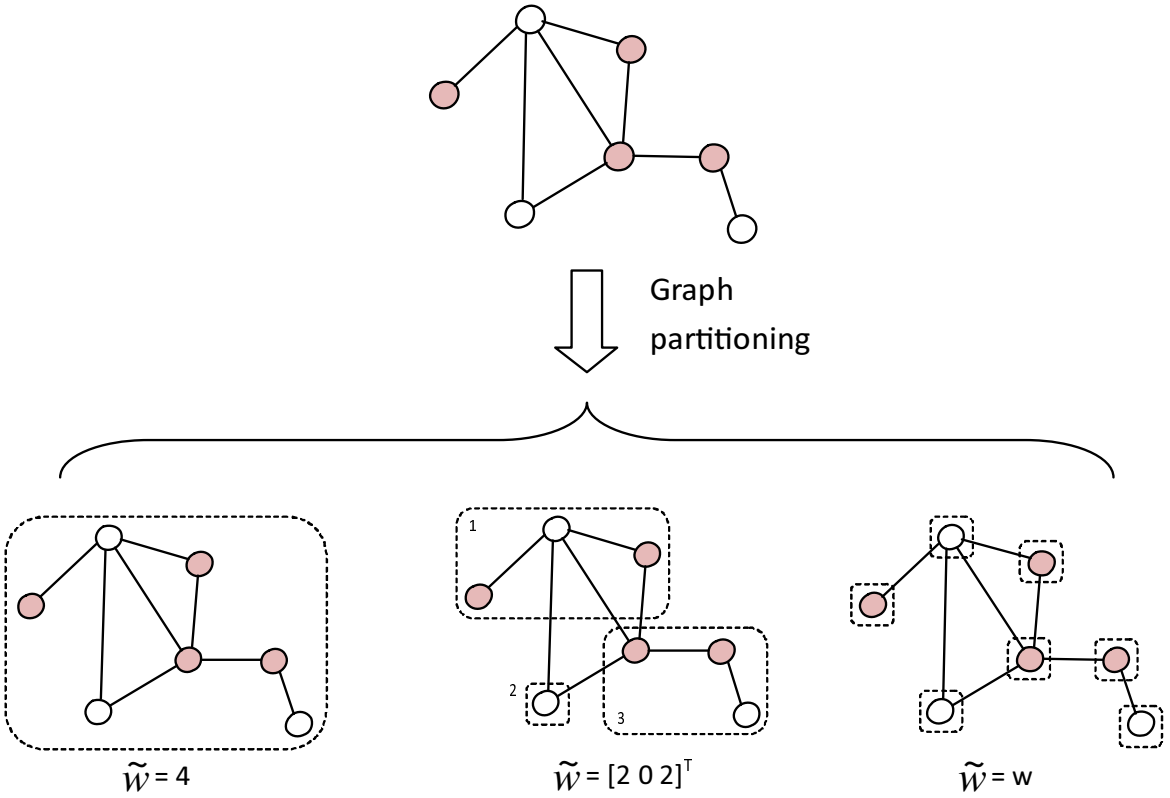

Figure 2-4: UMFF approaches the SIS approximation by grouping nodes according to a graph partitioning. Instead of describing the disease state of each node, i.e. with the full-state vector w, it is then possible to describe the collective disease state of each partition, i.e. the reduced-state vector $\tilde{w}$. In the reduced state description, only the number of infected nodes in a partition is known. In this figure, we show three examples of graph partitioning in 1, 3 and 7 partitions from left to right. As a particular case, the exact SIS case corresponds to the (unique) partitioning with $K = N$ partitions, for which $\tilde{w} = w$. This means that UMFF also describes the exact SIS equations.

of different full states w (see also Appendix A-1-2). A number of additional notations follow from the state reduction, as defined in Table 2-1.

Based on the notion of a reduced state $\tilde{w}$, UMFF is defined as:

Definition 2 (Universal Mean-Field Framework)**.** *Consider a graph $G(\mathcal{N}, \mathcal{L})$, an SIS epidemic process with rates (β, δ) and a partitioning π of the nodes into K partitions. The UMFF equations are approximate equations for $\mathbf{E}[\widetilde{W}]$, the expected number of infected nodes in partition k:*

$$\frac{d\mathbf{E}[\widetilde{W}_k]}{dt} \approx -\delta \mathbf{E}[\widetilde{W}_k] + \beta \sum_{m=1}^{K} \tilde{a}_{km} \left(N_k - \mathbf{E}[\widetilde{W}_k]\right) \mathbf{E}[\widetilde{W}_m] \tag{2-4}$$

The UMFF equations follow from simplifying the exact SIS process description, using two approximations:

	Single node	Partition (π)
Node/Partition indicator	Node $i \in \{0, 1, \ldots, N\}$	Partition $k \in \{0, 1, \ldots, K\}$
Indicator vector	$e_i \in \mathbb{R}^N$ $(e_i)_j = \mathbb{1}_{\{i=j\}}$	$\tilde{e}_k \in \mathbb{R}^K$ $(\tilde{e}_k)_m = \mathbb{1}_{\{k=m\}}$
Partition sum-vector	$s_k \in \mathbb{R}^N$ $(s_k)_i = \mathbb{1}_{\{i \in \mathcal{N}_k\}}$	N.A.
All-one vector	$u = (1, 1, \ldots, 1)^T$	$\tilde{u} = (N_1, N_2, \ldots, N_K)^T$
State vector	$w = (w_1, w_2, \ldots, w_N)^T$ $w_i = \mathbb{1}_{\{\text{node i is infected}\}}$	$\tilde{w} = (\tilde{w}_1, \tilde{w}_2, \ldots, \tilde{w}_k)^T$ $\tilde{w}_k = s_k^T w$
Adjacency matrix	$A \in \mathbb{R}^{N \times N}$ $a_{ij} = \mathbb{1}_{\{(i,j) \in \mathcal{L}\}}$	$\widetilde{A} \in \mathbb{R}^{K \times K}$ $\tilde{a}_{km} = \frac{s_k^T A s_m}{N_k N_m} = \frac{L_{km}}{N_k N_m}$
Submatrix	$A^{(km)}$ $a_{ij}^{(km)} = a_{ij} \mathbb{1}_{\{i \in \mathcal{N}_k \text{ and } j \in \mathcal{N}_m\}}$	$\widetilde{A}^{(km)}$ $\tilde{a}_{ij}^{(km)} = \tilde{a}_{ij} \mathbb{1}_{\{i=k \text{ and } j=m\}}$

Table 2-1: Overview of the node-level and partition-level variables corresponding to a specific partitioning. The symbol $\mathbb{1}$ is the indicator function for which $\mathbb{1}_{\{S\}} = 1$ if statement S is true and zero otherwise.

Approximation 1 (Topological approximation)**.** *The number of infective links between susceptible nodes in partition k and infected nodes in partition m are approximated by:*

$$(u - w)^T A^{(km)} w \approx (\tilde{u} - \tilde{w})^T \widetilde{A}^{(km)} \tilde{w} = \tilde{a}_{km}(N_k - \tilde{w}_k)\tilde{w}_m \tag{2-5}$$

Remark: The relations

$$(u - w)^T A^{(km)} w = \sum_{i=1}^{N} \sum_{j=1}^{N} a_{ij}^{(km)} (1 - w_i) w_j = \sum_{i \sim j} \mathbb{1}_{\{(1 - w_{i \in \mathcal{N}_k}) w_{j \in \mathcal{N}_m}\}}$$

where $\sum_{i \sim j}$ runs over all links $(i, j) \in \mathcal{L}$, show that $(u-w)^T A^{(km)} w$ indeed equals the number of infective links between susceptible nodes in partition k and infected nodes in partition m.

Approximation 2 (Moment-closure approximation)**.** *The covariance between the random variables $\widetilde{W}_k$ and $\widetilde{W}_m$ is approximated by zero:*

$$\text{Cov}[\widetilde{W}_k, \widetilde{W}_m] \approx 0 \Rightarrow \mathbf{E}[\widetilde{W}_k \widetilde{W}_m] \approx \mathbf{E}[\widetilde{W}_k]\mathbf{E}[\widetilde{W}_m] \tag{2-6}$$

In the next section, we show how the UMFF equations are found from the exact SIS process description subject to approximations (2-5) and (2-6). The idea behind the topological approximation is further discussed in Section 2-7, while the moment-closure approximation is addressed in Appendix A-2.

2-5 Derivation of the Universal Mean-Field Framework

Figure 2-5 overviews the variables and approximations involved in UMFF, and how the UMFF equations are derived from the exact SIS equations. Additionally, it shows for which particular

choices of partitioning, UMFF is to equivalent to existing mean-field methods (see also Section 2-6). For $K = N$ partitions, each partition consists of exactly one node.

In the next sections, we follow the variables in Figure 2-5 from left to right to describe the

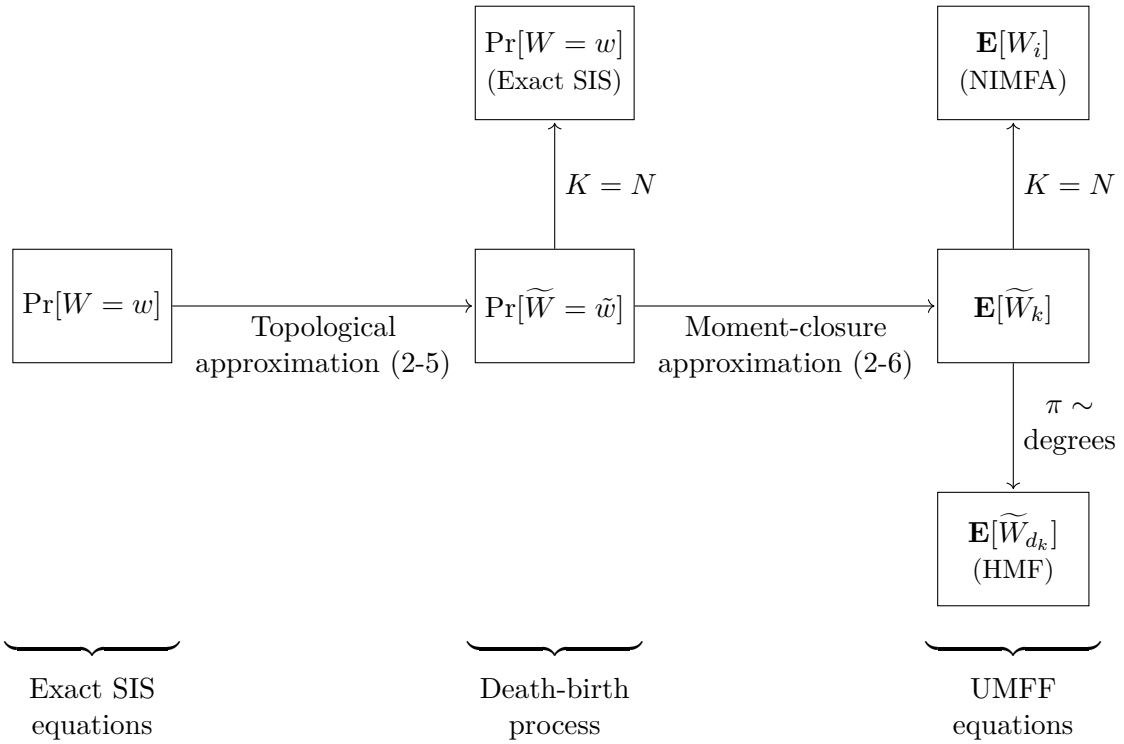

Figure 2-5: Schematic representation of the relationship between the different variables involved in the UMFF approximation steps. Overall, the UMFF description of the SIS process involves three variables: At the **exact SIS equations**-level, the probability of each state w is given by $\Pr[W = w]$. By graph partitioning, the state description changes to the reduced-state vector $\tilde{w}$. With the UMFF topological approximation (2-5), the probability of each reduced state $\Pr[\widetilde{W} = \tilde{w}]$ can be found, which we show to be equal to a **death-birth process**. Then, based on the moment-closure approximation (2-6), the **UMFF equations** for the expected number of infected nodes $\mathbf{E}[\widetilde{W}_k]$ in each partition k can be found. For specific choices of graph partitioning, the UMFF equations lead to existing mean-field methods.

derivation of the UMFF equations.

2-5-1 Exact SIS equations

The UMFF approximation of the SIS process is based on two process variables: the reduced-state probability $\Pr[\widetilde{W}(t) = \tilde{w}]$ for each reduced state $\tilde{w}$, and the expected number of infected nodes $\mathbf{E}[\widetilde{W}_k(t)]$ for each partition k. In Appendix A-1-2, the reduced-state probabilities are

derived as:

$$\begin{aligned}\frac{d\Pr[\widetilde{W}=\tilde{w}]}{dt} =& -\delta\sum_{k=1}^{K}\tilde{w}_k\Pr[\widetilde{W}=\tilde{w}]+\delta\sum_{k=1}^{K}(\tilde{w}_k+1)\Pr[\widetilde{W}=\tilde{w}+\tilde{e}_k]\\ &-\beta\sum_{k=1}^{K}\sum_{m=1}^{K}\sum_{w\in\mathcal{W}^k_{\tilde{w}_k}\cap\mathcal{W}^m_{\tilde{w}_m}}(u-w)^TA^{(km)}w\Pr[W=w]\\ &+\beta\sum_{k=1}^{K}\sum_{m=1}^{K}\sum_{w\in\mathcal{W}^k_{(\tilde{w}_k-1)}\cap\mathcal{W}^m_{\tilde{w}_m}}(u-w)^TA^{(km)}w\Pr[W=w]\end{aligned} \tag{2-7}$$

for any reduced-state vector $\tilde{w}$, where $\mathcal{W}^k_x=\left\{w\in\{0,1\}^N|w^Ts_k=x\right\}$ is the set of all full states w with x infected nodes in partition k.
In Appendix A-1-3, the equations for the expected number of infected nodes is derived as:

$$\frac{d\mathbf{E}[\widetilde{W}_k]}{dt}=-\delta\mathbf{E}[\widetilde{W}_k]+\beta\sum_{m=1}^{K}\sum_{\tilde{w}_k=0}^{N_k}\sum_{\tilde{w}_m=0}^{N_m}\sum_{w\in\mathcal{W}^k_{\tilde{w}_k}\cap\mathcal{W}^m_{\tilde{w}_m}}(u-w)^TA^{(km)}w\Pr[W=w] \tag{2-8}$$

for each partition k.

2-5-2 Death-birth process

By describing the SIS process with the reduced state rather than the full state, also the transition structure changes. Figure 2-6 illustrates this for the case of $K=1$ partition, i.e. $\tilde{w}$ is the number of infected nodes. Since $\tilde{w}$ is an integer between 0 and N_k, and each state transition corresponds to either a node healing or curing, the reduced-state transitions have a path structure. The problem, however, is that the transition rates between the reduced states don't depend on the reduced state only. In Appendix A-1-2 is shown that the rate of the infection transitions $\tilde{w}\to\tilde{w}+\tilde{e}_k$ and $\tilde{w}-\tilde{e}_k\to\tilde{w}$, depends on the number of infective links. The consequence is that equation (2-7) for the reduced-state probability $\Pr[\widetilde{W}=\tilde{w}]$ depends on the full-state probability $\Pr[W=w]$, which means that equations (2-7) are not a closed set of equations.
This closure problem is solved by invoking the UMFF topological approximation (2-5)

$$(u-w)^TA^{(km)}w\approx(\tilde{u}-\tilde{w})^T\widetilde{A}^{(km)}\tilde{w}$$

which enables the simplifications

$$\begin{cases}\displaystyle\sum_{w\in\mathcal{W}^k_{\tilde{w}_k}\cap\mathcal{W}^m_{\tilde{w}_m}}(u-w)^TA^{(km)}w\Pr[W=w]\approx(\tilde{u}-\tilde{w})^T\widetilde{A}^{(km)}\tilde{w}\Pr[\widetilde{W}_k=\tilde{w}_k,\widetilde{W}_m=\tilde{w}_m]\\ \displaystyle\sum_{w\in\mathcal{W}^k_{(\tilde{w}_k-1)}\cap\mathcal{W}^m_{\tilde{w}_m}}(u-w)^TA^{(km)}w\Pr[W=w]\approx(\tilde{u}-(\tilde{w}-\tilde{e}_k))^T\widetilde{A}^{(km)}\tilde{w}\Pr[\widetilde{W}_k=\tilde{w}_k-1,\widetilde{W}_m=\tilde{w}_m]\end{cases} \tag{2-9}$$

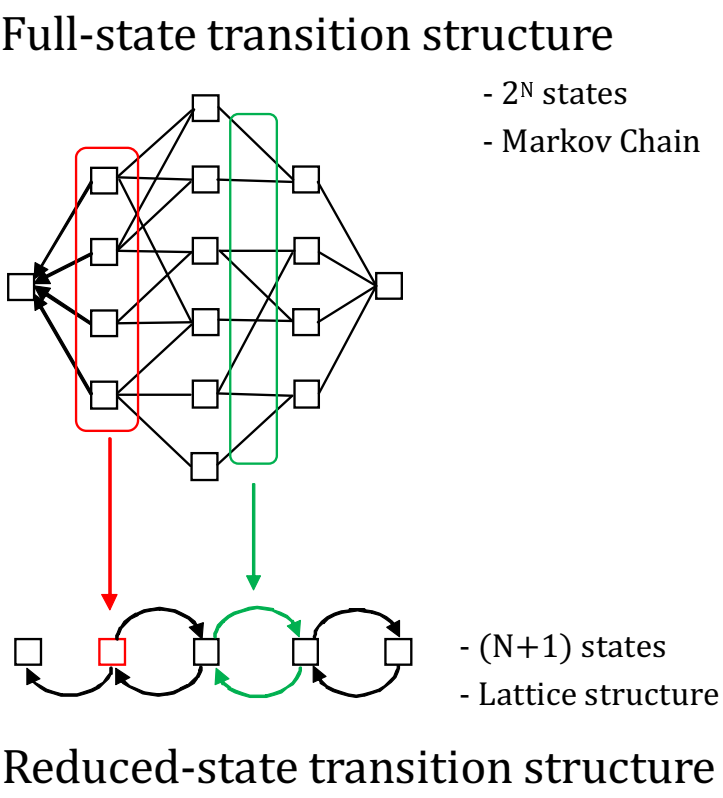

Figure 2-6: A comparison between the full-state transition structure and the reduced-state transition structure for a four-node network and a partitioning with one partition. The state reduction combines all full states with the same number of infected nodes into a single reduced state. Additionally, the reduced-state transition rates are combinations of the full-state transition rates. Appendix A-1-2 describes this reduction in more detail.

to be made in equation (2-7). Filling in (2-9) in the exact equations (2-7) yields:

$$\begin{aligned}\frac{d\Pr[\widetilde{W}=\tilde{w}]}{dt} \approx &-\delta\sum_{k=1}^{K}\tilde{w}_k\Pr[\widetilde{W}=\tilde{w}]+\delta\sum_{k=1}^{K}(\tilde{w}_k+1)\Pr[\widetilde{W}=\tilde{w}+\tilde{e}_k]\\ &-\beta\sum_{k=1}^{K}\sum_{m=1}^{K}(\tilde{u}-\tilde{w})\widetilde{A}^{(km)}\tilde{w}\Pr[\widetilde{W}_k=\tilde{w}_k,\widetilde{W}_m=\tilde{w}_m]\\ &+\beta\sum_{k=1}^{K}\sum_{m=1}^{K}(\tilde{u}-(\tilde{w}-\tilde{e}_k))\widetilde{A}^{(km)}\tilde{w}\Pr[\widetilde{W}_k=\tilde{w}_k-1,\widetilde{W}_m=\tilde{w}_m]\end{aligned} \tag{2-10}$$

which no longer depends on the full-state probability $\Pr[W=w]$. While equation (2-10) has a cumbersome form, it is a closed set of equations that completely characterizes $\Pr[\tilde{W}(t)=\tilde{w}]$ for a given initial distribution $\Pr[\tilde{W}(0)=\tilde{w}]$.

As Figure 2-6 already illustrates, the reduced state transitions have a particular structure. For the $K=1$ partitioning, the transition structure is a path, since for the number of infected nodes $\tilde{w}$ the transitions $\tilde{w}\to\tilde{w}\pm1$ and $\tilde{w}\pm1\to\tilde{w}$ exist. For any other partitioning, the possible transitions are still always of the form $\tilde{w}\to\tilde{w}\pm\tilde{e}_k$ and $\tilde{w}\pm\tilde{e}_k\to\tilde{w}$, since only single nodes are infected or cured during one event. In other words, $\tilde{w}$ can be seen

as a coordinate in an $(N_1 + 1) \times (N_2 + 1) \times \cdots \times (N_K + 1)$ lattice. As a result, equation (2-10) is equivalent to the description of a K-dimensional death-birth process on this lattice. Furthermore, equation (2-10) indicates that the birth rates are quadratic in $\tilde{w}$ and the death rates are linear in $\tilde{w}$, which means that the SIS process is equivalent to a higher-dimensional quadratic death-birth process. While no analytical solutions exist for the quadratic death-birth process [26], the equivalence between the SIS and the quadratic death-birth process is an interesting observation. It means that insights in one setting translate directly to the other (see also Section 2-10).

2-5-3 UMFF equations

The exact equations (2-8) for the expected number of infected nodes $\mathbf{E}[\widetilde{W}_k]$ are not "closed" for two reasons: the exact SIS dynamics depend on the number of infective links (i.e. on full-state probability $\Pr[W = w]$) and on higher-order moments, i.e. the first-order moment equations (2-8) depend on the second-order moments $\mathbf{E}[\widetilde{W}_k\widetilde{W}_m]$ (see also Appendix A-2). Similar to the derivation of the death-birth process, invoking the UMFF topological approximation (2-5) results in simplifications (2-9), which allows equation (2-8) to be approximated by:

$$\frac{d\mathbf{E}[\widetilde{W}_k]}{dt} = -\delta\mathbf{E}[\widetilde{W}_k] + \beta \sum_{m=1}^{K} \sum_{\tilde{w}_k=0}^{N_k} \sum_{\tilde{w}_m=0}^{N_m} (\tilde{u} - \tilde{w})^T \tilde{A}^{(km)} \tilde{w} \Pr[\widetilde{W}_k = \tilde{w}_k, \widetilde{W}_m = \tilde{w}_m] \tag{2-11}$$

While the dependence on the full-state probability $\Pr[W = w]$ is solved in equation (2-11), it still contains higher-order moment terms:

$$\sum_{\tilde{w}_k=0}^{N_k} \sum_{\tilde{w_m}=0}^{N_m} \tilde{w}_k\tilde{w}_m \Pr[\widetilde{W}_k = \tilde{w}_k, \widetilde{W}_m = \tilde{w}_m] = \mathbf{E}[\widetilde{W}_k\widetilde{W}_m] \tag{2-12}$$

for partition pairs (k, m). In general, these second-order moments $\mathbf{E}[\widetilde{W}_k\widetilde{W}_m]$ cannot be determined from $\mathbf{E}[\widetilde{W}_k]$ and $\mathbf{E}[\widetilde{W}_m]$ alone. Invoking the UMFF moment-closure approximation (2-6)

$$\mathrm{Cov}[\widetilde{W}_k, \widetilde{W}_m] \approx 0 \Rightarrow \mathbf{E}[\widetilde{W}_k\widetilde{W}_m] \approx \mathbf{E}[\widetilde{W}_k]\mathbf{E}[\widetilde{W}_m]$$

solves this closure problem by enabling equation (2-11) to be approximated by

$$\frac{d\mathbf{E}[\widetilde{W}_k]}{dt} \approx -\delta\mathbf{E}[\widetilde{W}_k] + \beta \sum_{m=1}^{K} \tilde{a}_{km}(N_k - \mathbf{E}[\widetilde{W}_k])\mathbf{E}[\widetilde{W}_m]$$

which are the UMFF equations (2-4).
In Appendix A-2, an extension of the UMFF equations for higher-order moments is described. These higher-order equations are more general, but a detailed description is not the focus of this article.

Bounds on the moment-closure approximation

For the particular case of $K = N$ partitions (for which UMFF is equivalent to NIMFA, see Section 2-6), the infection probabilities of nodes are non-negatively correlated [27], i.e. $\mathrm{Cov}[\widetilde{W}_k, \widetilde{W}_m] \geq 0$. Based on the definition of the covariance

$$\mathrm{Cov}[\widetilde{W}_k, \widetilde{W}_m] = \mathbf{E}[\widetilde{W}_k\widetilde{W}_m] - \mathbf{E}[\widetilde{W}_k]\mathbf{E}[\widetilde{W}_m] \tag{2-13}$$

we can rewrite the exact equation (2-11) as:

$$\frac{d\mathbf{E}[\widetilde{W}_k]}{dt} = -\delta\mathbf{E}[\widetilde{W}_k] + \beta \sum_{m=1}^{K} \tilde{a}_{km}(N_k - \mathbf{E}[\widetilde{W}_k])\mathbf{E}[\widetilde{W}_m] - \beta \sum_{m=1}^{N} \tilde{a}_{km} \operatorname{Cov}[\widetilde{W}_k, \widetilde{W}_m] \tag{2-14}$$

Omitting the negative term $-\tilde{a}_{km} \operatorname{Cov}[\widetilde{W}_k, \widetilde{W}_m]$ in equation (2-14) implies that for $K = N$ partitions, the moment-closure approximation is an upper-bound of the true process. However, for any other partitioning ($K \neq N$) we do not know about any such results for $\operatorname{Cov}[\widetilde{W}_k, \widetilde{W}_m]$. In other words, we do not know how to bound the UMFF moment-closure approximation error.

2-6 Existing mean-field methods contained by UMFF

An important feature of UMFF is that by particular choices of graph partitioning, the UMFF equations are equivalent to existing mean-field methods. In particular, the widely-used N-Intertwined Mean-Field Approximation [11] and Heterogeneous Mean-Field approximation [10] are contained by UMFF. Additionally, by the higher-order extension of UMFF described in Appendix A-2, also second-order NIMFA [27] and pair Quenched Mean-Field theory [14] are contained by (higher-order) UMFF.

2-6-1 N-Intertwined Mean-Field Approximation (NIMFA)

The N-Intertwined Mean-Field Approximation [11] incorporates the full topological information of the graph in its system of equations. The only approximation consists of assuming independence between the infection states of adjacent nodes. Denoting the infection probability of node k by $\rho_k = \Pr[W_k = 1]$, the NIMFA equations for $1 \leq k \leq N$ are given by [11]:

$$\frac{d\rho_k}{dt} = -\delta\rho_k + \sum_{m=1}^{N} \beta a_{km}(1 - \rho_k)\rho_m, \tag{2-15}$$

The same NIMFA equations (2-15) are retrieved from UMFF with $K = N$ partitions, which corresponds to each node being in a separate partition. The expected number of infected nodes in a partition $\mathbf{E}[\widetilde{W}_k]$ is then equal to the infection probability ρ_k of node k that makes up that partition. For this partitioning, we have $N_k = 1$ and $\widetilde{A} = A$, illustrating that the NIMFA equations (2-15) are indeed a particular case of the UMFF equations (2-4).

2-6-2 Heterogeneous mean-field method (HMF)

Pastor-Satorras and Vespignani [10] introduced the Heterogeneous Mean-Field method, which approximates the SIS process based on the assumption that all nodes of a certain degree are equivalent (in their connections with other nodes). Consequently, the SIS process is described based on the degree distribution of the underlying graph.
Different from UMFF and NIMFA, HMF [10] does not assume a known graph G, but rather considers a class of graphs. Specifically, in HMF the epidemic is assumed to take place on a graph with a specified degree distribution and with the link probability between pairs of

nodes independent of their degrees. For each degree $d_1 \leq d_k \leq d_K$, the probability distribution $\Pr[D = d_k]$ denotes the probability that a randomly chosen node has degree d_k. The variable $0 \leq \tilde{\rho}_k \leq 1$ reflects the expected fraction of infected nodes with degree d_k:

$$\frac{d\tilde{\rho}_k}{dt} = -\delta\tilde{\rho}_k + \beta k(1-\tilde{\rho}_k)\Theta \tag{2-16}$$

where Θ is the probability that a healthy node is linked to an infected node. The value of Θ is calculated in [10], based on the connection probability of nodes of degree d_k to infected nodes in the rest of the network, as:

$$\Theta = \sum_{m=1}^{K} \tilde{\rho}_m \frac{d_m \Pr[D = d_m]}{\sum_{i=1}^{K} d_i \Pr[D = d_i]} \tag{2-17}$$

Substituting expression (2-17) for Θ in (2-16) gives:

$$\frac{d\tilde{\rho}_k}{dt} = -\delta\tilde{\rho}_k + \beta \sum_{m=1}^{K} \frac{d_k d_m \Pr[D = d_m]}{\sum_{i=1}^{K} d_i \Pr[D = d_i]}(1-\tilde{\rho}_k)\tilde{\rho}_m \tag{2-18}$$

Introducing the variable $\rho_k = \Pr[D = d_k]\tilde{\rho}_k$ then yields:

$$\frac{d\rho_k}{dt} = -\delta\rho_k + \beta \sum_{m=1}^{K} \frac{d_k d_m}{\sum_{i=1}^{K} d_i \Pr[D = d_i]} \left(\Pr[D = d_k] - \rho_k\right) \rho_m \tag{2-19}$$

While the above equations (2-19) are derived in HMF for a probabilistic graph, the same equations are found from UMFF for a particular graph with the same degree distribution, namely $N_k = c \Pr[D = d_k]$ nodes of degree d_k for some scalar $c \in \mathbb{R}$, and degree-uncorrelated links. For such a graph, the number of links $L_{km} = s_k^T A s_m$ between nodes of degree d_k and degree d_m obeys the consistency relation $\sum_{m=1}^{K} L_{km} = N_k d_k$ as:

$$L_{km} = \frac{d_k d_m N_k N_m}{\sum_{i=1}^{K} d_i N_i},$$

from which the UMFF equations follow as:

$$\frac{d\mathbf{E}[\widetilde{W}_k]}{dt} = -\delta\mathbf{E}[\widetilde{W}_k] + \beta \sum_{m=1}^{K} \frac{d_k d_m}{\sum_{i=1}^{K} d_i N_i} \left(N_k - \mathbf{E}[\widetilde{W}_k]\right) \mathbf{E}[\widetilde{W}_m] \tag{2-20}$$

Equations (2-20) are equivalent to (2-19) for the scaling $\mathbf{E}[\widetilde{W}_k] = c\rho$, where c is the same scalar relating N_k to $\Pr[D = d_k]$. Hence, the HMF equations are found from the UMFF framework by considering a specific graph realization consistent with the random graph properties assumed by HMF.
Since HMF is a particular case of UMFF, HMF implicitly uses the UMFF moment-closure approximation (2-6) with respect to the partitioning according to node degree. As discussed in Section 2-5-3, this means that we do not know whether the HMF equations give an upper-bound or a lower-bound on the infection probabilities, or how they relate to the exact SIS process in general.

Boguñá and Pastor-Satorras [24] extend the HMF model to random graphs with correlated

degrees. Instead of only assuming $\Pr[D = d_k]$, also the probability $\Pr[i \sim j | i \in \mathcal{N}_k, j \in \mathcal{N}_m]$ that a node i of degree d_k links with a node j of degree d_m is assumed to be known for any pair of degrees (d_k, d_m). With these extra assumptions in the HMF methodology, the SIS process is then approximately described based on the degree distribution and the linking probabilities. If we now consider a specific graph realization with $N_k = c_1 \Pr[D = d_K]$ nodes of degree d_k and with $L_{km} = c_2 \Pr[i \sim j | i \in \mathcal{N}_k, j \in \mathcal{N}_m]$ links between nodes with degree d_k and d_m (for some scalars $c_1, c_2 \in \mathbb{R}$), then again the UMFF equations (2-4) are equivalent to the correlated HMF equations.
In the same way that the HMF equations are fully determined by the degree distribution and the linking probabilities, also the UMFF equations are fully determined by N_k and L_{km}. A consequence of the equivalence between UMFF (2-4) and (correlated) HMF (2-19), is that we can bound the topological approximation errors of HMF (with respect to a specific realization of the probabilistic graph model).

Since the partitions $\mathcal{N}_k$ do not need to correspond to node degrees specifically, UMFF enables the SIS dynamics to be described for a wider range of graph classes. For any graph model, where a probability distribution $\Pr[K = k]$ of a graph belonging to partition $\mathcal{N}_k$ is given, together with a linking probability $\Pr[i \sim j | i \in \mathcal{N}_k, j \in \mathcal{N}_m]$, the UMFF equations can be directly found. Such graph models are more general than graphs with degree-based partitions only and, in some settings, specific structure in the graph might suggest a natural way to partition the nodes such that grouped nodes have a similar connectivity to the rest of the network (see also further directions in Section 2-10).

2-6-3 Second-order NIMFA and Pair Quenched Mean-Field theory

Apart from containing NIMFA and HMF, the extension to higher-order UMFF (Appendix A-2) allows to unify the higher-order mean-field approximations. Both in [28] and [14], second-order mean-field equations are derived as an extended version of NIMFA and Quenched Mean-Field theory (QMF) [29]. These sNIMFA and pQMF equations approximate the SIS process by second-order and first-order moments, instead of first-order moments only for NIMFA and QMF.
With $K = N$ partitions, order $n = 2$ and the corresponding moment-closure function f in Equation (A-16), the higher-order UMFF equations contain second-order NIMFA [28] and pair QMF [14].

2-7 The *Isoperimetric Problem* in SIS epidemics

In this section, we focus on the UMFF topological approximation:

$$(u - w)^T A^{(km)} w \approx (\tilde{u} - \tilde{w})^T \tilde{A}^{(km)} \tilde{w}$$

We first describe how the closure problem of equations (2-7) and (2-8) can be related to the isoperimetric problem. Then, we show how this analogy leads to approximation (2-5) and bounds on the approximation error.

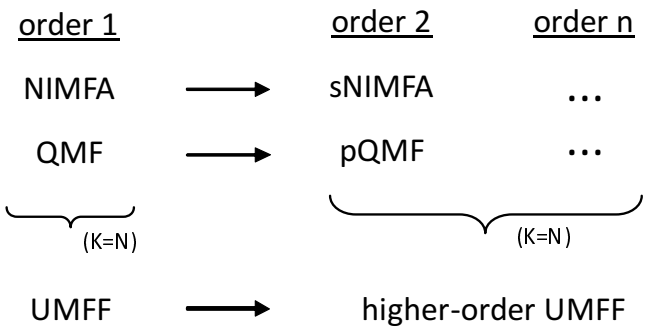

Figure 2-7: Higher-order UMFF extends the UMFF equations in the first-order moments $\mathbf{E}[\widetilde{W}_k]$ to equations in higher order moments $\mathbf{E}[\widetilde{W}_k \dots \widetilde{W}_m]$. As such, higher-order UMFF contains second-order NIMFA [28] and pair QMF [14], for $K = N$ partitions, order $n = 2$ and the appropriate moment-closure approximation.

2-7-1 The isoperimetric problem

The isoperimetric problem is an ancient problem that has interested many mathematicians throughout history. For the most basic form of the isoperimetric problem, we cite Blåsjö [20], who provides a broad historical and conceptual overview of the isoperimetric problem:

Problem 1 (The isoperimetric problem)**.** *Among all figures in the plane with a given perimeter P, which one encloses the greatest area A?*

Theorem 1 (The isoperimetric theorem)**.** *The solution to the isoperimetric problem is the circle of perimeter P.*

Theorem 2 (The isoperimetric inequality)**.** *For all figures with a given perimeter P and area A, it holds that $P^2 - 4\pi A \geq 0$ and equality only occurs for the circle.*

While the isoperimetric problem might seem simple, and its solution intuitive, it took until the 20'th century to rigorously prove the isoperimetric theorem. After the extensive historical study of the isoperimetric problem in the 2D plane, similar problems were studied in different geometric contexts. The basic interest in these problems always consisted of describing the relationship between the *volume* and *surface* of a certain object, leading to isoperimetric inequalities of the form:

$$\theta_{\min} \leq f(\text{volume}) + g(\text{surface}) \leq \theta_{\max} \tag{2-21}$$

For instance, Osserman [21] describes isoperimetric inequalities in higher dimensions, on curved surfaces and on general Riemannian manifolds. The geometric context of interest for UMFF, is the study of the isoperimetric problem on graphs (see for instance [30]).

2-7-2 Infective links and infected nodes: an isoperimetric analogy

The dynamics of SIS epidemics are governed by two processes: infected are cured and infection takes place on infective links, i.e. the links between healthy and infected nodes. *The*

curing process is proportional to the number of infected nodes while the infection process is proportional to the number of infective links. In a non-technical way we can associate the number of infected nodes to a volume on the graph, while the infective links accord to a surface or interface around the infected volume. *The curing process is then proportional to the infected volume while the infection process is proportional to the infective surface.* This relation is illustrated in Figure 2-8, which represents a specific disease state on a toy-network. To use the concepts of volume and surface in a more technical way in the context of graphs,

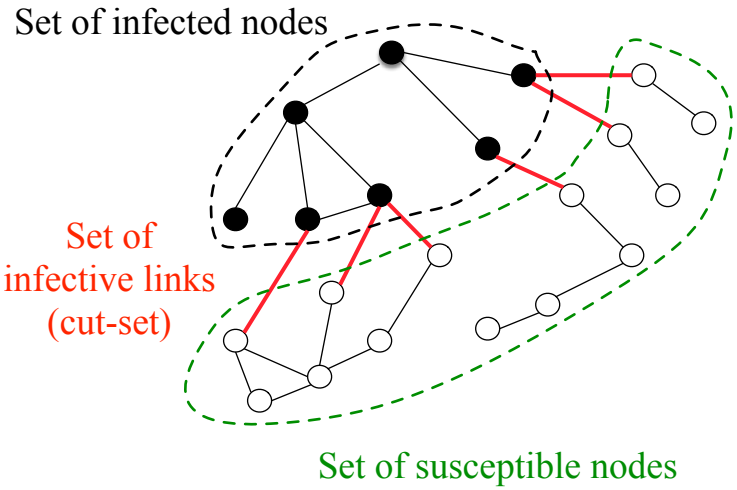

Figure 2-8: Example of a disease state in a toy network. The infected and healthy nodes make up two separate partitions in the network, with the cut-set between them determining the set of infective links. These two partitions can also be seen as volumes on the graph, and the cut-set between them as a surface.

we define a set of one node to have unit volume, and a set of one link to have unit surface. Other choices are possible, e.g. the volume of a node being proportional to its degree, but for the purpose of deriving and bounding the UMFF topological approximation (2-5), this would be a less natural choice.

In the derivation of the exact reduced-state Kolmogorov equations (2-7), the transition rate between reduced states depends on the number of infective links. As a result, the exact equations (2-7) for $\Pr[\widetilde{W} = \tilde{w}]$ and (2-8) for $\mathbf{E}[\widetilde{W}]$ are not closed. In particular, these equations contain terms of the form $(u-w)^T A^{(km)} w \Pr[W = w]$. In the language of the isoperimetric problem, this *closure problem* translates to the volume equations (2-7) and (2-8) containing terms related to the surface.

The UMFF topological approximation (2-5) replaces the surface term by a function of volume terms and thus solves the closure problem. Now, by analogy with the isoperimetric problem, we can bound the approximation error caused by this replacement, as shown in Figure 2-9, where ϵ represents the introduced error. It remains to find the correct translation of the isoperimetric inequality into the setting of SIS epidemics, such that the isoperimetric bounds translate to bounds on the UMFF approximation. The UMFF topological approximation is defined as (2-5):

$$(u-w)^T A^{(km)} w \approx (\tilde{u}-\tilde{w})^T \widetilde{A}^{(km)} \tilde{w}$$

which we can rewrite by introducing an error term $\epsilon \in \mathbb{R}$ as:

$$(u-w)^T A^{(km)} w = (\tilde{u}-\tilde{w})^T \widetilde{A}^{(km)} \tilde{w} + \epsilon \tag{2-22}$$

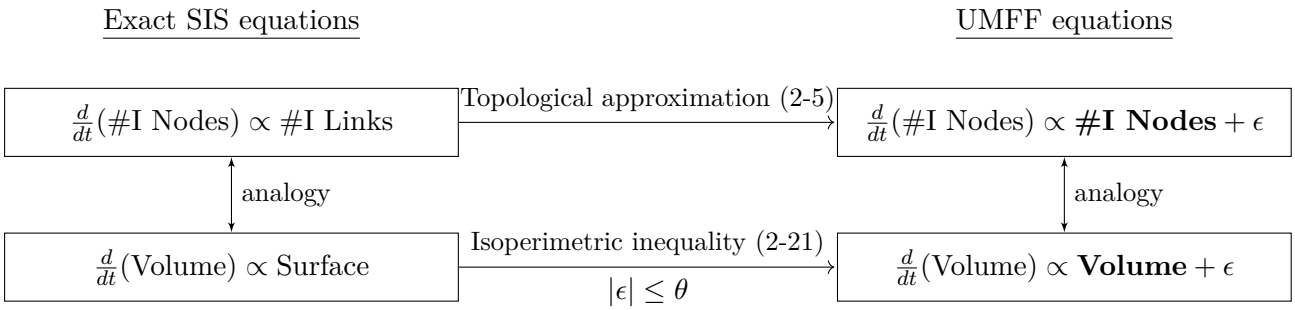

Figure 2-9: Conceptual diagram of how the UMFF topological approximation (2-5) fits into the context of the isoperimetric problem and the isoperimetric inequality (2-21). As a result of the analogy, the UMFF approximation ϵ can be bounded.

or, by upper-bounding the error term $|\epsilon| \leq \theta$, as:

$$\left|(u-w)^T A^{(km)} w - (\tilde{u}-\tilde{w})^T \widetilde{A}^{(km)} \tilde{w}\right| \leq \theta \tag{2-23}$$

In the next subsection, we specify the error bound θ based on the isoperimetric inequalities on graphs. Figure 2-10 is another illustration of how the isoperimetric inequality leads to bounds on the UMFF topological approximation. In the plane, any perimeter P corresponds to a bounded range of areas $A \in [A_{min}, A_{max}]$ it can enclose. Hence, for a certain range of P, this leads to a *feasibility region* of possible (A, P) pairs. Similarly, for any graph G, a feasibility region of possible $\left(u^T w, (u-w)^T A w\right)$ or $(\tilde{w}, (u-w)^T A w)$ exists based on the isoperimetric inequality on graphs. A similar notion of feasibility regions is developed by Agaskar and Lu [31], but for different definitions of volume and surface and applied in the context of an "uncertainty principle" for signals on graphs. More than just providing an error bound, the analogy with the isoperimetric problem and the mathematical techniques used in the proofs (see Appendix A-3) also provide a motivation for the specific form of the UMFF topological approximation (2-5).

2-7-3 Isoperimetric inequalities for the number of infective links

The bound for the approximation error is based on the isoperimetric and discrepancy inequalities of Chung [30]:

Theorem 3 (General-graph isoperimetric inequality)**.** *For a graph $G(\mathcal{N}, \mathcal{L})$ and a partitioning π, the error of the UMFF topological approximation* (2-5) *between any two partitions k and m is bounded as:*

$$\left|(u-w)^T A^{(km)} w - (\tilde{u}-\tilde{w})^T \widetilde{A}^{(km)} \tilde{w}\right| \leq \frac{\theta}{N} \sqrt{\tilde{w}_m (N-\tilde{w})(N_k - \tilde{w}_k)(N-(N_k-\tilde{w}_k))} \tag{2-24}$$

where $|\tilde{a}_{km} - \mu_i| \leq \theta$ holds for $1 \leq i < N$, with μ_i the eigenvalues of the Laplacian matrix based on $A^{(km)}$.

For bi-regular graphs $A^{(km)}$, meaning that $A^{(km)} s_m = c_1 s_m$ and $s_k^T A^{(km)} = c_2 s_k^T$ for some constants $c_1, c_2 \in \mathbb{R}$, a tighter bound can be given based on interlacing techniques of Haemers [32]:

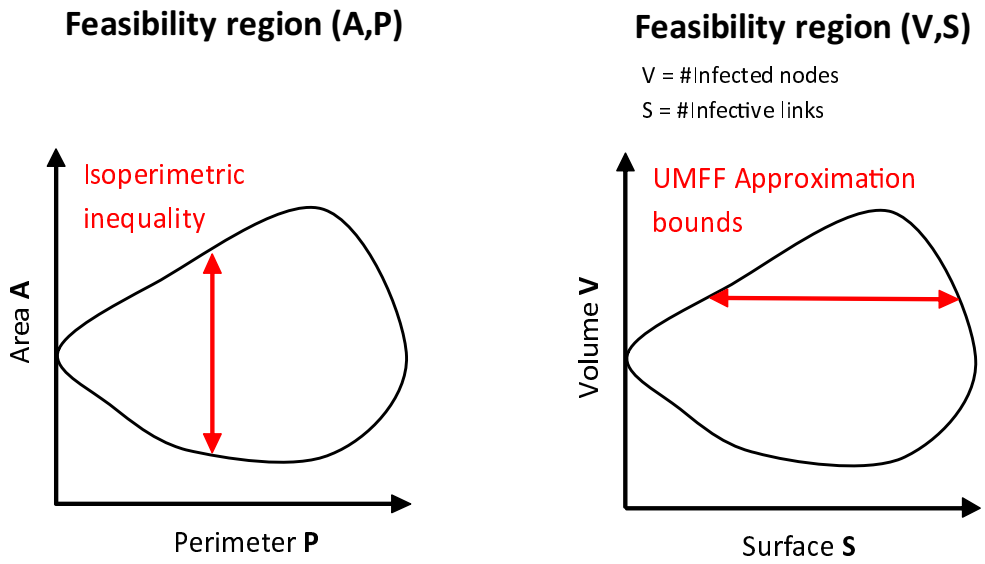

Figure 2-10: In general, isoperimetric inequalities specify restrictions on the combinations of volume (V) and surface (S) any shape can have in a certain geometric context. As a result, a *feasibility region* of possible (V, S) combinations is defined in that geometry. The UMFF topological approximation (2-5) is related to this concept, in that a volume term is approximated by a surface term. Hence, the (V, S) feasibility region on graphs allows to determine for a certain volume V what the error bounds are if we approximate the real surface S with an approximation $S^\star(V)$, i.e. $|S - S^\star(V)|$.

Theorem 4 (Bi-regular-graph isoperimetric inequality)**.** *For a graph $G(\mathcal{N}, \mathcal{L})$ and a partitioning π such that $A^{(km)}$ is bi-regular for some partitions k and m, the error of the UMFF topological approximation* (2-5) *is bounded as:*

$$\left|(u-w)^T A^{(km)} w - (\tilde{u}-\tilde{w})^T \tilde{A}^{(km)} \tilde{w}\right| \leq \frac{\lambda_2}{N} \sqrt{\tilde{w}_k (N_k - \tilde{w}_k) \tilde{w}_m (N_m - \tilde{w}_m)} \tag{2-25}$$

where λ_2 is the second-largest eigenvalue of $A^{(km)}$.

The proofs of Theorem 3 and Theorem 4 are given in appendix A-3 and rely heavily on proofs given by Chung [30] and Haemers [32].

2-8 UMFF and Szemerédi's regularity lemma

The isoperimetric problem is a well-studied mathematical problem that appears in many different fields, including graph theory and network science, and thus provides a conceptual link between those fields. For instance Szemerédi's regularity lemma (SRL) is a lemma with interesting implications for UMFF, which follows from the relation of both UMFF and SRL with the isoperimetric problem. We will discuss how SRL may indicate for which graphs the UMFF topological approximation (2-5) is expected to be accurate, and for which the SIS dynamics are thus well approximated by the UMFF equations.

Szemerédi's regularity lemma

The following definitions and interpretations are based on Diestel's [33] description of SRL. We start by defining a so-called regularity condition between pairs of partitions, which is related to the isoperimetric inequality.

Definition 3 (ϵ-regular partition pair)**.** *[33] Consider a graph $G(\mathcal{N}, \mathcal{L})$ and two disjoint node partitions $\mathcal{N}_k, \mathcal{N}_m \subseteq \mathcal{N}$. If for any pair of subsets $\mathcal{N}_x \subseteq \mathcal{N}_k$ and $\mathcal{N}_y \subseteq \mathcal{N}_m$ of size N_x and N_y with $N_x \geq \epsilon N_k$ and $N_y \geq \epsilon N_m$ for some real $\epsilon > 0$, the inequality*

$$\left| \frac{(u - s_x)^T A^{(km)} s_y}{N_x N_y} - \frac{s_k^T A^{(km)} s_m}{N_k N_m} \right| \leq \epsilon \tag{2-26}$$

holds, then we say that the partition pair (k, m) is ϵ-regular.

Inequality (2-26) can be rewritten as

$$\left| (u - s_x)^T A^{(km)} s_y - \frac{L_{km}}{N_k N_m} N_x N_y \right| \leq \epsilon N_x N_y \tag{2-27}$$

which shows that the regularity condition (2-26) is related to the difference between the size of the cut-set $(u - s_x)^T A^{(km)} s_y$ (for all subsets of partitions k, m with N_x, N_y nodes, respectively) and the approximate size of the cut-set: $\frac{L_{km}}{N_k N_m} N_x N_y$. For lower values of ϵ, the regularity condition becomes stronger. Firstly, because the true size of the cut-set can deviate less from the approximate cut-set size if ϵ is smaller, and secondly because the regularity condition must hold for a larger range of subsets $(\mathcal{N}_x, \mathcal{N}_y)$, since $N_x \geq \epsilon N_k$ is a less stringent condition if ϵ is lower (and similarly for $\mathcal{N}_y$).
Based on the notion of ϵ-regular partition pairs, we define a regularity condition on a partitioning π of a graph:

Definition 4 (ϵ-regular graph partitioning)**.** *[33] Consider a graph $G(\mathcal{N}, \mathcal{L})$ with a partitioning π of the nodes into $K+1$ partitions $\{\mathcal{N}_0, \mathcal{N}_1, \ldots, \mathcal{N}_K\}$. Such a graph partitioning is called ϵ-regular if it meets the following conditions:*

(i) $N_0 \leq \epsilon N$

(ii) $N_1 = N_2 = \cdots = N_K$

(iii) All except at most ϵK^2 of the partition pairs (k,m) for $1 \leq k < m \leq K$ are ϵ-regular

Roughly speaking, a graph partitioning is ϵ-regular if it contains K equally sized partitions (ii) such that most partition pairs are regular (iii), where one additional "small" partition is allowed to exist (i) on which conditions (ii) and (iii) do not apply. For a given K, a smaller ϵ strengthens the regularity conditions. Firstly, because the regularity condition between partition pairs becomes stronger, secondly, because $N_0 \leq \epsilon N$ means that a lower number of nodes are allowed to make up the "leftover partition" $\mathcal{N}_0$ and, finally, because ϵK^2 becomes smaller, implying that an increasing proportion of the partition pairs need to satisfy the regularity condition (2-26). Since condition (iii) holds for partition pairs (k, m) with $k \neq m$, the regularity conditions only applies to links between partitions and not within partitions.
Based on the regularity notion of a graph partitioning, Szemerédi's regularity lemma is a statement about the existence of finding a regular partitioning in arbitrary graphs, with a number K of partitions effectively independent of the size N of the graph.

Definition 5 (Szemerédi's regularity lemma)**.** *[33] For every $\epsilon > 0$ and every integer $K_{min} \geq 1$, there exists an integer K_{max} such that every graph on $N \geq K_{min}$ nodes admits an ϵ-regular graph partitioning in K partitions, with $K_{min} \leq K \leq K_{max}$.*

The proof of SRL can be found in Diestel [33]. We exemplify the lemma: if we take a certain ϵ and choose $K_{min} = 10$, then SRL states that there is an integer K_{max}, such that for any graph with $N > 10$ nodes there exists an ϵ-regular partitioning of $10 \leq K \leq K_{max}$ partitions. While for $N \leq K_{max}$, the existence of an ϵ-regular partitioning automatically holds by choosing the $K = N$ partitioning, the result becomes stronger for $N > K_{max}$. For very large graphs, i.e. $N \gg K_{max} \geq K$, it is still always possible to have an ϵ-regular K-partitioning.
An interesting interpretation of SRL is given by Tao [34] who states that, roughly speaking: "SRL can be viewed as a structure theorem for large dense graphs, approximating such graphs to any specified accuracy by objects whose complexity is bounded independently of the number of nodes in the original graph". Applied to UMFF, this means that, for any large dense graph and any desired accuracy ϵ, there exists a partitioning in $K \ll N$ partitions, such that the topological approximation of UMFF between most (k, m) partition pairs ($k \neq m$) is ϵ-accurate, in the sense that (k, m) are ϵ-regular partition pairs. While a regular graph partitioning does not imply any regularity conditions on the within-partition links, Diestel [33] mentions that by choosing K_{min} large "we may increase the proportion of links running between different partition sets (rather than inside one), i.e. the proportion of links that are subject to the regularity assertion". In other words, if we take K_{min} large enough for a given ϵ, then most links will be *between* partitions (rather than *within*) and will thus satisfy the regularity conditions.

Implications of SRL for UMFF

We believe that SRL can be translated to a statement about the scaling behavior of the SIS process on large graphs. We will describe the conceptual idea here, realizing that a more rigorous investigation would be necessary to proof any of the claims.
Since the regularity inequality (2-26) can be rewritten as (2-27), which has the same form as the isoperimetric inequality, the ϵ-regularity of a partition pair also implies that the UMFF topological approximation (2-5) has an ϵ-bounded approximation error (for subsets of sufficiently large size). For an ϵ-regular graph partitioning with $K + 1$ pairs, this isoperimetric interpretation then means that for most of the partition pairs ($\geq \epsilon K^2$) the UMFF topological approximation error is ϵ-bounded. Finally, SRL indicates that for any chosen accuracy ϵ and sufficiently large minimum number of partitions K_{min}, an integer K_{max} exists such that for any graph on $N \geq K_{min}$ nodes, a partitioning can be found with $K_{min} \leq K \leq K_{max}$ partitions, such that most links are between partitions and most of the partition pairs have ϵ-bounded approximation errors. Applied to UMFF, this means that *for large graphs on N nodes, a partitioning in $K_{min} < K \ll N$ partitions can always be found such that the UMFF topological approximation between most partition pairs is bounded by a chosen ϵ, where choosing a large enough K_{min} results in most links being between partitions* (by Diestel's argument). The UMFF approximation being ϵ-bounded on a large graph implies that the dynamics of the SIS process on that graph can approximately be described by the dynamics on a much smaller, weighted graph of dimension $K \ll N$.
Remark: The regularity of SRL only holds for subsets of size $N_x \geq \epsilon N_k$, where $N_k \approx \frac{N}{K}$.

Hence, the regularity weakens for growing N, because it no longer holds for cut-sets between small subsets. The consequence for UMFF is that the regularity, and thus the boundedness of the topological approximation error, only holds, if a sufficiently large fraction of nodes is infected in both partitions, i.e. N_x infected nodes in $\mathcal{N}_k$ and N_y in $\mathcal{N}_m$ for any (k, m). Thus, the dynamics are well approximated by lower-dimensional dynamics, only for disease states where enough nodes are infected between any pair of partitions.

2-9 Related work

NIMFA on graphs with an equitable partitioning

Bonaccorsi et al. [35] study the NIMFA equations on graphs with an equitable partitioning. A partitioning π is equitable if the subgraph between any two (possibly the same) partitions, is bi-regular (regular). If a graph has such an equitable partitioning, and the initial infection probability is the same for all nodes within one partition, then the NIMFA equations for the SIS process on that graph can be exactly described by K rather than N equations [35]. This result follows from the observation that equality in the UMFF topological approximation (2-5) holds, i.e.

$$(u - w)^T A^{(km)} w = (\tilde{u} - \tilde{w})^T \widetilde{A}^{(km)} \tilde{w} = \tilde{a}_{km}(N_k - \tilde{w}_k)\tilde{w}_m$$

when $A^{(km)}$ is bi-regular, and that

$$\Pr[W(0) = w] = \left|\mathcal{W}^k_{\tilde{w}_k} \cap \mathcal{W}^m_{\tilde{w}_m}\right|^{-1} \Pr\left[\widetilde{W}_k(0) = \tilde{w}_k, \widetilde{W}_m(0) = \tilde{w}_m\right] \quad \forall w \in \mathcal{W}^k_{\tilde{w}_k} \cap \mathcal{W}^m_{\tilde{w}_m}$$

holds, when nodes from the same partition have equal initial infection probabilities. Hence, the main point of [35] is that for this specific type of graph and initial condition, the number of infective links between any two partitions only depends on the number of infected nodes in those partitions, which enables a lower-dimensional description of the SIS process (within the NIMFA approximation). This result is based on similar ideas as the UMFF framework, but from a very different perspective: UMFF describes how the topological approximation (2-5) applied to *any graph*, followed by a moment-closure approximation (2-6), results in a lower-dimensional *approximate* description of the SIS process.

Approximating the number of infective links in SIS

A central concept of UMFF is the description of the topological approximation (2-5) from the perspective of the isoperimetric problem. This approach of approximating the SIS process by approximating the number of infective links has appeared before.
Ganesh et al. [36] find an upper-bound for the epidemic threshold, by relating the infection terms in the SIS process to the isoperimetric problem. The isoperimetric, or Cheeger constant [19] of a graph with adjacency matrix A is defined as:

$$\eta_c(A) = \min_{w \in \{0,1\}^N} \frac{(u - w)^T A w}{w^T w}$$

which leads to a lower-bound for the number of infective links as:

$$(u-w)^T Aw \geq \eta_c(A)\tilde{w} \tag{2-28}$$

for any $w \in \{0,1\}^N$ and where $\tilde{w} = w^T w$ is the number of infected nodes. By assuming equality in (2-28), the SIS process is approximated by a linear death-birth process, from which an approximate epidemic threshold is derived in [36].

Van Mieghem [37], [38] also approximated the SIS process by approximating the size of the cut-set. Rather than relying on the isoperimetric problem, the most dominant terms in the spectral decomposition of the quadratic form $w^T Qw$, which equals the number of infective links, approximate the cut-set. Specifically, the approximation

$$(u-w)^T Aw \approx \frac{\mu_{N-1}}{N}\tilde{w}(N-\tilde{w})$$

is made. If this approximation error can be bounded by a constant $\theta \in \mathbb{R}$, i.e.

$$\left|(u-w)^T Aw - \frac{\mu_{N-1}}{N}\tilde{w}(N-\tilde{w})\right| \leq \theta \tag{2-29}$$

then the exact equation for the expected number of infected nodes can be bounded as

$$\mathbf{E}[\widetilde{W}_{-\theta}(t)] \leq \mathbf{E}[\widetilde{W}_{\text{exact}}(t)] \leq \mathbf{E}[\widetilde{W}_{+\theta}(t)] \tag{2-30}$$

where the bounds follow from the differential equations:

$$\begin{cases} \dfrac{d\mathbf{E}[\widetilde{W}_{+\theta}(t)]}{dt} = -\delta\mathbf{E}[\widetilde{W}_{+\theta}] + \beta\dfrac{\mu_{N-1}}{N}\mathbf{E}[\widetilde{W}_{+\theta}](N - \mathbf{E}[\widetilde{W}_{+\theta}]) + \theta \\ \dfrac{d\mathbf{E}[\widetilde{W}_{-\theta}(t)]}{dt} = -\delta\mathbf{E}[\widetilde{W}_{-\theta}] + \beta\dfrac{\mu_{N-1}}{N}\mathbf{E}[\widetilde{W}_{-\theta}](N - \mathbf{E}[\widetilde{W}_{-\theta}]) - \theta \end{cases} \tag{2-31}$$

which are Riccati differential equations, whose analytic solution are known and have a hyperbolic-tangent form [37]. In other words, the method of [37] and [38] gives bounds on the exact expected number of infected nodes $\mathbf{E}[\widetilde{w}_{\text{exact}}(t)]$, if a constant bound θ on the approximation error (2-29) is known.
By filling in $c = \mu_{N-1}$ in Lemma 1 from Appendix A-3, we can show that $\theta \leq \frac{N(\mu_1 - \mu_{N-1})}{4} = \theta^\star$. Although not a tight bound, filling in $\theta = \theta^\star$ in equations (2-31) gives:

$$\mathbf{E}[\widetilde{W}(t)_{-\theta^\star}] \leq \mathbf{E}[\widetilde{W}_{\text{exact}}(t)] \leq \mathbf{E}[\widetilde{W}(t)_{+\theta^\star}]$$

which is a new result based on the spectral decomposition methodology of [37] and [38].

2-10 Summary of Chapter 2

2-10-1 Features of UMFF

We have introduced a novel approximation framework for the description of the Markovian SIS process on complex networks. The main features of this Universal Mean-Field Framework (UMFF) are:

- UMFF unifies and generalizes a number of existing mean-field methods for approximating SIS epidemics on complex networks. In particular, two widely-used techniques, the N-Intertwined Mean-Field Approximation [11] and the Heterogeneous Mean-Field method [10] are shown to be contained by UMFF.
- The accuracy of UMFF and of all its the contained methods can be assessed based on the isoperimetric analogy:

  $$\text{infected nodes} \leftrightarrow \text{graph volume}$$
  $$\text{infective links} \leftrightarrow \text{graph surface}$$

  which provides bounds on the error of the UMFF topological approximation.
- UMFF leads to a conceptual description of the scaling behavior of SIS epidemics on large graphs. Since the UMFF accuracy is related to the notion of regularity on which Szemerédi's regularity lemma (SRL) is based, we can translate the statements of SRL about the structural regularity of large graphs to statements about the possibility to accurately approximate SIS dynamics on large graphs by a lower-dimensional description.

2-10-2 Future directions

By providing a universal description of mean-field approximation techniques for the SIS process, UMFF offers a framework, in which the existing techniques can be compared and which enables their respective accuracy to be assessed. In principle, UMFF could prescribe which existing (or new) mean-field method is more suitable, for a certain graph specification and for a specific SIS process parameter of interest.
While derived specifically for SIS epidemics, the UMFF approach is applicable to more general epidemic models. Sahneh et al. [39] for instance, describe the Generalized Epidemic Mean-Field model (GEMF), which is a generalization of the NIMFA approach to epidemic models with any number of compartments, and with a general transition structure between different compartments. The global dynamics of this general epidemic model follow from *node-based* compartmental transitions and *edge-based* compartmental transitions, which translates to *volume-based* transitions and *surface-based* transitions in context of the isoperimetric problem. Hence, by exploiting the same problem structure and the isoperimetric analogy, UMFF could generalize GEMF in a similar vein as UMFF generalizes NIMFA for the SIS compartmental process.
The general partitioning feature of UMFF also creates the possibility to develop new approximation techniques for the SIS process. Specifically, if nodes can be grouped in partitions based on some parameter such that similarity in that parameter corresponds to similarity in connectivity, then UMFF is expected to yield a good approximation of the SIS process. For instance, the embedding of graphs in metric spaces is studied in [40] and [41]. Nodes are considered to be embedded in a metric space with linking probabilities between node pairs dependent on the distance between them. Similarity in spatial coordinates (i.e. a small distance) between a pair of nodes means that their distance to other nodes is also similar. Hence, for such graph models, spatial closeness of nodes seems to provide a good partitioning criterion for UMFF, and the coarse-graining of the infection state would then correspond to

the intuitively attractive notion of spatial coarse-graining.
Furthermore, the observation that both the exact and approximate Markovian SIS processes are equivalent to a higher-dimensional quadratic death-birth process opens up new perspectives on modeling the SIS process. Some questions about the epidemic process have tractable solutions if properly formulated in terms of death-birth processes. Ganesh et al. [36] for instance, characterized the disease die-out probability [42] of the SIS process, based on the gambler's ruin problem [25] of a death-birth process. Conversely, the knowledge about the epidemic process might provide valuable insights in the quadratic death-birth process, whose exact solution is still an open problem [26].

Chapter 3

The Circuit-Graph-Simplex equivalence and Robustness of networks

3-1 Overview

This chapter discusses the thesis contributions related to the equivalence between passive electrical circuits and weighted graphs. As discussed in the introduction, Chapter 1, this circuit-graph equivalence is an interesting connection with both practical applications and theoretical consequences. Figure 1-4 illustrated how this equivalence links the physical intuition and knowledge from electrical circuits to the wide range of tools in graph theory and network science. We will exploit the extended circuit-graph-simplex equivalence, and further relations, to propose a graph robustness measure which is complementary to the existing 'effective graph resistance' robustness measure [17].

In Section 3-2 passive electrical circuits are introduced and the equivalence with weighted graphs is defined. Next, Section 3-3 describes the electrical circuit laws and the compact description of these laws with characteristic graph matrices. Section 3-4 introduces the effective resistance from the perspective of electrical circuits and describes the translation of this concept to the context of graphs. Additionally, two interpretations and an application of the effective resistance are given. In Section 3-5, the circuit-graph equivalence is extended to equivalence with another mathematical object: a hyperacute simplex. We describe the properties and representations of simplices and derive a new formula for the volume of a hyperacute simplex in terms of Laplacian eigenvalues of its equivalent graph. Based on this new formula, we propose to consider the simplex volume as a new graph robustness metric. Section 3-6 concludes the Chapter with a summary of the results.

3-2 Introduction: the Circuit-Graph equivalence

An electrical circuit is a simplified model of an interconnected system of electrical components. A wide variety of real-world electrical components can be characterized by circuit model components. Any real interconnection of components can then be modeled by a circuit of circuit models, which enables the electromagnetic field to be characterized throughout the system.
The most basic electrical circuit consists only of passive, linear components: resistors. These resistors are characterized by a resistance value[1]. To form a circuit, these resistors are connected by ideal wires of zero Ohm resistance. Figure 3-1 shows how any passive electrical circuit is composed of these two elements. Graphs, on the other hand, are composed of nodes

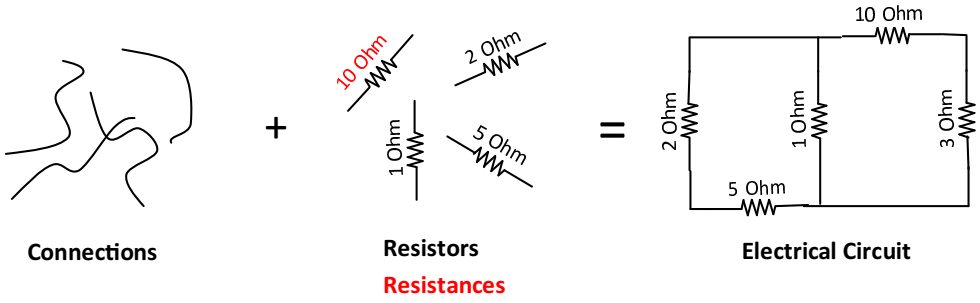

Figure 3-1: Passive electrical circuits are composed of resistors, resistance values, and ideal wires. Each resistor corresponds to one resistance value and is connected to two wires.

and links. Additionally, a positive, real value can be assigned to each link, which we call the link weights. A weighted graph can thus be characterized as $G(\mathcal{N}, \mathcal{L}, \mathcal{W})$, where $\mathcal{N}$ is the set of N nodes, $\mathcal{L}$ the set of L links between pairs of nodes and $\mathcal{W}$ the set of L weights, defined for each link. Figure 3-2 illustrates how any weighted graph is composed by the node, link and weight sets. As introduced in Chapter 1, the relation between electrical circuits and weighted

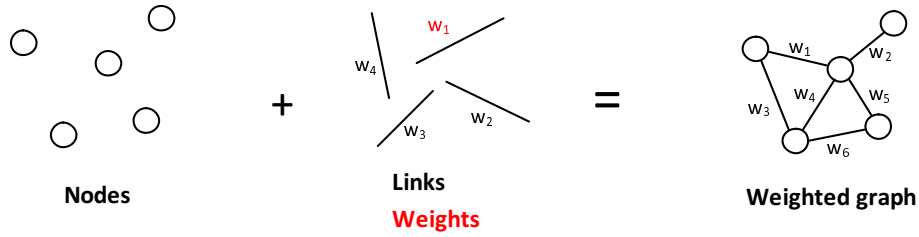

Figure 3-2: Weighted graphs are composed of nodes, links between nodes and link weights.

graphs is widely studied. In particular, electrical circuits and weighted graphs are known to be equivalent [43] in the sense that the description of each circuit corresponds to exactly one weighted graph. Additionally, both representations contain the same information necessary to constitute the relationship between the electrical signals in the circuit (see Section 3-3.

[1]The unit of resistance is Ohm $[\Omega] = \left[\frac{\text{volt}}{\text{ampere}}\right]$. To avoid confusion with the effective resistance matrix (see Section 3-4), which we will also denote by the symbol Ω, we will use "Ohm" to refer to a resistance value.

Definition 6 (Circuit-graph equivalence)**.** *Any passive electrical circuit corresponds to an equivalent weighted graph. Conversely, every weighted graph has a corresponding electrical circuit. This circuit-graph equivalence is defined by the following rules:*

(i) Each uninterrupted stretch of ideal wire in the circuit corresponds to a node in the graph.

(ii) A resistor between two wires corresponds to a link between the two nodes which correspond to those wires.

(iii) The weight of a link equals the reciprocal of the resistance value of the resistor corresponding to that link.

The circuit-graph equivalence is further illustrated by Figure 3-3.

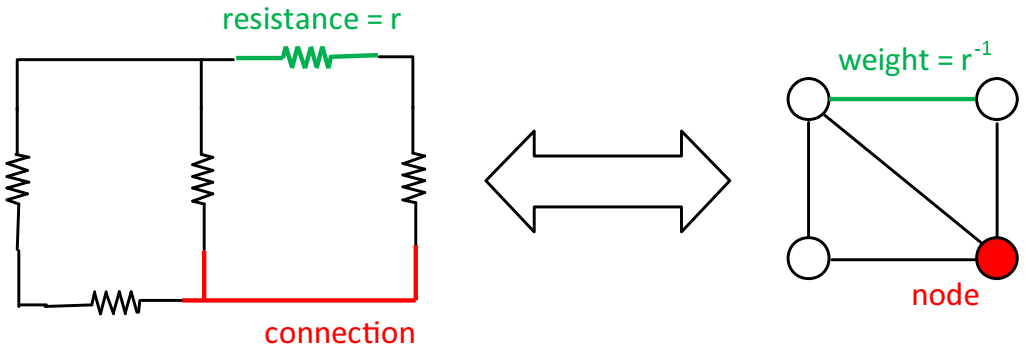

Figure 3-3: The circuit-graph equivalence means that every passive electrical circuit can be translated in a weighted graph and conversely. Each node corresponds to a wire, each link corresponds to a resistor and the link-weight equals the inverse of the corresponding resistors' resistance.

Additional characteristic graph matrices

We define an additional characteristic matrix for an unweighted, directed graph $G(\mathcal{N}, \mathcal{L})$: the incidence matrix B. The incidence matrix is an $N \times L$ matrix, defined by

$$Be_l = e_i - e_j \quad \text{for all links } l = (i, j) \in \mathcal{L}$$

where we allow the link element $l \in \mathcal{L}$ to index the columns of B. In other words, each column of the incidence matrix B corresponds to one link, and this column has a value $+1$ on the position of the node to which the link points, and a value -1 for the node where the arrow comes from. Since by definition each link leaves exactly one node and points to exactly one node, we can see that $B^T u = 0$.
For undirected graphs, the incidence matrix can still be defined by assigning an arbitrary direction to each link, i.e. $Be_l = \pm(e_i - e_j)$. Additionally, the incidence matrix is related to the Laplacian matrix by the identity $Q = BB^T$.

For weighted graphs, the previous graph definition $G(\mathcal{N}, \mathcal{L})$ can be modified to incorporate

the link weights. The link-weight information, i.e. a weight $w_{ij} \in \mathbb{R}$ for each link $(i,j) \in \mathcal{L}$, can be represented by an $L \times L$ diagonal matrix $W = \text{diag}(w_1, w_2 \ldots, w_L)$. Combined with the incidence matrix, the weighted Laplacian matrix $\widetilde{Q}$ can then be written as $\widetilde{Q} = BWB^T$ which gives:

$$\widetilde{Q}_{ij} = \begin{cases} -w_{ij} & \text{if } (i,j) \in \mathcal{L} \\ \sum_{k=1}^{N} w_{ki} & \text{if } i = j \\ 0 & \text{otherwise} \end{cases}$$

In the rest of this Chapter, the matrix $Q = \widetilde{Q}$ will denote the weighted Laplacian. The unweighted Laplacian can be considered as a specific case of a weighted graph, with $w_{ij} = 1$ for all links $(i,j) \in \mathcal{L}$.

3-3 Electrical circuit characterization

3-3-1 Circuit laws

Broadly speaking, electrical circuits are used to study the electromagnetic field in an interconnection of electrical components. In a passive electrical circuit model, the electromagnetic field throughout the whole circuit is characterized by defining one *voltage* value for each ideal wire. To include external influences in the circuit model, an additional *external current* in each wire is added to the description.

For N uninterrupted ideal wires, this means that the voltage is described by an $N \times 1$ **voltage vector**, denoted by $v = [v_1 \; v_2 \; \ldots \; v_N]^T$. Since all voltages in a circuit are necessarily defined with respect to a common, but arbitrary, reference level, only voltage differences are important. In other words, the voltage vector v is equivalent to the voltage vector $\tilde{v} = v + cu$ for some scalar c because the voltage difference v_{ij} between any pair of wires i and j is the same: $v_{ij} = (e_i - e_j)^T v = (e_i - e_j)^T (v + cu)$. As a result, we may choose the specific reference voltage such that $u^T v = 0$ holds, which is a useful choice for further notations and derivations. With the knowledge of the voltage in each of the wires, it is also possible to calculate the currents flowing through the resistors. Ohm's law, which is based on the electrical properties of resistive materials, provides a relation between the voltage over a resistor and the current that flows through it:

Definition 7 (Ohm's Law)**.** *In an electrical circuit, the current y_{ij} that flows from wire i with voltage v_j to wire j with voltage v_j, through a resistor with r_{ij} Ohm resistance, equals*

$$y_{ij} = \frac{v_{ij}}{r_{ij}}$$

If we combine the current through all links in an $L \times 1$ **link-current vector** $y = [y_1 \; y_2 \; \ldots \; y_L]^T$, where $e_l^T y = y_l$ is the current through any link $l \in \mathcal{L}$, then Ohm's law can be compactly written as

$$y = R^{-1} B^T v$$

where R and B are the characteristic graph matrices from the equivalent graph. The direction of a link, as specified in B, determines the sign of the current through that link. In particular, if $Be_l = (e_i - e_j)$ for some link $l = (i, j) \in \mathcal{L}$, then $y_l > 0$ corresponds to a current flowing from wire i to j and opposite for $y_l < 0$.

Without any external influence, a passive electrical circuit is in a trivial balance situation: the voltage is constant throughout the network, i.e. $v = 0$, and as a result all the link currents are zero, i.e. $y = 0$. Hence, to extend the modeling possibilities of electrical circuits, additional external currents are considered. In each wire i, such an external current x_i is added, where $x_i > 0$ means that the current flows into the wire and opposite for $x_i < 0$. All external currents together can be represented by the $N \times 1$ **external-current vector** $x = [x_1 \; x_2 \; \dots \; x_N]^T$. External currents "excite" the circuit from its passive all-zero state because of the physical principle of *conservation of charge*. Roughly speaking, this principle means that there can be no build-up of charge, anywhere in the circuit. If an external current is flowing into a wire, this means that there is a net-influx of charge. In order for no charge to build up, there must be a resulting current flowing out of that wire, and thus into the network. This principle is formalized by Kirchhoff's current law:

Definition 8 (Kirchhoff's current law)**.** *The total net current arriving at, or leaving from any wire equals zero. For any wire i, with currents y_{ij} flowing from i to its neighbors $j \in \mathcal{N}(i)$, this means that*

$$x_i = \sum_{j \in \mathcal{N}(i)} y_{ij}$$

must hold.

Again, it is possible to compactly describe Kirchhoff's current law based on the characteristic matrices of the equivalent graph:

$$x = By$$

Now, because $B^T u = 0$ it automatically follows that the external current vector has to satisfy $u^T x = 0$. In other words, the total sum of all the external currents introduced in the circuit has to be zero. This observation also follows directly from the conservation of charge principle, since the passive electrical circuit has no means of "adding" or "removing" charge, it can only displace charge by link-currents.

3-3-2 (x, v, y)-Characterization

Based on the two circuit laws, i.e. Ohm's law and Kirchhoff's current law, any passive electrical circuit defines a particular relation between voltage vectors v, external-current vectors x and link-current vectors y. In other words, an electrical circuit determines a set of possible (x, v, y) couples. In that sense, as shown in Figure 3-4, the electrical circuit can be seen as a black box that simply defines these possible couples. From this perspective, the circuit-graph equivalence can then understood as an equivalent graph and circuit defining the same possible couples, which we will call (x, v, y)-equivalence.

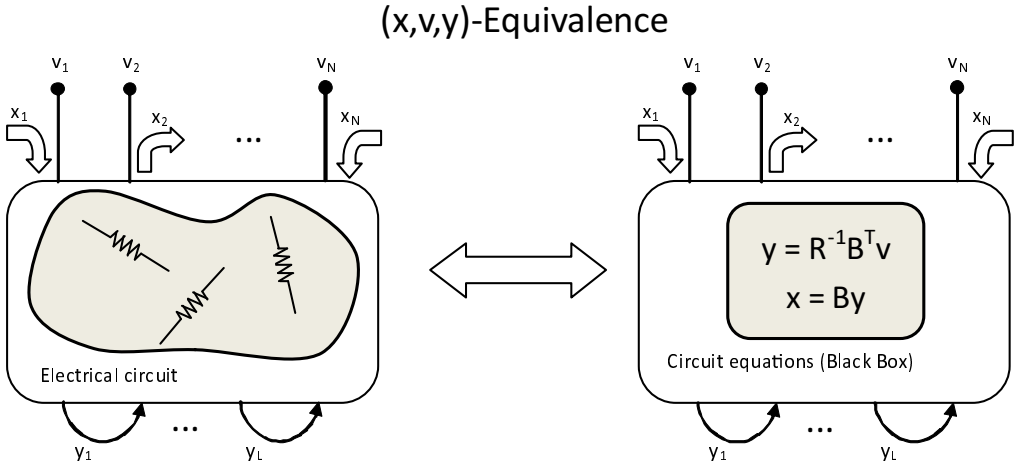

Figure 3-4: As a model, the electrical circuit describes the relation between three signals in the circuit: the external-currents x, the wire voltages v and the link currents y. In other words, it describes the possible (x, v, y)-combinations that can occur on the circuit. The electrical circuit can thus be modeled as a black-box, specifying certain (x, v, y)-relations.

3-3-3 Graph Laplacian and pseudo-inverse Laplacian

From the three signals (x, v, y), it is possible to directly eliminate the link-current vector y from this description by combining Ohm's law and Kirchhoff's current law. Because the weighted Laplacian equals $Q = BR^{-1}B^T$, we find the relation

$$x = Qv \tag{3-1}$$

Apart from being a compact description of the (x, v) relation, equation (3-1) is particularly interesting because the Laplacian matrix Q is a well-studied matrix in graph theory and network theory [19]. For instance, because we know the eigendecomposition of the Laplacian matrix Q, we can rewrite equation (3-1) as

$$x = \left(\sum_{i=1}^{N-1} \mu_i z_i z_i^T\right) v \iff v = \left(\sum_{i=1}^{N-1} \frac{1}{\mu_i} z_i z_i^T\right) x$$

This pseudo-inversion, which is an inversion in the subspace orthogonal to the u-vector, holds because both the external-current vector x and the voltage vector v are orthogonal to the zero-eigenvector $u/\sqrt{N}$, i.e. $u^T x = 0$ and $u^T v = 0$. If by $Q^\dagger = \sum_{i=1}^{N-1} \mu_i^{-1} z_i z_i^T$ we denote the pseudo-inverse of the Laplacian matrix, then we can write the alternative (x, v) relation:

$$v = Q^\dagger x \tag{3-2}$$

In the rest of this chapter, the practical applicability of the inverse relation (3-2) will become apparent. Additionally, in other work, this pseudo-inverse relation is studied in other contexts and deep theoretical implications are discussed. For instance Chung et al. [44] and Bendito et al. [45] investigate the equation $x = \widetilde{Q}v$, where $\widetilde{Q}$ is a more general form of the Laplacain. Chung relates $\widetilde{Q}$ to the continuous Laplacian operator, and the pseudo-inverse $\widetilde{Q}^\dagger$ in that setting is shown to be related to the Green's operator of the Laplacian. Bendito et al.

generalize the Laplacian operator to the Schrödinger operator, and concepts from the circuit-graph equivalence setting are related to similar concepts in this generalized setting. Both examples illustrate the deep theoretic nature and the wide applicability of the concepts that we are describing in the (limited) context of passive electrical circuits.

3-4 Effective Resistance

3-4-1 Effective resistance in electrical circuits

When studying electrical circuits, one is often not interested in the signals throughout the whole circuit. For this reason, the effective resistance can be introduced, which effectively "lumps" the whole-system response by one equivalent resistor. In particular, consider introducing an external current of I_c ampere in a wire i, and extracting the same current from j. As a result, there will be a distribution of voltages over the wires in the circuit, and a certain voltage difference between wires i and j, i.e. $v_{ij} = v_i - v_j$, will be established. In other words, the equivalent effect of the whole network distributing the currents, is that an "input" current of I_c ampere between wires i and j is related to an "output" voltage difference v_{ij} between them. Moreover, the relationship between the introduced current and measured voltage is linear: if this setup is repeated for multiple current values, i.e. $I_c^{(1)}, I_c^{(2)}, \dots$, then the proportionality with the measured voltage differences $v_{ij}^{(1)}, v_{ij}^{(2)}, \dots$ is constant and equal to ω_{ij}:

$$\omega_{ij} = \frac{I_c^{(1)}}{v_{ij}^{(1)}} = \frac{I_c^{(2)}}{v_{ij}^{(2)}} = \dots \tag{3-3}$$

where we define ω_{ij} as the *effective resistance* between wires i and j. The name effective resistance stems from the the fact that the whole-network effect leads to a linear current-voltage relationship, which can be characterized by a single resistor with the effective resistance as resistance value. Figure 3-5 further illustrates this concept.

While definition (3-3) is a measurement-based definition, the effective resistance it is a property that follows directly from the circuit structure. Figure 3-6 shows the two combination rules with which any network can be transformed into an equivalent resistor between two specified wires. It is interesting to remark the conceptual meaning of the combination rules: a series of resistors can be replaced by one resistor with the sum of the individual resistances. Hence, adding resistors in series always increases the effective resistance between the endpoints of the series. Resistors in parallel, on the other hand, result in an effective resistance which is lower than any of the individual resistances. Even stronger, adding resistors in parallel always decreases the effective resistance. As we will discuss later, these properties of series and parallel connections are related to the concept of distance functions. The effective resistance ω_{ij} can be calculated for any pair of wries i and j, which can be represented all together in the $N \times N$ effective resistance matrix Ω, where $\omega_{ij} = e_i^T \Omega e_j$. The diagonal elements of Ω are zero, i.e. $\omega_{ii} = 0$ for all i, because introducing and subtracting the same current in one wire is equivalent to introducing no current, and because $v_{ii} = 0$ by definition.

Because the effective resistances ω_{ij} only model the current-voltage relationship between distinct wire pairs, it is not immediately clear how Ω could capture the whole (x, v)-characteristic of a circuit. However, with equation (3-5), we will show that this Ω contains enough information for this characterization. Secondly, since the effective resistance lumps the network

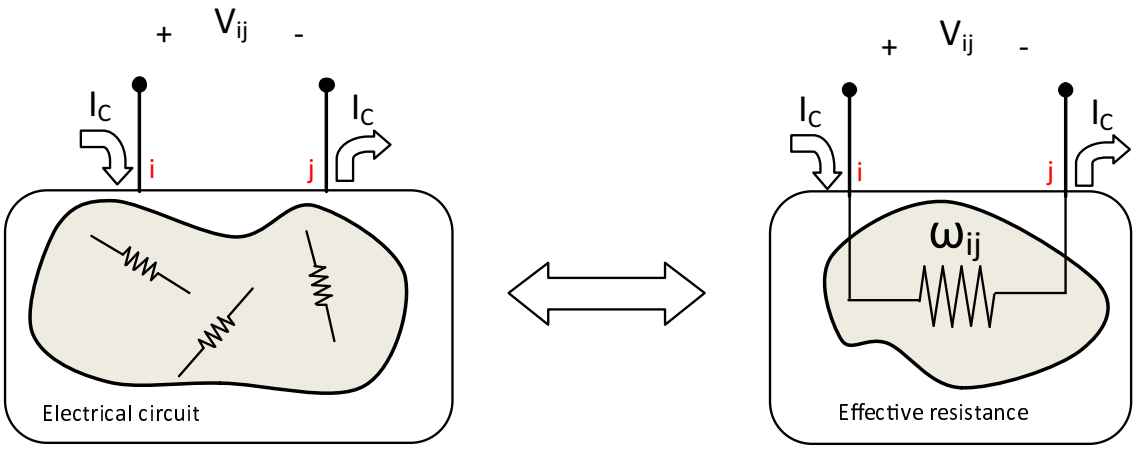

Figure 3-5: The effective resistance between a pair of wires represents the linear whole-network effect that relates an external current of I_c ampere between these wires, to a voltage difference of $v_{ij} = \omega_{ij} I_c$ between them.

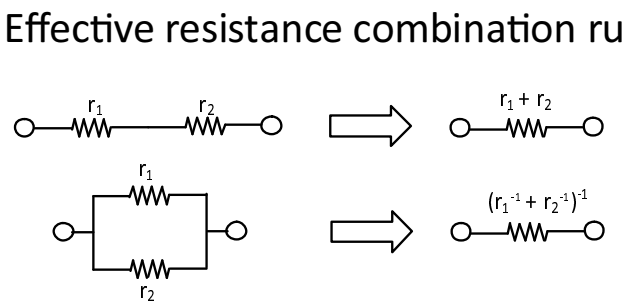

Figure 3-6: The effective resistance between a pair of nodes can be found based on two resistor combination rules. For two resistors in series, with resistances r_1 and r_2 in *series*, the equivalent resistor has a resistance of $r_1 + r_2$. For two resistors in *parallel*, with resistances r_1 and r_2, the equivalent resistor has a resistance of $\left(r_1^{-1} + r_2^{-1}\right)^{-1}$.

topology to a single resistor, it could be expected that this topological information can not be reconstructed from Ω and that it wouldn't be possible to also provide the full (x, v, y) characterization, i.e. including also the link currents y. Again, we will show with equation (3-7) that this full characterization is contained in the effective resistance matrix Ω. This idea is further developed in Section 3-5 by considering an additional representation to complement the circuit-graph equivalence.

3-4-2 Effective resistance in graphs

Based on the circuit laws and the resulting relations $x = Qv$ and $v = Q^{\dagger}v$, it is possible to derive an alternative expression for the effective resistance. We translate the effective resistances measurement setup to the setting of circuit equations, based on $v_{ij} = (e_i - e_j)^T v$.

For the definition of the effective resistance, this yields:

$$\omega_{ij} = \frac{v_{ij}}{I_c} = \frac{1}{I_c}(e_i - e_j)^T v$$

Now, because introducing an external current of I_c ampere in wire i and subtracting the same current from j corresponds to an external-current vector $x = (e_i - e_j)I_c$, and because of the (x, v)-relation $v = Q^\dagger x$ (equation (3-2)), this can be rewritten as:

$$\omega_{ij} = (e_i - e_j)^T Q^\dagger (e_i - e_j) = Q^\dagger_{ii} + Q^\dagger_{jj} - 2Q^\dagger_{ij} \tag{3-4}$$

Apart from showing how the effective resistance can be calculated from the pseudo-inverse of the Laplacian of the equivalent graph, equation (3-4) also enables the effective resistance to be further studied in terms of linear equations. In Appendix B-1, we derive the following equation:

$$v = -\frac{1}{2}\left(I - \frac{uu^T}{N}\right)\Omega x \tag{3-5}$$

which shows that the effective resistance matrix Ω indeed contains enough information to fully characterize the (x, v)-relation of the circuit.

3-4-3 Applications of the effective resistance in graphs

While the effective resistance is originally defined based on electrical circuit concepts, expression (3-4) means that the effective resistance can be derived directly from the (pseudo-inverse) graph Laplacian, without an explicit connection to electrical circuits. As a result, we can talk about the effective resistance ω_{ij} between pairs of nodes for any graph.
An interesting property of the effective resistance on graphs is that it defines a **distance function** between the nodes. This property can be understood conceptually by considering the effective resistance combination rules depicted in Figure 3-6. Roughly speaking, introducing resistors (and thus links) in a series connection increases the effective resistance, in other words the distance, between a pair of nodes. Adding resistors (or links) in parallel however, adds alternative paths between the nodes which reduces the effective distance. The resistance distance is thus reflecting the (path-)length of the paths between two nodes, as well as the number of alternative paths between then. The distance property was introduced in 1993 by Randic and Klein [16]. In a paper with the telling title “Resistance distance”, they showed the following fact:

Theorem 5 (Resistance is distance)**.** *[16] For any weighted graph, the effective resistance defines a distance function between nodes. In other words, for all nodes $i, j, k \in \mathcal{N}$, the following conditions hold:*

(i) $\omega_{ij} \geq 0$

(ii) $\omega_{ij} = 0 \iff i = j$

(iii) $\omega_{ij} = \omega_{ji}$

(iv) $\omega_{ij} \leq \omega_{ik} + \omega_{kj}$

Compared to other distance functions on graphs, like the shortest-path distance, the resistance distance is a "nice" distance function in the sense that it has a tractable description in terms of the characteristic graph matrices.

A second interpretation of effective resistances on graphs, this time in terms of **random walks**, is given by Doyle and Snell [46] and Chandra et al. [47]. A random walk is a process on a graph that describes the probability $p_i[t]$ of a "random walker" to be on a certain node i in the network at a given time-step t. This random walker moves through the network according to the following process:
(a) At time-step t=0, the walker is at node i with probability $p_i[0]$ for each i.
(b) From any time t to the next time-step $t+1$, the random walker moves from a node i to one of its neighboring nodes $j \in \mathcal{N}(i)$ with a probability P_{ij} proportional to the link-weight w_{ij}. All transition probabilities can be represented by the transition matrix $P = \Delta^{-1}A$.
(c) All together, the random walk can be characterized as:

$$p[t] = P^t p[0] \quad \text{for } t = 0, 1, \dots$$

where the $N \times 1$ vector $p[t] = [p_1[t]\ p_2[t]\ \dots\ p_N[t]]^T$ contains the random walker position probabilities at time-step t.
For the random walk process, the *commute time* C_{ij} is defined as the expected time it takes for a random walker that starts at node i to reach node j and return to node i. Chandra et al. show the following result:

Theorem 6 (Resistance is commute time)**.** *[47] In a weighted graph $G(\mathcal{N}, \mathcal{L}, \mathcal{W})$ with $W = \sum_{\forall l \in \mathcal{L}} w_l$ the sum of all link weights, the commute time C_{ij} between a pair of nodes is related to the effective resistance ω_{ij} as*

$$W\omega_{ij} = C_{ij} \quad \forall i, j \in \mathcal{N}$$

From Theorem 6, we can conclude that the effective resistance on a network reflects how well pairs of nodes are connected, with respect to random walks taking place on that network.

A third interpretation of the effective resistance is given in the context of **network robustness**. Ellens et al. [17] define the *effective graph resistance* R_G as the sum of all effective resistances:

$$R_G = \frac{1}{N} \sum_{i=1}^{N} \sum_{j=i+1}^{N} \omega_{ij} = \frac{1}{2N} u^T \Omega u \tag{3-6}$$

Interestingly, the effective graph resistance equals the arithmetic mean of the inverse Laplacian eigenvalues [16]:

$$R_G = \frac{1}{N} \sum_{i=1}^{N-1} \frac{1}{\mu_i}$$

Several arguments are given in [17] as to why the effective graph resistance R_G is related to the robustness of a graph. In Section [ref], these arguments are discussed in more detail. Conceptually, a low R_G value corresponds to a low average resistance distance between nodes, which means a good connectivity between all node pairs.
The same value R_G is also used as a graph invariant in the context of molecular graphs, i.e.

graphs representing the structural formula of a molecule, where R_G is called the Kirchhoff index [15]. Additionally, Ghosh et al. [48] provide an excellent overview of optimization problems related to the effective resistance, including optimization problems for the effective graph resistance.

3-4-4 The inverse $Q - \Omega$ relation

From the circuit perspective, the effective resistance is a characterization of the current-voltage relation between pairs of wires (equation (3-3) and Figure 3-5):

$$\omega_{ij} = \frac{v_{ij}}{I_c}$$

Based on the circuit laws, we then found that the effective resistance matrix Ω captures the full (x, v)-relationship of the circuit (equation (3-5)):

$$v = -\frac{1}{2}\left(I - \frac{uu^T}{N}\right)\Omega x$$

Furthermore, we can show that the effective resistance matrix Ω also contains enough information for a full (x, v, y)-characterization of the network. This result follows from the inverse relation between the Laplacian Q and the effective resistance matrix Ω:

Definition 9 (Inverse Q-Ω relation)**.** *For any weighted graph with Laplacian matrix Q and effective resistance matrix Ω, the following inverse relation holds:*

$$-\frac{1}{2}\begin{bmatrix} 0 & u^T \\ u & \Omega \end{bmatrix} = \begin{bmatrix} \zeta^T Q\zeta + \frac{4R_G}{N^2} & -(Q\zeta + \frac{2}{N}u)^T \\ -(Q\zeta + \frac{2}{N}u) & Q \end{bmatrix}^{-1} \tag{3-7}$$

where the $N \times 1$ vector $\zeta = \begin{bmatrix} Q^\dagger_{11} & Q^\dagger_{22} & \dots & Q^\dagger_{NN} \end{bmatrix}^T$ contains the diagonal elements of the pseudo-inverse Laplacian.

This equation can be checked with the inversion formulas for block-matrices [19]. While we do not have an immediate intuitive explanation[2] for the precise form of the block-matrix extension of Q with the value $\zeta^T Q\zeta + \frac{4R_G}{N^2}$ and the vector $(Q\zeta + \frac{2}{N}u)$, we can understand that the inverse Q-Ω relation (3-7) represents the same conceptual inverse relationship between Ω and Q as suggested by equation (3-5):

$$-\frac{1}{2}(e_i - e_j)^T\Omega(e_k - e_m) = (e_i - e_j)^T Q^\dagger (e_k - e_m)$$

The interesting implication of equation (3-7) is that Q can be calculated directly from Ω. In other words, we can retrieve the topology of the graph based on Ω alone. This means that the (x, v)-equivalence between circuits, graphs and the effective resistance representation is effectively an (x, v, y)-equivalence.

[2] Based on the circuit-graph-simplex equivalence (Theorem 7) it is possible to find an interpretation of the term $\zeta Q\zeta + \frac{4R_G}{N^2}$: if by R we denote the radius of the circumsphere of the equivalent simplex, then the relation $R^2 = \zeta Q\zeta + \frac{4R_G}{N^2}$ holds. This was first described by Coxeter [49] in 1930.

3-5 Circuit-graph-simplex equivalence

In the previous section, we showed that based on the inverse relation (3-7), the distance matrix Ω is an equivalent representation to weighted graphs and circuits. However, it is not immediately clear which restrictions exist on the properties of the matrix Ω such that it corresponds to a weighted graph and an electrical circuit. Can we just pick any distance matrix (i.e. with ω_{ij} values satisfying the distance-function conditions) and find the corresponding circuit-graph representations? In other word, is the full class of distance matrices equivalent to the class of weighted graphs and electrical circuits, or only a sub-class of distance matrices due to additional restrictive conditions on the form of Ω?
These questions are answered by Fiedler [43] in the context of another object: a simplex.

Definition 10 (Simplex). *An N-simplex $\mathcal{S}$ is the convex hull of $N+1$ points in $\mathbb{R}^N$. More specifically, for the set $\mathcal{P} = \{p_0, p_1, \ldots, p_N\}$ containing N points $p_i \in \mathbb{R}^N$, and with the set of vectors $\{p_i - p_j\}_{\forall i<j}$ linearly independent, the simplex $\mathcal{S}(\mathcal{P})$ defined by this set of point equals the following N-dimensional polyhedron:*

$$\mathcal{S}(\mathcal{P}) = \left\{ \sum_{i=0}^{N} \theta_i p_i \middle| \sum_{i=0}^{N} \theta_i = 1 \text{ and } \theta_i \geq 0 \text{ for all } i \right\}$$

A simplex can be seen as a higher-dimensional generalization of a triangle (2-simplex) or a prism (3-simplex). An N-simplex is called *hyperacute*, if all interior angles between $(N-1)$-dimensional faces are acute or right, i.e. less than or equal to $\frac{\pi}{2}$ radians.
Since a simplex is a geometric object, it is natural to talk about distances. For an N-simplex with vertex set $\mathcal{P}$, we can write an $N \times N$ matrix which contains the pairwise distances between points in $\mathcal{P}$. For the squared Euclidean distance specifically, we define:

Definition 11 (Squared Euclidean distance (SED) matrix). *For an N-simplex with corresponding point set $\mathcal{P} = \{p_1, p_2, \ldots, p_N\}$, the squared Euclidean distance matrix H is defined by the pairwise distances:*

$$h_{ij} = e_i^T H e_j = (p_i - p_j)^T (p_i - p_j)$$

We will further also use $\widetilde{H}$ to denote the function that maps a simplex $\mathcal{S}$ to its corresponding SED matrix H, i.e. $\widetilde{H}(\mathcal{S}) = H$. Since the SED matrix only contains information about the pairwise distances between points, it is possible for different simplices $\mathcal{S}_1$ and $\mathcal{S}_2$ to correspond to the same SED matrix, i.e. $\widetilde{H}(\mathcal{S}_1) = \widetilde{H}(\mathcal{S}_2)$. In this case, we call $\mathcal{S}_1$ and $\mathcal{S}_2$ *congruent simplices*. In 2D, congruent triangles are rotated, translated and mirrored versions of each other. Shrinking or changing the angles of the triangles is not allowed since, indeed, this would change the distances between the vertices.
A class of congruent simplices $\widetilde{\mathcal{S}}(H)$ can be defined as[3]:

$$\widetilde{\mathcal{S}}(H) = \left\{ \mathcal{S}^\star | \widetilde{H}(\mathcal{S}^\star) = H \right\} \tag{3-8}$$

Since also the simplex volume is invariant with respect to congruence, we can define the simplex volume based on the class of congruent simplices:

$$V(\widetilde{\mathcal{S}}(H)) = f(H)$$

[3] Alternatively, classes of congruent simplices can be defined by other invariants, for instance by all interior angles between $N-1$-dimensional faces combined with the simplex volume

where the function $f(H)$ illustrates that the volume depends only on H, i.e. the volume is an invariant for the $\widetilde{\mathcal{S}}(H)$.
The observation that an SED matrix corresponds to a class of congruent hyperacute simplices leads to the following extension of the circuit-graph equivalence [43]:

Theorem 7 (Circuit-graph-simplex (CGS) equivalence)**.** *The following objects are equivalent: weighted graphs, passive electrical circuits and classes of congruent hyperacute simplices.*

In other words, each of these objects can be translated one-to-one to all the others. The proof is given by Fiedler in [43], and can be sketched based on the provided context as follows:
(i) Each graph-circuit pair is equivalent to an Ω matrix (Equation (3-7))
(ii) Ω is an SED matrix (Appendix B-3)
(iii) Each SED matrix corresponds to a class of congruent simplices (Equation (3-8))
(iv) Specifically the subclass of hyperacute simplices is equivalent (see [50],[18])

3-5-1 The volume of a hyperacute simplex

Based on the numerous connections between electrical circuits, weighted graphs and hyperacute simplices that follow from the CGS equivalence, we introduce a new formula for the volume of a hyperacute simplex:

Theorem 8. *The volume V_G of a hyperacute $(N-1)$-simplex $\mathcal{S}$ equals*

$$V_G = |\mathcal{S}| = \frac{1}{(N-1)!\sqrt{\xi}} \tag{3-9}$$

where $\xi = \frac{1}{N}\prod_{i=1}^{N-1}\mu_i$ is the product of the non-zero Laplacian eigenvalues of the equivalent weighted graph.

In order to proof Theorem 8, we start by introducing a formula for the volume of a general simplex.
Motivated by the particular block-matrix form of the inverse Q-Ω relationship, specifically the matrix $\left[\begin{smallmatrix} 0 & u^T \\ u & \Omega \end{smallmatrix}\right]$, we consider the simplex-volume problem in the context of distance geometry. A particular result by Menger [51] relates the volume of a simplex to the corresponding SED matrix:

Theorem 9 (General simplex volume)**.** *The volume of an N-simplex with corresponding SED matrix H is given by:*

$$V\left(\widetilde{\mathcal{S}}(H)\right)^2 = \frac{(-1)^{N+1}}{2^N (N!)^2} \det \begin{bmatrix} 0 & u^T \\ u & H \end{bmatrix}$$

The determinant $\det\left[\begin{smallmatrix} 0 & u^T \\ u & H \end{smallmatrix}\right]$ for some SED matrix H, is called the *Cayley-Menger determinant.* This general expression for the volume of a simplex provides the starting point for the proof of Theorem 8:
Proof of Theorem 8:
For the specific case of hyperacute simplices, we know that the SED matrix H can be seen

as an effective resistance matrix Ω. For a hyperacute $(N-1)$-simplex with corresponding $N \times N$ effective resistance matrix Ω, Theorem 9 allows us to write:

$$V_G^2 = V\left(\widetilde{\mathcal{S}}(\Omega)\right)^2 = \frac{(-1)^N}{2^{N-1}((N-1)!)^2} \det \begin{bmatrix} 0 & u^T \\ u & \Omega \end{bmatrix} \tag{3-10}$$

Moreover, from the inverse Q-Ω relation, we know that

$$\det \begin{bmatrix} 0 & u^T \\ u & \Omega \end{bmatrix} = \det \left(-2 \begin{bmatrix} \zeta^T Q \zeta + \frac{4R_G}{N^2} & -(Q\zeta + \frac{2}{N}u)^T \\ -(Q\zeta + \frac{2}{N}u) & Q \end{bmatrix}^{-1} \right)$$

In Appendix B-2, we show how the expression $\det\left(Q_{\setminus\{i,j\}}\right) = (-1)^{i+j}\xi$, which is related to Kirchhoff's matrix-tree theorem [19], enables the Cayley-Menger determinant to be calculated as:

$$\det \begin{bmatrix} 0 & u^T \\ u & \Omega \end{bmatrix} = \frac{(-1)^N 2^{N-1}}{\xi} \tag{3-11}$$

Filling in equation (3-11) in the simplex volume expression (3-10) then leads to Theorem 8. □

3-5-2 Simplex volume as a complementary robustness measure

In [17], Ellens et al. propose the effective graph resistance R_G as a robustness measure. They provide four arguments why *a lower R_G reflects a higher robustness*:
(a) The effective resistance ω_{ij} between a pair of nodes represents the distance between these nodes, including parallel 'back-up paths', which is thus a measure of how well connected a pair is. Since the effective graph resistance is the average effective resistance between all node pairs, it reflects how well nodes are connected on average.
(b) The effective resistance can be approximated by the inverse second smallest Laplacian eigenvalue, i.e. $R_G \sim \mu_{N-1}^{-1}$, which is known to reflect network robustness.
(c) R_G decreases strictly when links are added to a network, which corresponds to the intuitive notion that the robustness of a network would increase by adding links[4].
(d) Because the effective resistance is proportional to the commute time 6, it reflects how well nodes are linked together.

We adopt the idea from [17] that R_G reflects the robustness of a network, and propose the simplex volume V_G as a complementary robustness measure. The main motivation is that for graphs with the same effective graph resistance R_G, the simplex volume V_G can discriminate between the different graphs, where a higher simplex volume corresponds to a higher robustness. Figure 3-7 illustrates this for the example of three graphs, and their corresponding triangles (2-simplices). The triangles have the same sum of squared edge lengths R_G, but they enclose a different area V_G. Additionally, it can be seen that a larger V_G corresponds to a more narrow distribution of the edge lengths ω_{ij} in the triangles, and thus a more balanced network topology. Extrapolating this observation to N-simplices, leads to the suggestion that

[4] In theory, adding nodes to a network can also deteriorate the "performance" of that network. This counterintuitive effect is commonly called Braess's paradox [52].

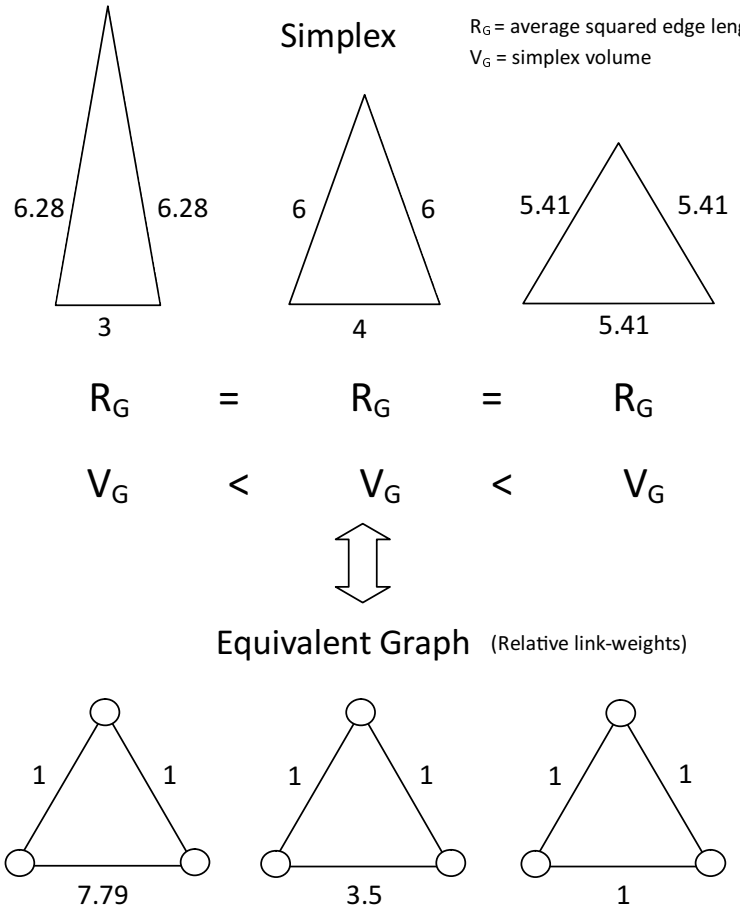

Figure 3-7: Three triangles (2-simplices) with the same effective graph resistance value R_G, but with different enclosed areas V_G. Amongst triangles with the same R_G value, a higher volume corresponds to more similar edge-lengths, i.e. a more narrow distribution of the effective resistances ω_{ij}.

graphs with the same R_G value can be distinguished based on V_G. Furthermore, we argue that a more narrow distribution of the effective resistance, i.e. a higher V_G, corresponds to a higher robustness, because it implies a smaller difference between the "worst connected" node pairs and the "best connected" node pairs.
Remark: Maximizing V_G without regarding R_G is not a good strategy because this maximization can work in the "opposite direction" of minimizing R_G. A large simplex volume can be achieved by evenly distributed effective resistances (the desired property), but it can also be achieved by large values for the effective resistances (an undesired property). Hence, it is necessary to compare V_G for fixed, or similar R_G values, such that V_G differences correspond to differences in the effective resistance distribution.

An additional argument to consider simplex volume as a complementary measure to the effective resistances, follows from comparing the equations for both measures. The effective

graph resistance R_G equals (3-6):

$$R_G = \frac{1}{N}\sum_{i=1}^{N-1}\frac{1}{\mu_i} \propto \sum_{i=1}^{N-1}\frac{1}{\mu_i} \tag{3-12}$$

while the simplex volume is given by Theorem 8:

$$V_G = \frac{1}{(N-1)!\sqrt{\xi}} \propto \sqrt{\prod_{i=1}^{N-1}\frac{1}{\mu_i}} \tag{3-13}$$

where the proportionality sign "$\propto$" denotes that additive and multiplicative constants related to N are omitted. Equation (3-12) shows that R_G is related to the *arithmetic mean*, while V_G is related to the *geometric mean*[5] Hence, complementing R_G with V_G is closely related to complementing the arithmetic mean with the geometric mean. This illustrates that, indeed, the simplex volume provides additional information compared to R_G only.

3-6 Summary of Chapter 3

The main subject of this chapter is the circuit-graph-simplex (CGS) equivalence. An overview of this equivalence is given, starting from the description of passive electrical circuits and the circuit laws. Then, based on the circuit-graph equivalence, the circuit concept of effective resistance is translated to graphs, where it has many applications. Finally, a description of the relation between simplices, squared Euclidean matrices and the effective resistance matrix Ω leads to the CGS equivalence.
In the context of the CGS equivalence, a new formula is introduced for the volume V_G of a hyperacute simplex. The formula expresses V_G in terms of the Laplacian eigenvalues of the corresponding graph, which leads to a network robustness interpretation of the simplex volume. The main argument for this interpretation is the observation that for fixed R_G values, a difference in V_G corresponds to a difference in the connectivity homogeneity.

[5]For a set of numbers $x_1, x_2, \ldots, x_N$, the arithmetic mean M_a is defined as $M_a = \frac{1}{N}\sum_{i=1}^{N} x_i$, while the geometric M_g is defined as $M_g = \sqrt[N]{\prod_{i=1}^{N} x_i}$. This means that $M_g = V_G^{\frac{2}{N}}$ corresponds to the geometric mean. Since the function $f(x) = \sqrt[N]{x^2}$ is monotonically increasing, i.e. $x_1 > x_2 \iff f(x_1) > f(x_2)$, the geometric mean of the inverse Laplacian eigenvalues reflects the same order between graphs: $M_g^{(1)} > M_g^{(2)} \iff V_G^{(1)} > V_G^{(2)}$.

Chapter 4

Conclusion

This thesis describes the contribution to two problems in network science. The first problem relates to the general pursuit of better understanding the behavior of dynamical processes on networks. As a particular dynamical process, the spreading of the Susceptible-Infected-Susceptible disease model on networks is studied. Secondly, the theoretical equivalence between electrical circuits and graphs is used as a starting point to study the network topology and network robustness. While at first sight these problems appear to be unrelated, a more elaborate description in the 'language' of networks leads to the conclusion that both problems can be approached with a same set of tools. In both problems, for instance, the Laplacian eigenvalues play an important role. These eigenvalues are related to the Laplacian-matrix representation, in one case of the contact network over which the disease spreads, and in the other case of the circuit-equivalent graph. For the epidemics problem, we found that the Laplacian eigenvalues can be used to bound topological mean-field approximations, based on the geometric notion of the isoperimetric problem. For the circuit-related problem, we found that a geometric representation of circuits and graphs, i.e. a simplex, could be used to quantify the robustness of those circuits and graphs. The specific formula that represents this robustness measure, i.e. the simplex volume, is an expression in terms of the Laplacian eigenvalues. This somewhat surprising connection between network epidemics and electrical circuits is a good example of the strength of the 'network approach' to solve certain problems. By providing the common language of networks and dynamical processes, seemingly disparate problems can be approached with the same set of tools. Hence, developments in analysis tools or in one of the many fields related to network science, have the possibility to translate to other fields, and lead to solutions for problems in those fields. In the same line of thought, the contributions of this thesis might be related to problems in a different context in the future, which is in itself an interesting direction for future work

Summary of the Chapters

Chapter 1 describes the *context and motivation* of the thesis contributions, starting from an introductory description of network science. A general discussion of networks and their use

in modeling complex systems, provides the context in which the two specific topics of this thesis are discussed: dynamical processes on networks and electrical circuits.

The work on *network epidemics* in Chapter 2 consists of an overview of the Markovian SIS model, the proposal of the Universal Mean-Field Framework as a general framework for SIS approximation methods, and a discussion of the implications of UMFF in terms of new approximation bounds and a link to Szemerédi's regularity lemma.
While this thesis mainly focused on introducing the framework and its properties, possible further work could focus on (i) a practical comparison of different existing mean-field methods based on the insights from UMFF, (ii) a quantitative investigation of the isoperimetric inequalities for the UMFF approximation and (iii) further studying the connection with Szemerédi's regularity lemma, and the possible implications it has for epidemics on large graphs.

The work on *the circuit-graph-simplex equivalence* in Chapter 3 consists of an overview of electrical circuit models, the implications of the circuit-graph equivalence and finally of the effective resistance as a combining ingredient for the CGS equivalence. Then, based on this equivalence, we introduce a new formula for the volume of a hyperacute simplex and interpret this volume as a network robustness measure.
Since the simplex volume is discussed only briefly, future work should focus on (i) a deeper investigation of the implications of the new formula, (ii) a broader literature research to combine the different perspectives related to the result, i.e. simplex geometry, network robustness, etc. and (iii) experimental quantification of the simplex volume as a robustness measure. All together, these further steps should make out whether the simplex volume has a practical use as a robustness measure.

Bibliography

[1] A. Fornito, A. Zalesky, and E. T. Bullmore. *Fundamentals of Brain Network Analysis*. San Diego: Academic Press, 2016. ISBN: 978-0-12-407908-3.

[2] H. Jeong et al. "The large-scale organization of metabolic networks." In: *Nature* 407.6804 (2000), pp. 651–654. DOI: 10.1038/35036627.

[3] V. Colizza et al. "Modeling the Worldwide Spread of Pandemic Influenza: Baseline Case and Containment Interventions". In: *PLOS Medicine* 4.1 (2007), pp. 1–16. DOI: 10.1371/journal.pmed.0040013.

[4] F. Xie and D. Levinson. "Measuring the Structure of Road Networks". In: *Geographical Analysis* 39.3 (2007), pp. 336–356. DOI: 10.1111/j.1538-4632.2007.00707.x.

[5] J. O. Kephart and S. R. White. "Directed-Graph Epidemiological Models of Computer Viruses". In: *Proc. IEEE Comput. Soc. Symp. Research in Security and Privacy* (1991), pp. 343–359. DOI: 10.1109/RISP.1991.130801.

[6] L. Euler. "Solutio problematis ad geometriam situs pertinentis". In: *Commentarii academiae scientiarum Petropolitanae 8* (1741), pp. 128–140.

[7] D. J. Watts and S. H. Strogatz. "Collective dynamics of 'small-world' networks." In: *Nature* 393.6684 (1998), pp. 409–10. DOI: 10.1038/30918.

[8] A. L. Barabási and R. Albert. "Emergence of Scaling in Random Networks". In: *Science* 286.5439 (1999), pp. 509–512. DOI: 10.1126/science.286.5439.509.

[9] M. Girvan and M. E. J. Newman. "Community structure in social and biological networks". In: *Proceedings of the National Academy of Sciences* 99.12 (2002), pp. 7821–7826. DOI: 10.1073/pnas.122653799.

[10] R. Pastor-Satorras and A. Vespignani. "Epidemic Spreading in Scale-Free Networks". In: *Phys. Rev. Lett.* 86 (14 2001), pp. 3200–3203. DOI: 10.1103/PhysRevLett.86.3200.

[11] P. Van Mieghem, J. Omic, and R. Kooij. "Virus Spread in Networks". In: *IEEE/ACM Trans. Netw.* 17.1 (2009), pp. 1–14. DOI: 10.1109/TNET.2008.925623.

[12] R. Pastor-Satorras et al. "Epidemic processes in complex networks". In: *Rev. Mod. Phys.* 87 (3 2015), pp. 925–979. DOI: 10.1103/RevModPhys.87.925.

[13] W. Wang et al. "Unification of theoretical approaches for epidemic spreading on complex networks". In: *Reports on Progress in Physics* 80.3 (2017), p. 036603. DOI: 10.1088/1361-6633/aa5398.

[14] A. S. Mata and S. C. Ferreira. "Pair quenched mean-field theory for the susceptible-infected-susceptible model on complex networks". In: *Europhysics Letters* 103.4 (2013). DOI: 10.1209/0295-5075/103/48003.

[15] I. Lukovits, S. Nikolić, and N. Trinajstić. "Resistance distance in regular graphs". In: *International Journal of Quantum Chemistry* 71.3 (1999), pp. 217–225. DOI: 10.1002/(SICI)1097-461X(1999)71:3<217::AID-QUA1>3.0.CO;2-C.

[16] D. J. Klein and M. Randić. "Resistance distance". In: *Journal of Mathematical Chemistry* 12.1 (1993), pp. 81–95. DOI: 10.1007/BF01164627.

[17] W. Ellens et al. "Effective graph resistance". In: *Linear Algebra and its Applications* 435.10 (2011), pp. 2491–2506. DOI: 10.1016/j.laa.2011.02.024.

[18] G. E. Sharpe. "On the (m+1)-terminal resistive-network problem". In: *Electrical Engineers, Proceedings of the Institution of* 116.4 (1969), pp. 503–509. DOI: 10.1049/piee.1969.0103.

[19] P. Van Mieghem. *Graph Spectra for Complex Networks*. Cambridge, U.K.: Cambridge University Press, 2011. ISBN: 9780511921681.

[20] V. Blåsjö. "The Isoperimetric Problem". In: *The American Mathematical Monthly* 112.6 (2005), pp. 526–566. DOI: 10.2307/30037526.

[21] R. Osserman. "The isoperimetric inequality". In: *Bulletin of the American Mathematical Society* 84.6 (1978), pp. 1182–1238. DOI: 10.1090/S0002-9904-1978-14553-4.

[22] W. O. Kermack and A. G. McKendrick. "A Contribution to the Mathematical Theory of Epidemics". In: *Proceedings of the Royal Society of London A: Mathematical, Physical and Engineering Sciences* 115.772 (1927), pp. 700–721. DOI: 10.1098/rspa.1927.0118.

[23] E. Cator, R. van de Bovenkamp, and P. Van Mieghem. "Susceptible-infected-susceptible epidemics on networks with general infection and cure times". In: *Phys. Rev. E* 87 (6 2013), p. 062816. DOI: 10.1103/PhysRevE.87.062816.

[24] M. Boguñá and R. Pastor-Satorras. "Epidemic spreading in correlated complex networks". In: *Phys. Rev. E* 66 (4 2002), p. 047104. DOI: 10.1103/PhysRevE.66.047104.

[25] P. Van Mieghem. *Performance Analysis of Complex Networks and Systems*. Cambridge, U.K.: Cambridge University Press, 2014. ISBN: 9781107415874.

[26] P. Van Mieghem. "Time evolution of SIS epidemics on the Complete Graph". In: *Delft University of Technology, report20170405* (2017).

[27] E. Cator and P. Van Mieghem. "Nodal infection in Markovian susceptible-infected-susceptible and susceptible-infected-removed epidemics on networks are non-negatively correlated". In: *Phys. Rev. E* 89 (5 2014), p. 052802. DOI: 10.1103/PhysRevE.89.052802.

[28] E. Cator and P. Van Mieghem. "Second-order mean-field susceptible-infected-susceptible epidemic threshold". In: *Phys. Rev. E* 85 (5 2012), p. 056111. DOI: 10.1103/PhysRevE.85.056111.

[29] C. Castellano and R. Pastor-Satorras. "Thresholds for Epidemic Spreading in Networks". In: *Phys. Rev. Lett.* 105 (21 2010), p. 218701. DOI: 10.1103/PhysRevLett.105.218701.

[30] F. Chung. "Discrete Isoperimetric Inequalities". In: *Discrete Mathematics and Theoretical Computer Science* (1996).

[31] A. Agaskar and Y. M. Lu. "A Spectral Graph Uncertainty Principle". In: *IEEE Transactions on Information Theory* 59.7 (2013), pp. 4338–4356. DOI: 10.1109/TIT.2013.2252233.

[32] W. H. Haemers. "Interlacing eigenvalues and graphs". In: *Linear Algebra and its Applications* 226 (1995), pp. 593–616. DOI: 10.1016/0024-3795(95)00199-2.

[33] R. Diestel. *Graph Theory, 5th Edition*. Vol. 173. Graduate texts in mathematics. Springer, 2016. ISBN: 978-3-662-53621-6.

[34] T. Tao. "Szemerédi's regularity lemma revisited". In: *Contributions to Discrete Mathematics* 1 (2006).

[35] S. Bonaccorsi et al. "Epidemic Outbreaks in Networks with Equitable or Almost-Equitable Partitions". In: *SIAM Journal on Applied Mathematics* 75.6 (2015), pp. 2421–2443. DOI: 10.1137/140995829.

[36] A. Ganesh, L. Massoulie, and D. Towsley. "The effect of network topology on the spread of epidemics". In: *Proceedings IEEE 24th Annual Joint Conference of the IEEE Computer and Communications Societies.* 2 (2005), 1455–1466 vol. 2. DOI: 10.1109/INFCOM.2005.1498374.

[37] P. Van Mieghem. "Universality of the SIS prevalence in networks". In: *ArXiv e-prints* (2016).

[38] P. Van Mieghem. "Approximate formula and bounds for the time-varying susceptible-infected-susceptible prevalence in networks". In: *Phys. Rev. E* 93 (5 2016), p. 052312. DOI: 10.1103/PhysRevE.93.052312.

[39] F. D. Sahneh, C. Scoglio, and P. Van Mieghem. "Generalized Epidemic Mean-Field Model for Spreading Processes Over Multilayer Complex Networks". In: *IEEE/ACM Transactions on Networking* 21.5 (2013), pp. 1609–1620. DOI: 10.1109/TNET.2013.2239658.

[40] M. A. Serrano, D. Krioukov, and M. Boguñá. "Self-Similarity of Complex Networks and Hidden Metric Spaces". In: *Phys. Rev. Lett.* 100 (7 2008), p. 078701. DOI: 10.1103/PhysRevLett.100.078701.

[41] D. Krioukov et al. "Hyperbolic geometry of complex networks". In: *Phys. Rev. E* 82 (3 2010), p. 036106. DOI: 10.1103/PhysRevE.82.036106.

[42] Q. Liu and P. Van Mieghem. "Die-out Probability in SIS Epidemic Processes on Networks". In: *Complex Networks & Their Applications V: Proceedings of the 5th International Workshop on Complex Networks and their Applications*. Springer International Publishing, 2017, pp. 511–521. DOI: 10.1007/978-3-319-50901-3_41.

[43] M. Fiedler. "Some characterizations of symmetric inverse M-matrices". In: *Linear Algebra and its Applications* 275 (1998), pp. 179–187. DOI: 10.1016/S0024-3795(97)10022-2.

[44] F. Chung and S.-T. Yau. "Discrete Green's Functions". In: *Journal of Combinatorial Theory, Series A* 91.1 (2000), pp. 191–214. DOI: 10.1006/jcta.2000.3094.

[45] E. Bendito et al. "Generalized inverses of symmetric M-matrices". In: *Linear Algebra and its Applications* 432.9 (2010), pp. 2438–2454. DOI: 10.1016/j.laa.2009.11.008.

[46] P. G. Doyle and J. L. Snell. *Random walks and electric networks*. Carus mathematical monographs. Mathematical Association of America, 1984. ISBN: 978-0883850244.

[47] A. K. Chandra et al. "The Electrical Resistance of a Graph Captures Its Commute and Cover Times". In: STOC '89 (1989), pp. 574–586. DOI: 10.1145/73007.73062.

[48] A. Ghosh, S. Boyd, and A. Saberi. "Minimizing Effective Resistance of a Graph". In: *SIAM Review* 50.1 (2008), pp. 37–66. DOI: 10.1137/050645452.

[49] H. S. M. Coxeter. "The Circumradius of the General Simplex". In: *The Mathematical Gazette* 15.210 (1930), pp. 229–231.

[50] D. J. H. Moore. "A geometric theory for resistive networks with positive element values". In: *Proceedings of the Hawaii international conference on system sciences* (1969).

[51] K. Menger. "New Foundation of Euclidean Geometry". In: *American Journal of Mathematics* 53.4 (1931), pp. 721–745. DOI: 10.2307/2371222.

[52] D. Braess. "Über ein Paradoxon aus der Verkehrsplanung". In: *Unternehmensforschung* 12.1 (1968), pp. 258–268. DOI: 10.1007/BF01918335.

[53] M. Taylor et al. "From Markovian to pairwise epidemic models and the performance of moment closure approximations". In: *Journal of Mathematical Biology* 64.6 (2012), pp. 1021–1042. DOI: 10.1007/s00285-011-0443-3.

[54] M. Fiedler. "Geometry of the Laplacian". In: *Linear Algebra and its Applications* 403 (2005), pp. 409–413. DOI: 10.1016/j.laa.2005.02.017.

Appendix A

Appendix UMFF

A-1 Derivation of exact SIS equations for $\widetilde{W}$ and $\mathbf{E}[\widetilde{W}]$

A-1-1 The Kolmogorov equations for Markov Chains

As a background for the further derivation of the UMFF equations (2-4), we start with a toy example to illustrate how the Kolmogorov equations are found for a Markov Chain. Further details can be found in [25]. Consider the 3-state Markov chain in $W(t)$ below: The Markov

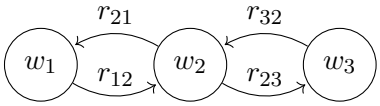

chain has three states: w_1,w_2 and w_3, with state probabilities $\Pr[W(t) = w_i]$ and transition rates r_{ij}, for $1 \leq i \neq j \leq 3$. By the subscript "ij" in the rates r_{ij}, we denote the transition from state i to state j, i.e. $i \to j$. As mentioned in Section 2-3, we assume that the transition processes are independent Poisson processes with exponentially distributed inter-event times, for example for the transition r_{12} this yields:

$$\Pr[W(t+h) = w_2 | W(t) = w_1] = r_{12} e^{-r_{12} h}$$

For $h \to 0$, this transition leads to:

$$\begin{cases} \frac{d \Pr[W(t)=w_2]}{dt} = r_{12} \Pr[W(t) = w_1] \\ \frac{d \Pr[W(t)=w_1]}{dt} = -r_{12} \Pr[W(t) = w_1] \end{cases}$$

Combining all transitions then leads to the Kolmogorov equations:

$$\begin{cases} \frac{d \Pr[W(t)=w_1]}{dt} = -r_{12} \Pr[W(t) = w_1] + r_{21} \Pr[W(t) = w_2] \\ \frac{d \Pr[W(t)=w_2]}{dt} = r_{12} \Pr[W(t) = w_1] - (r_{23} + r_{21}) \Pr[W(t) = w_2] + r_{32} \Pr[W(t) = w_3] \\ \frac{d \Pr[W(t)=w_3]}{dt} = r_{23} \Pr[W(t) = w_2] - r_{32} \Pr[W(t) = w_3] \end{cases}$$

Hence, by identifying the state transitions and according rates, one obtains the Kolmogorov equations of a Markov Chain, which completely characterize the dynamics of the process for a given initial distribution $\Pr[W(0) = w_i]$, for each possible state w.

A-1-2 State probability $\Pr[\widetilde{W}(t) = \tilde{w}]$

As described in Sections 2-4 and 2-5, the reduced-state vector $\tilde{w}$ is introduced to compactly describe the disease state and to reduce the complexity of the SIS process description. Instead of describing the state of each node separately, the reduced-state vector $\tilde{w} = (\tilde{w}_1, \tilde{w}_2, \ldots, \tilde{w}_K)$ captures the number of infected nodes in each partition, by the relation $\tilde{w}_k = s_k^T w$. By $\mathcal{W}_x^k = \left\{ w \in \{0,1\}^N | s_k^T w = x \right\}$ we denote the set of all full-state vectors w with x nodes infected in partition k (and with any possible number of nodes nodes in the other partitions $m \neq k$). Each full-state vector $w \in \bigcap_{k=1}^K \mathcal{W}_{\tilde{w}_k}^k$ then corresponds to the reduced-state vector $\tilde{w}$, since each set $\mathcal{W}_{\tilde{w}_k}^k$ constrains the number of infected nodes in a specific partition k. Based on this notation, we can represent the coarse-graining of the full states to the reduced states as:

$$\bigcap_{k=1}^{K} \mathcal{W}_{\tilde{w}_k}^k \xrightarrow{\text{group by partitioning } \pi} \tilde{w}$$

The full-state and reduced-state probabilities are then related as:

$$\Pr[\widetilde{W} = \tilde{w}] = \sum_{w \in \bigcap_{k=1}^K \mathcal{W}_{\tilde{w}_k}^k} \Pr[W = w] \tag{A-1}$$

and similarly, the rates are related as:

$$r_{\tilde{w}_k(\tilde{w}_k \pm \tilde{e}_k)} \Pr[\widetilde{W}_k = \tilde{w}_k] = \sum_{w \in \bigcap_{i=1}^K \mathcal{W}_{\tilde{w}_i}^i} \sum_{j \in \mathcal{N}_k} r_{w(w+e_j)} \Pr[W = w] \tag{A-2}$$

which is illustrated in Figure 2-6. More can be said about the reduced-state transition structure: firstly, the entries $\tilde{w}_k$ represent the number of infected nodes in partition k, from which it follows that

$$\tilde{w} \in \{0, 1, \ldots, N_1\} \times \{0, 1, \ldots, N_2\} \times \cdots \times \{0, 1, \ldots, N_K\},$$

and secondly, since a state transition in the Markovian SIS process reflects a single infection or curing event, the possible transitions between reduced states are of the form

$$\tilde{w} \to \tilde{w} \pm \tilde{e}_k$$

Hence, the reduced states and their transitions constitute an $(N_1+1) \times (N_2+1) \times \cdots \times (N_K+1)$ lattice. This structure can be represented compactly by the chain below, which depicts one specific “direction" in the lattice, corresponding to one partition k. However, since the transition rates between reduced states depend on the full states (A-2), the transitions at the reduced-state level do not describe a Markov chain. Nonetheless, it is still possible to write the exact, but not-closed differential equations for the reduced-state probabilities by grouping the Kolmogorov equations according to the partitions:

$$\frac{d \Pr[\widetilde{W} = \tilde{w}]}{dt} = \sum_{w \in \bigcap_{k=1}^K \mathcal{W}_{\tilde{w}_k}^k} \frac{d \Pr[W = w]}{dt}$$

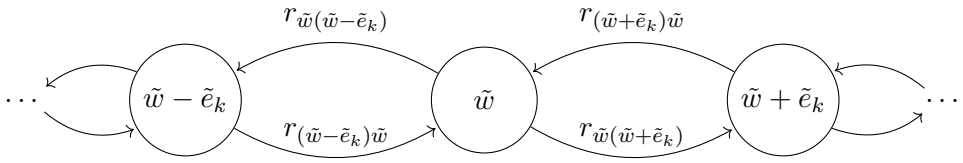

Considering the transitions within the partitions separately enables the Kolmogorov equations at the reduced-state level to be written as:

$$\begin{aligned}\frac{d\Pr[\widetilde{W}(t)=\tilde{w}]}{dt} = \sum_{k=1}^{K}\Big(&- r_{\tilde{w}(\tilde{w}-\tilde{e}_k)}\Pr[\widetilde{W}=\tilde{w}] + r_{(\tilde{w}+\tilde{e}_k)\tilde{w}}\Pr[\widetilde{W}=\tilde{w}+\tilde{e}_k] \\ &- r_{\tilde{w}(\tilde{w}+\tilde{e}_k)}\Pr[\widetilde{W}=\tilde{w}] + r_{(\tilde{w}-\tilde{e}_k)\tilde{w}}\Pr[\widetilde{W}=\tilde{w}-\tilde{e}_k]\Big)\end{aligned} \tag{A-3}$$

The transition rates at the reduced-state level are derived below.

Transition rates $r_{\tilde{w}(\tilde{w}-\tilde{e}_k)}$ and $r_{(\tilde{w}+\tilde{e}_k)\tilde{w}}$: node healing in partition k.

By the grouping relation (A-2) between the full states and the reduced states, the reduced-state transition rates are given by:

$$r_{\tilde{w}(\tilde{w}-\tilde{e}_k)}\Pr[\widetilde{W}=\tilde{w}] = \sum_{w\in\bigcap_{i=1}^{K}\mathcal{W}^i_{\tilde{w}_i}}\ \sum_{j\in\mathcal{N}_k} r_{w(w-e_j)}\Pr[W=w] \tag{A-4}$$

The transition rate $r_{w(w-e_j)}$ in equation (A-4) corresponds to node j healing in state w, i.e. the transition $W_j = 1 \to W_j = 0$. The healing rate in UMFF is δ for any node, hence the transition rate equals

$$r_{w(w-e_j)} = \delta w_j$$

for any full-state vector w and node j. The sum of the healing rates for all nodes in a partition k is then:

$$\sum_{j\in\mathcal{N}_k} r_{w(w-e_j)} = \delta s_k^T w = \delta\tilde{w}_k \tag{A-5}$$

Substituting (A-5) in the rate equation (A-4) and invoking (A-1) then yields

$$r_{\tilde{w}(\tilde{w}-\tilde{e}_k)}\Pr[\widetilde{W}=\tilde{w}] = \delta\tilde{w}_k\Pr[\widetilde{W}=\tilde{w}] \tag{A-6}$$

for the reduced-state transition rate corresponding to a node healing in partition k, in state $\tilde{w}$. A similar derivation yields

$$r_{(\tilde{w}+\tilde{e}_k)\tilde{w}}\Pr[\widetilde{W}=\tilde{w}+\tilde{e}_k] = \delta(\tilde{w}_k+1)\Pr[\widetilde{W}=\tilde{w}+\tilde{e}_k] \tag{A-7}$$

for the reduced-state transition rate corresponding to a node healing in partition k, in state $\tilde{w}+\tilde{e}_k$.

Transition rates $r_{\tilde{w}(\tilde{w}+\tilde{e}_k)}$ and $r_{(\tilde{w}-\tilde{e}_k)\tilde{w}}$: a node in partition k is infected.

By the grouping relation (A-2) between the full states and the reduced states, the reduced-state transition rates are given by equation:

$$r_{\tilde{w}(\tilde{w}+\tilde{e}_k)} \Pr[\widetilde{W} = \tilde{w}] = \sum_{w \in \bigcap_{i=1}^{K} \mathcal{W}^i_{\tilde{w}_i}} \sum_{j \in \mathcal{N}_k} r_{w(w+e_j)} \Pr[W = w] \tag{A-8}$$

The transition rate $r_{w(w+e_j)}$ in equation (A-8) corresponds to node j becoming infected in state w, i.e. the transition $W_j = 0 \to W_j = 1$. Since

$$e_j^T A w = \sum_{i=1}^{N} a_{ij} w_i$$

is the number of infected neighbors of node j, and since each infected neighbor infects node j at a rate β if $w_j = 0$, the full-state transition rate

$$r_{w(w+e_j)} = \beta(1 - w_j) e_j^T A w$$

is found. The sum of infection rates for all nodes in partition k is then:

$$\sum_{j \in \mathcal{N}_k} = \beta \sum_{m=1}^{K} (u - w)^T A^{(km)} w \tag{A-9}$$

where the sum over partitions $1 \leq m \leq K$ is introduced such that the block-matrix $A^{(km)}$, which naturally reflects the partition structure, can be used. Filling (A-9) into the rate equation (A-8) then yields:

$$r_{\tilde{w}(\tilde{w}+\tilde{e}_k)} \Pr[\widetilde{W} = \tilde{w}] = \beta \sum_{m=1}^{K} \sum_{w \in \mathcal{W}^k_{\tilde{w}_k} \cap \mathcal{W}^m_{\tilde{w}_m}} (u - w)^T A^{(km)} w \Pr[W = w] \tag{A-10}$$

for the reduced-state transition rate corresponding to a node becoming infected in partition k, in state $\tilde{w}$. A similar derivation yields

$$r_{(\tilde{w}-\tilde{e}_k)\tilde{w}} \Pr[\widetilde{W} = \tilde{w} - \tilde{e}_k] = \beta \sum_{m=1}^{K} \sum_{w \in \mathcal{W}^k_{(\tilde{w}_k - 1)} \cap \mathcal{W}^m_{\tilde{w}_m}} (u - w)^T A^{(km)} w \Pr[W = w] \tag{A-11}$$

for the reduced-state transition rate corresponding to a node becoming infected in partition k, in state $\tilde{w} - \tilde{e}_k$.

Resulting reduced-state equations

Introducing the rates (A-6),(A-7),(A-10) and (A-10) the Kolmogorov equations (A-3) establishes equation (2-7) in Section 2-5.

A-1-3 Expected number of infected nodes $\mathbf{E}[\widetilde{W}_k]$

The equations for the expected number of infected nodes $\mathbf{E}[\widetilde{W}_k]$ can be derived from the reduced-state probability equations (2-7), based on the definition of expectation and the law of total probability. For any partition k, we can write the expected number of infected nodes as:

$$\mathbf{E}[\widetilde{W}_k] = \sum_{\tilde{w}_k=0}^{N_k} \tilde{w}_k \Pr[\widetilde{W}_k = \tilde{w}_k] \tag{A-12}$$

Since by the law of total probability, the marginal probability can be written as:

$$\Pr[\widetilde{W}_k = \tilde{w}_k] = \underbrace{\sum_{\tilde{w}_1=0}^{N_1} \cdots \sum_{\tilde{w}_l=0}^{N_l} \cdots \sum_{\tilde{w}_K=0}^{N_K}}_{\forall l \neq k} \Pr[\widetilde{W} = \tilde{w}]$$

such that (A-12) equals

$$\mathbf{E}[\widetilde{W}_k] = \underbrace{\sum_{\tilde{w}_1=0}^{N_1} \cdots \sum_{\tilde{w}_l=0}^{N_l} \cdots \sum_{\tilde{w}_K=0}^{N_K}}_{\forall l} \tilde{w}_k \Pr[\widetilde{W} = \tilde{w}] \tag{A-13}$$

Differentiation with respect to time of equation (A-13) then yields:

$$\frac{d\mathbf{E}[\widetilde{W}_k]}{dt} = \underbrace{\sum_{\tilde{w}_1=0}^{N_1} \cdots \sum_{\tilde{w}_l=0}^{N_l} \cdots \sum_{\tilde{w}_K=0}^{N_K}}_{\forall l} \tilde{w}_k \frac{d\Pr[\widetilde{W} = \tilde{w}]}{dt} \tag{A-14}$$

After substitution of $\frac{d\Pr[\widetilde{W}=\tilde{w}]}{dt}$ from equation (2-7), we arrive at equation (2-8) in Section 2-5.

A-2 Higher-order UMFF

The UMFF equations can be extended to higher-order moments, in order to better capture the dynamic correlations of the SIS process.
For the case of $K = N$ partitions, Cator et al. [28] and Mata et al. [14] have described how the NIMFA [11] and Quenched Mean-Field (QMF) [29] equations can be extended to n'th-order moments:

$$\mathbf{E}[W_i] \rightarrow \mathbf{E}[W_i], \mathbf{E}[W_i W_j], \ldots, \mathbf{E}[\underbrace{W_i W_j \ldots W_l}_{n}]$$

based on the exact SIS dynamics. In order to have a closed set of equations for order n, the $(n+1)$'th-order moments must be approximated by lower-order moments, i.e. an approximation of the form:

$$\mathbf{E}[\underbrace{W_i W_j \ldots W_l}_{n+1}] \approx f\left(\mathbf{E}[\underbrace{W_i W_j \ldots W_l}_{\forall m \leq n}]\right)$$

where different choices for the moment-closure approximation f are given in [28] and [14]. Similarly, we can define the higher-order Universal Mean-Field Framework as:

Definition 12 (Higher-order UMFF)**.** *Consider a graph $\mathcal{G}(\mathcal{N},\mathcal{L})$, an epidemic process with rates (β,δ) and a graph partitioning π. For any integer $n \leq K$, the n'th-order UMFF equations are given by:*

$$\frac{d\mathbf{E}\left[\prod_{k=1}^{K}\widetilde{W}_k^{p_k}\right]}{dt} = \underbrace{\sum_{\tilde{w}_1=0}^{N_1}\cdots\sum_{\tilde{w}_k=0}^{N_k}\cdots\sum_{\tilde{w}_K=0}^{N_K}}_{\forall k}\prod_{k=1}^{K}\tilde{w}_k^{p_k}\frac{d\Pr[\widetilde{W}=\tilde{w}]}{dt} \tag{A-15}$$

for all vectors $p \in \left\{p \in \mathbb{N}^K | 0 \leq p_k \leq N_k, \forall k \text{ and } u^T p \leq n\right\}$ and with $\frac{d\Pr[\widetilde{W}=\tilde{w}]}{dt}$ given by equation (2-10). The $(n+1)$'th-order moments appearing in the higher-order UMFF equations are approximated by:

$$\mathbf{E}\left[\prod_{k=1}^{K}\widetilde{W}_k^{p_k}\right] \approx f\left(\left\{\mathbf{E}\left[\prod_{k=1}^{K}\widetilde{W}_k^{q_k}\right]\right\}_{\forall q\in\mathcal{Q}}\right) \tag{A-16}$$

for all vectors $p \in \left\{p \in \mathbb{N}^K | 0 \leq p_k \leq N_k, \forall k \text{ and } u^T p = n+1\right\}$ and with $\mathcal{Q} = \left\{q \in \mathbb{N}^K | 0 \leq q_k \leq p_k, \forall k \text{ and } u^T q \leq n\right\}$. The function f represents a generic moment-closure approximation.

Remark (1): The higher-order UMFF equations are found from the definition of expectation and the law of total probability, similar to the derivation of the first-order moments in Appendix A-1-3.
Remark (2): For a certain partition k, only the moments $\mathbf{E}\left[\ldots\widetilde{W}_k^{p_k}\ldots\right]$ for values $p_k \in \{1,\ldots,N_k\}$ are considered. Since $\tilde{w}_k \in \{0,1,\ldots,N_k\}$ has (N_k+1) possible values, the probability distribution $\Pr[\widetilde{W}_k = \tilde{w}_k]$ is fully determined by the first N_k moments. Hence the set $\left\{p \in \mathbb{N}^K | 0 \leq p_k \leq N_k, \forall k \text{ and } u^T p \leq n\right\}$ represents the set of powers of all n'th-order moments.

The approximation function f in the moment-closure approximation (A-16) is not further specified here. The current form of the moment-closure approximation expresses the condition that the higher-order moments need to be expressed in terms of lower-order moments, such that the set of equations (A-2) is closed in those moments.
Conceptually however, these moment-closure approximations are related to assumptions on the correlation of higher-order variables. Cator et al. [28] for instance, base their second-order moment-closure on the assumption[1]:

$$\mathrm{Cov}[W_iW_j, W_k] \approx 0$$

which, by definition of covariance yields:

$$\mathbf{E}[W_iW_jW_k] \approx \mathbf{E}[W_iW_j]\mathbf{E}[W_k]$$

[1]This specific approximation is used for third-order terms $\mathbf{E}[W_iW_jW_k]$ appearing in the equation of $\frac{d\Pr[W_i=w_i,W_j=w_j]}{dt}$.

for some triple of nodes (i, j, k). The accuracy of the moment-closure approximation thus depends on the actual covariance value which is assumed to be zero, which could be studied similar to how the investigation of the first-order moment-closure approximation in NIMFA [27].
As another example, Mata et al. [14] formulate a second-order moment-closure approximation, based on the assumption[2]:

$$\mathrm{Cov}\left[W_i, W_j | W_k\right] \approx 0$$

which, by definition of covariance, and because W_n is a Bernoulli random variable for each node n, yields:

$$\mathbf{E}[W_i W_j W_k] \approx \frac{\mathbf{E}[W_i W_k]\mathbf{E}[W_j W_k]}{\mathbf{E}[W_k]}$$

for some triple of nodes (i, j, k). Again, the accuracy of this approximation depends on the actual conditional covariance, which is assumed to be zero.
Taylor et al. [53] describe more elaborate moment-closure approximations by including topological information of the graph and discuss the accuracy of their approximation, based on simulations. For the more general case of higher-order UMFF however, it is not immediately clear which higher-order independence assumptions would work, and what difference it makes that the reduced-state variables $\widetilde{W}_k$ are not necessarily Bernoulli random variables.

A-3 Proof of isoperimetric inequalities

In this section, we prove the isoperimetric inequalities (2-24) and (2-25) of Theorem 3 and Theorem 4. We start by introducing some definitions and notations, based on the work of Haemers [32]. We then state and prove Lemma 1, from which Theorem 3 follows. Finally, we prove Theorem 4 based on the specific structure of bi-regular graphs.

A-3-1 Interlacing and quotient matrices

The following definitions are given in [32] and [19]:

Definition 13 (Interlacing sequences)**.** *Consider two sequences of real numbers:* $\alpha_1 \geq \alpha_2 \geq \cdots \geq \alpha_N$ *and* $\gamma_1 \geq \gamma_2 \geq \cdots \geq \gamma_K$ *with* $K \leq N$*. The second sequence is said to interlace the first whenever*

$$\alpha_i \geq \gamma_i \geq \alpha_{N-K+i} \quad \textit{for } i = 1, \ldots, K$$

[2]Mata et al. [14] define the approximation of third-order probabilities $\Pr[W_i = w_i, W_j = w_j, W_k = w_k]$ that appear in the equation of $\frac{d\Pr[W_i=w_i, W_j=w_j]}{dt}$ as:

$$\Pr[W_i = w_i, W_j = w_j, W_k = w_k] \approx \frac{\Pr[W_i = w_i, W_k = w_k]\Pr[W_j = w_j, W_k = w_k]}{\Pr[W_k = w_k]}$$

This approximation can be rewritten as a conditional independence approximation: $\Pr[W_i = w_i, W_j = w_j | W_k = w_k] \approx \Pr[W_i = w_i | W_k = w_k]\Pr[W_j = w_j | W_k = w_k]$, which implies $\mathrm{Cov}\left[W_i, W_j | W_k\right] \approx 0$. While independence of random variables is stronger than zero correlation, the latter suffices in this case to characterize the moment-closure approximation.

Definition 14 (Quotient matrix)**.** *The quotient matrix $A^{(\pi)}$ of an adjacency matrix A according to a partitioning π, is the matrix whose entries are the average row sums of the blocks of A. More precisely, $a_{km}^{(\pi)}$ is the entry in the quotient matrix according to the submatrix of A between nodes of $\mathcal{N}_k$ and $\mathcal{N}_m$ with value*

$$a_{km}^{(\pi)} = \frac{1}{N_k} s_k^T A s_m$$

These concepts can be combined by the interlacing theorem [32]:

Theorem 10 (Interlacing theorem)**.** *Suppose $A^{(\pi)}$ is the quotient matrix of a matrix A, then the eigenvalues of $A^{(\pi)}$ interlace the eigenvalues of A.*

The interlacing theorem is crucial for the proof of the isoperimetric inequality as will become clear in the proof of Lemma 1.

A-3-2 General isoperimetric inequality

We start by proving Lemma 1 below:

Lemma 1. *Consider a graph $G(\mathcal{N}, \mathcal{L})$ with N nodes. For any $c \in \mathbb{R}$ and any pair of Bernoulli vectors $w_x, w_y \in \{0,1\}^N$, with $N_x = u^T w_x$ and $N_y = u^T w_y$ ones, respectively, and with $w_x^T w_y = 0$, the following inequality holds:*

$$\left| w_x^T A w_y - \frac{c}{N} N_x N_y \right| \leq \frac{\theta}{N} \sqrt{N(N-N_x)N_y(N-N_y)} \tag{A-17}$$

where $|c - \mu_i| \leq \theta$ for $1 \leq i < N$ holds.

A first proof of Lemma 1 is given by Chung [30] in the context of isoperimetric inequalities and discrepancy inequalities on graphs. The proof is mainly based on algebraic manipulations of the term $w_x^T A w_y$ and the eigendecomposition of the Laplacian matrix Q. As mentioned in Section 2-3, the Laplacian Q is a positive semidefinite matrix possessing the eigendecomposition:

$$Q = ZMZ^T$$

where Z is the orthogonal eigen-matrix with eigenvectors z_i as columns, and $M = \text{diag}(\mu_1, \mu_2, \ldots, \mu_N)$, the diagonal matrix containing the eigenvalues. These eigenvalues can be ordered as $0 = \mu_N < \mu_{N-1} \leq \cdots \leq \mu_1$, where the 0 eigenvalue corresponds to the all-one eigenvector $z_N = \frac{u}{\sqrt{N}}$. Now, if we denote by $\widetilde{Z}$ the $N \times (N-1)$ matrix with z_N removed, and by $\widetilde{M}$ the $(N-1)\times(N-1)$ diagonal matrix $\widetilde{M} = \text{diag}(\mu_1, \ldots, \mu_{N-1})$, then we can also write:

$$Q = \widetilde{Z}\widetilde{M}\widetilde{Z}^T$$

If we further denote by $Q_K = NI - uu^T$ the Laplacian matrix of the complete graph, then we can write $\widetilde{Z}\widetilde{Z}^T = \frac{1}{N} Q_K$, which holds for $\widetilde{Z}$ of any Laplacian matrix.
Proof A:

We start by rewriting $w_x^T A w_y = w_x^T(\Delta - Q)w_y$. Due to the condition that $w_x^T w_y = 0$, we have $w_x^T \Delta w_y = 0$ and thus $w_x^T A w_y = -w_x^T Q w_y$. We then introduce the value $c \in \mathbb{R}$ as follows:

$$\begin{aligned} w_x^T A w_y &= -w_x^T Q w_y + \frac{c}{N} w_x^T Q_K w_y - \frac{c}{N} w_x^T Q_K w_y \\ &= w_x^T (\frac{c}{N} Q_K - Q) w_y - \frac{c}{N} w_x^T Q_K w_y \end{aligned}$$

Since $w_x^T Q_K w_y = -N_x N_y$, and using the eigendecomposition of Q and Q_K, we obtain:

$$w_x^T A w_y = w_x^T \widetilde{Z}(cI - \widetilde{M})\widetilde{Z}^T w_y + \frac{c}{N} N_x N_y$$

or,

$$w_x^T A w_y - \frac{c}{N} N_x N_y = w_x^T \widetilde{Z}(cI - \widetilde{M})\widetilde{Z}^T w_y$$

By introducing the variables $\alpha_i = w_x^T z_i$ and $\beta_i = w_y^T z_i$, we can write:

$$w_x^T A w_y - \frac{c}{N} N_x N_y = \sum_{i=1}^{N-1} \alpha_i \beta_i (c - \mu_i) \tag{A-18}$$

We can upper-bound the right-hand side as $\left|\sum_{i=1}^{N-1} \alpha_i \beta_i (c - \mu_i)\right| \leq \theta \sum_{i=1}^{N-1} |\alpha_i \beta_i|$, where we introduce θ with $|c - \mu_i| \leq \theta, \forall i \neq N$ as an upper bound. Equation (A-18) can then be written as:

$$\left| w_x^T A w_y - \frac{c}{N} N_x N_y \right| \leq \theta \sum_{i=1}^{N-1} |\alpha_i \beta_i|$$

Now, invoking the Cauchy-Schwartz inequality on the right-hand side of the equation and replacing α_i, β_i by their original values yields:

$$\left| w_x^T A w_y - \frac{c}{N} N_x N_y \right| \leq \theta \sqrt{\sum_{i=1}^{N-1} \alpha_i^2 \sum_{i=1}^{N-1} \beta_i^2} \leq \theta \sqrt{(w_x^T \widetilde{Z}\widetilde{Z}^T w_x)(w_y^T \widetilde{Z}\widetilde{Z}^T w_y)}$$

which by $\widetilde{Z}\widetilde{Z}^T = NI - uu^T$ and $w_x^T(NI - uu^T)w_x = N_x(N - N_x)$ proves (A-17). □

A second proof for Lemma 1 can be formulated based Haemers' interlacing theorem and applications [32]. Haemers ingeniously describes how quotient matrix constructions combined with the interlacing theorem can lead to algebraic expressions (i.e. involving Laplacian eigenvalues) for combinatorial quantities (i.e. possible number of links between subsets of nodes in a graph).

Proof B:

Haemers defines the block-matrix B

$$B = \begin{bmatrix} 0 & Q + cI \\ Q + cI & 0 \end{bmatrix} \tag{A-19}$$

for some graph Laplacian Q, and any scalar $c \in \mathbb{R}$. By the anti-diagonal blockform of B, we know that each eigenvalue μ_j of the Laplacian Q corresponds to two eigenvalues $\tilde{\lambda}_i = \mu_j + c$ and $\tilde{\lambda}_{2N-i} = -(\mu_j + c)$ of B.

We consider a specific partitioning π of the rows of B (nodes in the combined graph), for

which we can explicitly write the quotient matrix. For the Laplacian in the upper-right block, we partition the nodes $\mathcal{N}$ into a subset $\mathcal{N}_x$ of size N_x, and a remainder set $\mathcal{N}_{rx}$. For the Laplacian in the lower-left block, we partition the nodes $\mathcal{N}$ into a subset $\mathcal{N}_y$ of size N_y, where $\mathcal{N}_y$ is non-overlapping with the N_x-size block of the other Laplacian, and a remainder set $\mathcal{N}_{ry}$. Overall, this results in the partitioning $\{\mathcal{N},\mathcal{N}\} \to \{\mathcal{N}_x,\mathcal{N}_{rx},\mathcal{N}_y,\mathcal{N}_{ry}\}$ for matrix B. For this partitioning, and because $Bu = cu$ due to $Qu = 0$, we can write the quotient matrix $B^{(\pi)}$ explicitly as:

$$B^{(\pi)} = \begin{bmatrix} \frac{1}{N_x} & 0 & 0 & 0 \\ 0 & \frac{1}{N-N_x} & 0 & 0 \\ 0 & 0 & \frac{1}{N-N_y} & 0 \\ 0 & 0 & 0 & \frac{1}{N_y} \end{bmatrix} \begin{bmatrix} 0 & 0 & cN_x + m & -m \\ 0 & 0 & c(N - N_x - N_y) - m & cN_y + m \\ cN_x + m & c(N - N_x - N_y) - m & 0 & 0 \\ -m & cN_y + m & 0 & 0 \end{bmatrix} \tag{A-20}$$

where m is the number of links between subsets $\mathcal{N}_x$ and $\mathcal{N}_y$, i.e. $w_x^T A w_y$ in Lemma 1.
We can write the determinant of $B^{(\pi)}$ in two ways: an equality involving m and an inequality involving the eigenvalues of the Laplacian Q. Combining both expressions for the determinant then yields the isoperimetric inequality (A-17) of Lemma 1.
From (A-20), the determinant of $B^{(\pi)}$ can be calculated as:

$$\det\left(B^{(\pi)}\right) = \frac{c^2\left(cN_xN_y + Nm\right)^2}{N_x(N-N_x)N_y(N-N_y)} \tag{A-21}$$

Secondly, if we call $\delta_1 \geq \delta_2 \geq \delta_3 \geq \delta_4$ the eigenvalues of $B^{(\pi)}$, where $\delta_1 = -\delta_4$ and $\delta_2 = -\delta_3$ hold because of the anti-diagonal blockmatrix structure, then we have a second equation for the determinant:

$$\det\left(B^{(\pi)}\right) = \delta_1\delta_2\delta_3\delta_4 = \delta_1^2\delta_2^2 \tag{A-22}$$

From the definition of $B^{(\pi)}$, it follows that the all-one vector u is an eigenvector with eigenvalue c, i.e. $B^{(\pi)}u = cu$. This means that either $|\delta_1| = c$ or $|\delta_2| = c$. Additionally, because $B^{(\pi)}$ is a quotient matrix of B, we know that the eigenvalue sequence δ_i of $B^{(\pi)}$ interlaces the eigenvalue sequence $\tilde{\lambda}_i$ of B:

$$-\tilde{\lambda}_2 \leq \delta_1 \leq \tilde{\lambda}_1 \text{ and } -\tilde{\lambda}_3 \leq \delta_2 \leq \tilde{\lambda}_2$$

Because we know that either δ_1 or δ_2 equals $\tilde{\lambda}_i = \mu_N + c = c$, we can write:

$$\det\left(B^{(\pi)}\right) = \delta_1^2\delta_2^2 \leq c^2\left(\max_{\forall i \neq N} |\mu_i + c|\right) \tag{A-23}$$

Combining (A-21) and (A-23) gives:

$$\frac{c^2\left(cN_xN_y + Nm\right)}{N_x(N-N_x)N_y(N-N_y)} \leq c^2\theta^2, \tag{A-24}$$

with $|c + \mu_i| \leq \theta, \forall i \neq N$. By taking the square root of both sides, replacing m by $w_x^T A w_y$ and c by $-c$, we find again the isoperimetric inequality (A-17) in Lemma 1. □

Remark: Proofs A and B are two different ways to arrive at the same result. Proof A, based on Chung's approach, involves two approximations that upper-bound the cut-set approximation. The first approximation is upper bounding the $(c-\mu_i)$ values by θ, i.e. $\left|\sum_{i=1}^{N-1}\alpha_i\beta_i(c-\mu_i)\right| \leq \theta\sum_{i=1}^{N-1}|\alpha_i\beta_i|$. The second approximation involves the Cauchy-Schwartz inequality applied to the inner-product $\sum_{i=1}^{N-1}|\alpha_i\beta_i|$. Proof B based on Haemers' approach, involves one approximation step. The absolute value of the second largest eigenvalue $|\delta_2|$ of the quotient matrix $B^{(\pi)}$ is upper bounded by the second largest absolute eigenvalue $\max_{i\neq N}|\mu_i + c|$ of $Q + cI$, based on the interlacing theorem.
Since both approaches lead to the same result, we can conclude that the error due to interlacing is of the same nature as the error due to upper-bounding $(c - \mu_i)$ combined with the Cauchy-Schwartz inequality, which is a non-trivial relationship.

A-3-3 Proof of Theorem 3

Theorem 3 follows from Lemma 1 by particular choices of (c, A, w_x, w_y).
Proof:
First, we choose $w_x = (u - w) \circ s_k$ and $w_y = w \circ s_m$, where $(. \circ s_k)$ represents the Hadamard product (elementwise product) with s_k. For this choice of w_x and w_y, which are Bernoulli vectors satisfying $w_x^T w_y = 0$, and any adjacency matrix A, we can write:

$$w_x^T A w_y = (u_k \circ (u - w))^T A(w \circ u_m) = (u - w)^T A^{(km)} w$$

Secondly, we choose the specific value $c = N\tilde{a}_{km}$ which satisfies the condition $c \in \mathbb{R}$.
These choices allow us to rewrite Lemma 1 as:

$$\left|(u - w)^T A^{(km)} w - (\tilde{u} - \tilde{w})^T \widetilde{A}^{(km)} \tilde{w}\right| \leq \frac{\theta}{N}\sqrt{\tilde{w}_m(N - \tilde{w}_m)(N_k - \tilde{w}_k)(N - (N_k - \tilde{w}_k))}$$

for any adjacency matrix A, which equals equation (2-24) and thus proves Theorem 3. □

A-3-4 Proof of Theorem 4

Theorem 4 states that the topological approximation error can be bounded more tightly for bi-regular graphs $A_{km,r}$, which we prove based on Haemers' interlacing techniques [32].
Proof:
Consider a bi-regular graph $G_{km,r}$ with partitions $\mathcal{N}_k$ and $\mathcal{N}_m$, for which the adjacency matrix has the block-form:

$$A_{km,r} = \begin{bmatrix} 0 & B \\ B^T & 0 \end{bmatrix},$$

with $Bu = d_1 u$ and $u^T B = d_2 u^T$, because the graph is biregular. The values $d_1 = \frac{L}{N_k}$ and $d_2 = \frac{L}{N_m}$ are the degrees of the partitions.
Furthermore, we consider a partitioning π of the nodes of $G_{km,r}$ into four sets $\{\mathcal{N}_k^x, \mathcal{N}_k^r, \mathcal{N}_m^y, \mathcal{N}_m^r\}$ according to

$$\begin{cases} \mathcal{N}_k^x \cup \mathcal{N}_k^r = \mathcal{N}_k,\ \mathcal{N}_k^x \cap \mathcal{N}_k^r = \emptyset \text{ and } |\mathcal{N}_k^x| = N_x \\ \mathcal{N}_m^x \cup \mathcal{N}_m^r = \mathcal{N}_m,\ \mathcal{N}_m^x \cap \mathcal{N}_m^r = \emptyset \text{ and } |\mathcal{N}_m^x| = N_x \end{cases}$$

In other words, partition k is further refined into a subset of N_x nodes and a remainder subset, and similarly for partition m. For this partitioning π, the quotient matrix can be explicitly written as:

$$A^{(\pi)}_{km,r} = \begin{bmatrix} \frac{1}{N_x} & 0 & 0 & 0 \\ 0 & \frac{1}{N_k - N_x} & 0 & 0 \\ 0 & 0 & \frac{1}{N_y} & 0 \\ 0 & 0 & 0 & \frac{1}{N_m - N_y} \end{bmatrix} \begin{bmatrix} 0 & 0 & m & \frac{L}{N_k}N_x - m \\ 0 & 0 & \frac{L}{N_m}N_y - m & L\left(1 - \frac{N_x}{N_k} - \frac{N_y}{N_m}\right) + m \\ m & \frac{L}{N_m}N_y - m & 0 & 0 \\ \frac{L}{N_k}N_x - m & L\left(1 - \frac{N_x}{N_k} - \frac{N_y}{N_m}\right) + m & 0 & 0 \end{bmatrix} \tag{A-25}$$

where m is the number of links between partitions $\mathcal{N}^x_k$ and $\mathcal{N}^y_m$, i.e. the cut-set size $(u - w)^T A^{(km)} w$ in Theorem 4.

We can write the determinant of $A^{(\pi)}_{km,r}$ in two ways: an expression involving m, which follows directly from the block-matrix form and secondly, an inequality involving the eigenvalues of $A^{(\pi)}_{km,r}$. Combining both expressions for the determinant yields the isoperimetric inequality of Theorem 4. From (A-25), the determinant of $A^{(\pi)}_{km,r}$ can be calculated as:

$$\det\left(A^{(\pi)}_{km,r}\right) = \frac{L^2\left(m - \frac{L}{N_k N_m}N_x N_y\right)^2}{N_x(N_k - N_x)N_y(N_m - N_y)} \tag{A-26}$$

Secondly, if we call $\delta_1 \geq \delta_2 \geq \delta_3 \geq \delta_4$ the eigenvalues of $A^{(\pi)}_{km,r}$, where $\delta_1 = -\delta_4$ and $\delta_2 = -\delta_3$ hold because of the anti-diagonal block structure, then we have a second equation for the determinant:

$$\det\left(A^{(\pi)}_{km,r}\right) = \delta_1\delta_2\delta_3\delta_4 = \delta_1^2\delta_2^2 \tag{A-27}$$

Next, two facts about the eigenvalues of $A^{(\pi)}_{km,r}$ are combined to find expression (2-25). Firstly, because $A^{(\pi)}_{km,r}$ is a quotient matrix of $A_{km,r}$, we know by Theorem 10 that the eigenvalues of the first interlace those of the latter. In other words, we can bound δ_2 by:

$$\lambda_{N-K+2} \leq \delta_2 \leq \lambda_2$$

Because $\lambda_{N-k+2} = \lambda_{N-2} = -\lambda_3 \geq -\lambda_2$, we find

$$\delta_2^2 \leq \lambda_2^2 \tag{A-28}$$

The second fact we use is

$$\delta_1 = \frac{L}{\sqrt{N_k N_m}} \tag{A-29}$$

which can be verified by considering the eigenvalue equation:

$$\left(A^{(\pi)}_{km,r} - \frac{L}{\sqrt{N_k N_m}}\right)\begin{bmatrix}\sqrt{N_m}\\ \sqrt{N_m}\\ \sqrt{N_k}\\ \sqrt{N_k}\end{bmatrix} = 0$$

from which follows that $\left[\sqrt{N_m}, \sqrt{N_m}, \sqrt{N_k}, \sqrt{N_k}\right]^T$ is the right eigenvector of $A^{(\pi)}_{km,r}$ according to eigenvalue $\delta_1 = \frac{L}{N_k N_m}$. By the Perron-Frobenius theorem [19], we know that for non-negative matrices such as $A^{(\pi)}_{km,r}$, the largest (possibly non-unique) eigenvalue accords to an eigenvector with non-negative elements. This means that δ_1 is the largest eigenvalue of $A^{(\pi)}_{km,r}$ since its corresponding eigenvector is a vector with non-negative elements.
Combining (A-28) and (A-29) then yields an upper-bound for the determinant of $A^{(\pi)}_{km,r}$ in equation (A-27):

$$\det\left(A^{(\pi)}_{km,r}\right) \leq \frac{L^2}{N_k N_m}\lambda_2^2$$

Combined with (A-26) this gives

$$\frac{L^2\left(m - \frac{L}{N_k N_m}N_x N_y\right)^2}{N_x(N_k - N_x)N_y(N_m - N_y)} \leq \frac{L^2}{N_k N_m}\lambda_2^2$$

Which reduces to equation (2-25) if we replace m by $(u-w)^T A^{(km)} w$, and which thus proves Theorem 4. □

Appendix B

Appendix circuit-graph-simplex equivalence

B-1 Derivation of the (x, v)-characterization by Ω, equation (3-5)

Based on the definition of the effective resistance (3-4) and the fact that $\omega_{ii} = 0$ for all connections i, we can write:

$$\omega_{ij} = -\frac{1}{2}(e_i - e_j)^T \Omega (e_i - e_j) = (e_i - e_j)^T Q^\dagger (e_i - e_j)$$

for all connections i and j. Similarly, the following equality holds:

$$-\frac{1}{2}(e_k - e_m)^T \Omega (e_i - e_j) = (e_k - e_m)^T Q^\dagger (e_i - e_j) \tag{B-1}$$

for all connections i, j, k, m. Next, we introduce the external-current vector x with $u^T x = 0$, by noticing that x can always be written as a linear combination of $(e_i - e_j)$ vectors. In particular, for any external-current vector x, there exists weights α_{ij} for all pairs of connections i, j, such that

$$x = \sum_{i=1}^{N} \sum_{j=i}^{N} \alpha_{ij} (e_i - e_j)$$

holds. By linearity of equation (B-1), the external-current vector can be introduced as

$$-\frac{1}{2}(e_k - e_m)^T \Omega x = (e_k - e_m)^T Q^\dagger x$$

which by the (x, v)-relation $v = Q^\dagger x$ can be rewritten as:

$$-\frac{1}{2}(e_k - e_m)^T \Omega x = (e_k - e_m)^T v \tag{B-2}$$

Similar to the introduction of x, we can now introduce the matrix $\left(I - \frac{uu^T}{N}\right)$ by noticing that this matrix can be written as a linear combination of $(e_k - e_m)$ vectors. In particular, we have the relation

$$NI - uu^T = \sum_{k=1}^{N} \sum_{m=k}^{N} (e_k - e_m)(e_k - e_m)^T$$

Hence, by linearity of equation (B-2), the matrix $\left(I - \frac{uu^T}{N}\right)$ can be introduced as

$$-\frac{1}{2}\left(I - \frac{uu^T}{N}\right)\Omega x = \left(I - \frac{uu^T}{N}\right) v$$

which by $u^T v = 0$ leads to equation (3-5).

B-2 Proof of expression (3-11) for the Cayley-Menger determinant.

From Fiedlers inverse Q-Ω relation (3-7), we know that

$$-\frac{1}{2}\begin{bmatrix} 0 & u^T \\ u & \Omega \end{bmatrix} = \begin{bmatrix} \zeta^T Q \zeta + \frac{4R_G}{N^2} & -(Q\zeta + \frac{2}{N}u)^T \\ -(Q\zeta + \frac{2}{N}u) & Q \end{bmatrix}^{-1}$$

Hence, for the Cayley-Menger determinant [51] of the distance matrix Ω we have:

$$\det \begin{bmatrix} 0 & u^T \\ u & \Omega \end{bmatrix} = \det \left(-2 \begin{bmatrix} \zeta^T Q \zeta + \frac{4R_G}{N^2} & -(Q\zeta + \frac{2}{N}u)^T \\ -(Q\zeta + \frac{2}{N}u) & Q \end{bmatrix}^{-1} \right)$$

which by rules of the determinant reduces to

$$\det \begin{bmatrix} 0 & u^T \\ u & \Omega \end{bmatrix} = (-2)^{N+1} \det \left(\begin{bmatrix} \zeta^T Q \zeta + \frac{4R_G}{N^2} & -(Q\zeta + \frac{2}{N}u)^T \\ -(Q\zeta + \frac{2}{N}u) & Q \end{bmatrix} \right)^{-1} \tag{B-3}$$

For convenience, we rewrite the block-matrix by introducing the scalar $\alpha = \zeta^T Q \zeta + \frac{4R_G}{N^2}$ and the $N \times 1$ vector $\beta = [\beta_1 \ \beta_2 \ \dots \ \beta_N] = -(Q\zeta + \frac{2}{N}u)$. These replacements result in the simplified notation:

$$\begin{bmatrix} \zeta^T Q \zeta + \frac{4R_G}{N^2} & -(Q\zeta + \frac{2}{N}u)^T \\ -(Q\zeta + \frac{2}{N}u) & Q \end{bmatrix} = \begin{bmatrix} \alpha & \beta^T \\ \beta & Q \end{bmatrix} \tag{B-4}$$

By cofactor expansion along the first row, followed by cofactor expansion of the remaining first column, the determinant of the simplified matrix in equation (B-4) can be written as:

$$\det \begin{bmatrix} \alpha & \beta^T \\ \beta & Q \end{bmatrix} = \alpha \det(Q) + \sum_{i=1}^{N} (-1)^i \beta_i \sum_{j=1}^{N} (-1)^{j+1} \beta_j \det\left(Q_{\setminus\{i,j\}}\right)$$

or

$$\det \begin{bmatrix} \alpha & \beta^T \\ \beta & Q \end{bmatrix} = -\sum_{i=1}^{N} \sum_{j=1}^{N} (-1)^{i+j} \beta_i \beta_j \det\left(Q_{\setminus\{i,j\}}\right) \tag{B-5}$$

where we used $\det(Q) = 0$. The factor $\det\left(Q_{\setminus\{i,j\}}\right)$ is related to the Laplacian eigenvalues by the so-called *Kirchhoff's matrix-tree theorem*[1][19] :

$$\xi = \det\left(Q_{\setminus\{i,j\}}\right) = \frac{1}{N}\prod_{i=1}^{N-1}\frac{1}{\mu_i}$$

Introducing ξ in equation (B-5) yields the compact expression:

$$\det\begin{bmatrix}\alpha & \beta^T\\ \beta & Q\end{bmatrix} = -\xi(u^T\beta)^2$$

which, by definition of β, and $u^T\beta = -u^T(Q\zeta + \frac{2}{N}u) = -2$, equals

$$\det\begin{bmatrix}\zeta^T Q\zeta + \frac{4R_G}{N^2} & -(Q\zeta + \frac{2}{N}u)^T\\ -(Q\zeta + \frac{2}{N}u) & Q\end{bmatrix}^{-1} = -\frac{1}{4\xi} \tag{B-6}$$

Filling in equation (B-6) in equation (B-3) finally leads to equation (3-11) for the Cayley-Menger determinant of the effective resistance matrix Ω.

B-3 The effective resistance matrix Ω is an SED matrix

The result that electrical circuits are equivalent to hyperacute simplices, and that the effective resistance matrix is an SED matrix, is discussed by Sharpe in [18], who refers to earlier work by Moore [50]. In [43] uses this fact to establish the circuit-graph-simplex equivalence, amongst other results. In [54] on the "Geometry of the Laplacian", Fiedler gives a clear proof as to why the Ω matrix is an SED matrix:

Proof:

We start by considering the eigendecomposition of the Laplacian matrix Q:

$$Q = ZMZ^T = \sum_{i=1}^{N}\mu_i z_n z_n^T = [\sqrt{\mu_1}z_1\ \sqrt{\mu_2}z_2\ \dots\ \sqrt{\mu_N}z_N]\,[\sqrt{\mu_1}z_1\ \sqrt{\mu_2}z_2\ \dots\ \sqrt{\mu_N}z_N]^T$$

By omitting the zero eigenvalue $\mu_N = 0$ with corresponding eigenvector $z_N = u/\sqrt{N}$, this can can be rewritten as

$$Q = \left[\sqrt{\mu_1}z_1\ \sqrt{\mu_2}z_2\ \dots\ \sqrt{\mu_{N-1}}z_{N-1}\right]\left[\sqrt{\mu_1}z_1\ \sqrt{\mu_2}z_2\ \dots\ \sqrt{\mu_{N-1}}z_{N-1}\right]^T$$

By defining the $N \times (N-1)$ matrix $S = \left[\sqrt{\mu_1}z_1\ \sqrt{\mu_2}z_2\ \dots\ \sqrt{\mu_{N-1}}z_{N-1}\right]^T$, this yields $Q = S^T S$ which is commonly called the Gram decomposition, with S the Gram matrix. A nice

[1] A spanning tree of a graph $G(\mathcal{N}, \mathcal{L}, \mathcal{W})$ is a subgraph with links $T \subseteq \mathcal{L}$ such that all nodes are in the subgraph, and such that the subgraph contains no loops. If by $\mathbb{T}(G)$ we denote the set of all spanning trees of a graph, and by $\pi(T) = \prod_{\forall l\in T} w_l$ the weight of a spanning tree, then the weighted number of spanning trees ξ is defined as: $\xi = \sum_{\forall T\in\mathbb{T}(G)}\pi(T)$. Kirchhoff's matrix-tree theorem states the following relations for the weighted number of spanning trees:

$$\xi = \sum_{\forall T\in\mathbb{T}(G)}\pi(T) = \frac{1}{N}\prod_{i=1}^{N-1}\frac{1}{\mu_i} = (-1)^{i+j}\det\left(Q_{\setminus\{i,j\}}\right)$$

property of the Gram matrix is that inner products of its columns are directly related to the elements of Q, in particular:

$$Q_{ij} = s_i^T s_j$$

holds, with $s_i = Se_i$ the i'th column of the Gram matrix S. Repeating the same procedure for the pseudo-inverse Laplacian matrix $Q^\dagger$, yields the Gram decomposition

$$Q^\dagger = S^{\dagger T} S^\dagger$$

with the $N \times (N-1)$ Gram matrix $S^\dagger = \left[\frac{z_1}{\sqrt{\mu_1}} \; \frac{z_2}{\sqrt{\mu_2}} \; \dots \; \frac{z_{N-1}}{\sqrt{\mu_{N-1}}}\right]^T$. Again, the column inner products yield $Q_{ij}^\dagger = s_i^{\dagger T} s_j^\dagger$, which results in the following expression for the effective resistance:

$$(s_i^\dagger - s_j^\dagger)^T (s_i^\dagger - s_j^\dagger) = s_i^{\dagger T} s_i^\dagger + s_j^{\dagger T} s_j^\dagger - 2 s_i^{\dagger T} s_j^\dagger = Q_{ii}^\dagger + Q_{jj}^\dagger - 2Q_{ij}^\dagger = \omega_{ij}$$

that is, the effective resistance ω_{ij} equals the squared Euclidean distance between vectors $s_i^\dagger$ and $s_j^\dagger$. In other words, if we consider the N columns of $S^\dagger$ as a set of $(N-1)$-dimensional points, i.e. $\mathcal{P} = \{s_1^\dagger, s_2^\dagger, \dots, s_N^\dagger\}$, then the SED matrix of this point set equals the effective resistance matrix Ω. This can also be written as:

$$\widetilde{H}(\mathcal{S}(\mathcal{P})) = \Omega$$

which thus means that, indeed, Ω is an SED matrix. □